

**ASSESSING THE FUTURE OF THE ARCTIC SEA ICE  
COVER: PROCESSES, VARIABILITY AND  
IMPLICATIONS**

by

**PATRICIA DEREPIENTIGNY**

B.Sc., Université du Québec à Montréal, 2013

M.Sc., McGill University, 2016

A thesis submitted to the  
Faculty of the Graduate School of the  
University of Colorado in partial fulfillment  
of the requirements for the degree of  
Doctor of Philosophy  
Department of Atmospheric and Oceanic Sciences

2021

Committee Members:

Dr. Alexandra Jahn

Dr. Jennifer Kay

Dr. Marika Holland

Dr. Walt Meier

Dr. Clara Deser

# Assessing the Future of the Arctic Sea Ice Cover: Processes, Variability and Implications

DeRepentigny, Patricia (Ph.D., Atmospheric and Oceanic Sciences)

Thesis directed by Dr. Alexandra Jahn

## Abstract

Uncertainty in climate predictions arises from three distinct sources: the internal variability of the climate system, which refers to natural fluctuations in climate that occur even in the absence of external forcing, model or structural uncertainty, as different models make different assumptions and hence simulate somewhat different changes in climate in response to the same forcing, and scenario uncertainty, which represents humankind's free will concerning future climate change. In this thesis, we evaluate projections of Arctic sea ice in the context of these different sources of uncertainty. In particular, we show that internal variability, not scenario uncertainty, will ultimately determine the year of first summer ice-free conditions in the Arctic, in addition to the contribution from model uncertainty. Moreover, the increased inter-annual variability in late historical biomass burning forcing is found to cause a strong acceleration in sea ice decline in the early 21<sup>st</sup> century in several CMIP6 models, with model uncertainty affecting how different CMIP6 models respond to this forcing. Finally, we focus on the implications of scenario uncertainty on the changing sea ice cover through the lens of trans-border exchange of sea ice between the exclusive economic zones of the Arctic states. These different perspectives on climate model uncertainty allow for an improved understanding of the processes, variability and implications of a diminishing Arctic sea ice cover.

## DEDICATION

*À mes parents, Monique et Robert,  
qui m'ont toujours encouragé à aller au bout de mes rêves.*

## ACKNOWLEDGEMENTS

My time at CU Boulder has been a wild, awesome, stressful, and sometimes infuriating journey, but altogether a life-changing experience. It involved a lot of growth and evolution, and with that came a part of sacrifice, the loss of guidance, of familiar structures, as well as lots of doubt as I tried to find my way through this uncharted territory. I had to leave behind what I used to know and build a new understanding of myself and the world. Now that I have walked this path, I cannot go back, as I am forever changed.

None of my accomplishments would have been possible without the unconditional love and support from my family. To my parents, Monique and Robert, who gave me the world, thank you for the many sacrifices you made for my education that have allowed me to reach for the stars, and for putting up with me as I watched MétéoMédia for hours on end. Your hard work, passion and fearlessness have shaped my life and motivated me to follow my dreams. To my little sister Sophie, thank you for being your colorful and enthusiastic self and for always knowing how to make me laugh. In my moments of despair, you have been there to remind me that this is what I have been passionate about since I was 8 years old. You have always looked up to me and, because of you, I aspire to be the very best version of myself every day.

To Ben, who supports me in all that I do and never stops believing in me, I could not have done this without you. I am so grateful that we embarked on this journey of moving to another country and starting a PhD together. Thank you for being there to put me back on my feet when I fall into the abyss of self-doubt and to remind me to celebrate all of my successes, no matter how small.

To John, thanks for being the best friend anyone could ever ask for and for continuing to be even as I decided to move thousands of miles away. Thank you for always being there when I just need someone to listen and for being so patient when I take a long time to respond. You've seen me both at my best and my worst, and I am so grateful to know that I can always count on you whatever the future holds.

To Hannah, my personality twin, thank you for being your true unapologetic self, for always be willing to answer my questions about the English language or American culture, and for lending an open ear every time I needed to talk, cry, scream, or celebrate. Thank you for spending every working hour (and more!) on Zoom with me since the start of the COVID-19 pandemic and for keeping me accountable, I honestly do not know how I will be able to get anything done once we both move on to the next chapter in our career. I know that initially, the prospect of moving to a new city and starting a second postdoc came with a lot of doubts, but I am so grateful that it allowed us to cross paths and to develop a friendship that will undoubtedly stand the test of time and distance. I wish you all the best in Wisconsin, but most of all I hope you find happiness and peace, in whatever form it might come.

I want to thank all of my professors, friends, and classmates from the University of Colorado Boulder. To my first-year cohort—Tessa, Nicki, Elina, Marissa, Matt, Nick, Margot, Allyson, Mark, Nicola and Camden—I do not know how I would have passed my classes without all of the long hours spent studying and doing homework together at SEEC. It is an honor to have embarked on this journey with such a curious, lively, and intelligent bunch. To my fellow members of the Polar and Paleoclimate Modeling Group—Abigail Smith, Rory Laiho, Aaron Schroeder, Kerrie Ellzey (previously Dochen), Clara Burgard, Hannah Zanowski, Chris Wyburn-Powell and Sara Jean Reinelt—thank you for always providing supportive and constructive feedback, as well as a sense of community. To the cubicrew—Hannah, Holly, Geneviève and Riley—thank you for tolerating my obsession with plants, for creating such a supportive work environment and for the many discussions around a cup of tea or a pint of beer. To my fellow ATOC students, thank you for your scientific assistance and research suggestions when I was motivated, and for a welcome distraction when I

was not. To my friends and colleagues at the National Center for Atmospheric Research—Marika Holland, Alice DuVivier, David Bailey, Laura Landrum and Kristen Krumhardt—thank you for always helping me feel welcome and inspired during my time at the Mesa Lab. A very special thank you to Laurie Conway for making the logistics of graduate school and finances as smooth as imaginable and for being such a positive force in the department.

To my advisor, Alexandra Jahn, for her selfless encouragement and support both in my personal and professional life. Thank you for pushing me when I needed to be pushed and for telling me to rest when I needed to rest. You are a model advisor for all other scientists and I could not have done this without you. To my committee members—Alexandra Jahn, Jennifer Kay, Marika Holland, Walt Meier and Clara Deser—thank you for the guidance, support, mentorship and time you have selflessly provided for the last 4 years. I am honored to have had the opportunity to learn and work alongside you and to have developed into a capable scientist under your expert guidance. I also want to thank my master’s adviser and first mentors, Bruno Tremblay, Jean-François Lemieux and André Plante, for the endless advice, support, and knowledge provided which jump-started my passion for sea ice and climate science. To my co-authors—Alexandra Jahn, Marika Holland, Alice DuVivier, Bruno Tremblay, Robert Newton, Stephanie Pfirman, Jerry Meehl, John Fasullo, Dirk Notz, Jakob Dörr, Jennifer Kay, and many more—thank you for your hard work and the time you committed to solving new problems together.

The work presented in this thesis was supported by the Natural Sciences and Engineering Council of Canada (NSERC), the Fonds de recherche du Québec – Nature et Technologies (FRQNT) and the Canadian Meteorological and Oceanographic Society (CMOS) through doctoral scholarships, as well as NSF-OPP awards 1847398 and 1504348 and A. Jahn’s start-up funds from the University of Colorado Boulder. I am forever grateful to NSERC, FRQNT and CMOS for their financial support throughout my PhD studies. It means the world to me to have been supported by Canadian agencies who believed in my research abilities, even as I decided to pursue my doctoral studies outside of Canada.

The CESM project is supported primarily by NSF. We thank all the scientists, software en-

gineers, and administrators who contributed to the development of CESM and the CESM1 and CESM2 Large Ensemble Community Projects. We would like to acknowledge high-performance computing support from Yellowstone (<http://n2t.net/ark:/85065/d7wd3xhc>) and Cheyenne (doi: 10.5065/D6RX99HX) provided by NCAR's Computational and Information Systems Laboratory (CISL), sponsored by the National Science Foundation (NSF). We also acknowledge supercomputing resources provided by the IBS Center for Climate Physics in South Korea for the CESM2 Large Ensemble Project. We also thank the climate modeling groups for producing and making available their model output, the Earth System Grid Federation (ESGF) for archiving the data and providing access, and the multiple funding agencies who support CMIP6 and ESGF.

## CONTENTS

<b>CHAPTER</b>	
<b>1</b>	<b>INTRODUCTION</b> <span style="float: right;"><b>1</b></span>
<b>2</b>	<b>ARCTIC SEA ICE IN TWO CONFIGURATIONS OF THE CESM2 DURING THE 20TH AND 21ST CENTURIES</b> <span style="float: right;"><b>4</b></span>
2.1	Introduction . . . . . 5
2.2	Data and Methods . . . . . 7
2.2.1	The Community Earth System Model Version 2 (CESM2) . . . . . 7
2.2.2	The Community Earth System Model Large Ensemble (CESM-LE) . . . . . 10
2.2.3	Observational Datasets for Comparison . . . . . 10
2.3	Historical Arctic Sea Ice . . . . . 10
2.3.1	September – Arctic Sea Ice Minimum . . . . . 10
2.3.2	March – Arctic Sea Ice Maximum . . . . . 12
2.4	Ice-Free Conditions . . . . . 16
2.5	Accelerated Decline in Winter and Spring Ice Cover . . . . . 20
2.6	Sea Ice Trends at the Historical-Scenario Transition . . . . . 28
2.7	Conclusions . . . . . 30
2.8	Acknowledgements . . . . . 32
2.9	Supplementary Material . . . . . 34

<b>3</b>	<b>ENHANCED EARLY 21<sup>ST</sup> CENTURY ARCTIC SEA ICE LOSS DUE TO CMIP6 BIOMASS BURNING EMISSIONS</b>	<b>38</b>
3.1	Introduction . . . . .	38
3.2	Results . . . . .	40
3.2.1	Accelerated sea ice loss in the CESM2-LE compared to the CESM1-LE . . . . .	40
3.2.2	Impact of BB emissions on simulated Arctic climate . . . . .	41
3.2.3	Impact of BB emissions on sea ice sensitivity . . . . .	44
3.3	Discussion . . . . .	46
3.4	Conclusions . . . . .	48
3.5	Methods . . . . .	50
3.5.1	Observational data . . . . .	50
3.5.2	CESM simulations . . . . .	50
3.5.3	CESM2 sensitivity experiments with homogenized forcing . . . . .	52
3.5.4	CMIP6 simulations . . . . .	53
3.5.5	Criteria for determining sensitive versus not sensitive models . . . . .	54
3.6	Acknowledgements . . . . .	54
3.7	Author contributions . . . . .	55
3.8	Competing interests . . . . .	56
3.9	Data and materials availability . . . . .	56
3.10	Supplementary Information . . . . .	57
<b>4</b>	<b>INCREASED TRANSNATIONAL SEA ICE TRANSPORT BETWEEN NEIGHBORING ARCTIC STATES IN THE 21<sup>ST</sup> CENTURY</b>	<b>63</b>
4.1	Introduction . . . . .	64
4.2	Methods . . . . .	68
4.2.1	Community Earth System Model (CESM) . . . . .	68
4.2.2	Sea Ice Tracking Utility (SITU) . . . . .	72

4.3	Results . . . . .	74
4.3.1	Increase in Transnational Ice Exchange . . . . .	74
4.3.2	Impact of the Future Emissions Scenario . . . . .	78
4.4	Discussion . . . . .	82
4.5	Conclusions . . . . .	84
4.6	Acknowledgements . . . . .	87
4.7	Supplementary Material . . . . .	88
4.7.1	Observational Datasets . . . . .	88
4.7.2	Comparison of the CESM with Observations . . . . .	89
4.7.3	Supplementary Figures . . . . .	92
<b>5</b>	<b>CONCLUSION</b>	<b>101</b>
5.1	Summary of Major Findings . . . . .	101
5.2	Future Work . . . . .	104
	<b>BIBLIOGRAPHY</b>	<b>106</b>

## TABLES

### Table

2.1	Number of Ensemble Members for the Different CESM2 Simulations and the CESM-LE. . . . .	9
S4.1	Annual mean average areal flux of ice exchanged between all EEZs for the CESM-LE over the three time periods. The EEZ of formation is indicated in the first column and the EEZ of melt in the first row. All numbers are in km <sup>2</sup> /year. The last column contains the total annual mean average areal flux of ice formed in each EEZ, only considering ice floes that melted before the end of the time period. The numbers in bold highlight the pathways that are statistically different between the CESM-LE and the CESM-LW over a same time period at the 95% confidence level using a t-test.	99
S4.2	As in Table S4.1, but for the CESM-LW and for the time periods of 2031–2050 and 2081–2100 only. . . . .	100

## FIGURES

### Figure

- 2.1 Time evolution of (a) September and (b) March Arctic sea ice area in the observations (red), the CESM2(CAM6) (orange), the CESM2(WACCM6) (blue), the CESM-LE (dark grey) and the CMIP6 model spread (light grey). The vertical double-dashed lines indicate the transition year between historical and future simulations in CMIP6. Note that the reduction in the spread of CMIP6 models at the historical-scenario transition is due to a lower number of available simulations under the SSP5-8.5 scenario compared to historical simulations. The CMIP6 range shown here is the same as in SIMIP Community (2020). . . . . 11
- 2.2 Ensemble mean, decadal mean September sea ice concentration during the 1980s (left), 1990s (center) and 2000s (right) in the CESM2(CAM6) (top), the CESM2(WACCM6) (middle) and the CESM-LE (bottom). The decadal-averaged observed sea ice edge (defined as the 15% sea ice concentration contour) is indicated by the pink line. . . . 13

- 2.3 Fraction of total March ice area (where ice concentration is greater or equal to 15%) for different ice thickness categories during the (a) 1980s, (b) 1990s, (c) 2000s and (d) 2010s in the CESM2(CAM6) (orange), the CESM2(WACCM6) (blue) and the CESM-LE (grey). The solid line and the lower/upper dotted lines show the mean and the minimum/maximum across all ensemble members, respectively. In (d), given the different number of ensemble members in the CESM2(CAM6) between the historical (2010–2014) and the SSP5-8.5 (2015–2019) simulations, only ensemble members that cover the full decade are used. . . . . 14
- 2.4 Ensemble mean, decadal mean March ice thickness during the 1980s (left), 1990s (center) and 2000s (right) in the CESM2(CAM6) (top), the CESM2(WACCM6) (middle) and the CESM-LE (bottom). Note that the spacing of the color shading is uneven to highlight the thinner ice categories. . . . . 15
- 2.5 **Timing of first ice-free Arctic:** (a) Year of first September ice-free conditions in the CESM2(CAM6) (circles) and the CESM2(WACCM6) (diamonds) over the historical period (black) and the different future simulations (colors). The symbols with a dot in the middle indicate that two ensemble members reach first ice-free conditions in the same year. (b) Percentage of the total number of ensemble members reaching first September ice-free conditions in a given year in the CESM2(CAM6) (orange; total of 13 ensemble members), the CESM2(WACCM6) (blue; total of 10 ensemble members) and the CESM-LE (grey; total of 40 ensemble members). For the CESM2(CAM6) and the CESM2(WACCM6), this is done by combining the historical and all future simulations into one single distribution. . . . . 17

- 2.6 **Ice-free Arctic as a function of global warming:** (a) September sea ice extent as a function of 5-year annual mean global temperature anomaly in the CESM2(CAM6) (orange circles), the CESM2(WACCM6) (blue diamonds) and the CESM-LE (grey squares) over the historical period and the different future simulations. The horizontal dashed line indicates ice-free conditions of 1 million km<sup>2</sup> and the vertical dash-dotted line indicates 1.5°C of global warming. (b) Probability of September ice-free conditions for different values of 5-year annual mean global temperature anomaly in the CESM2(CAM6) (top), the CESM2(WACCM6) (middle) and the CESM-LE (bottom). The probability is calculated for temperature anomalies within  $\pm 0.1^\circ\text{C}$  of each target level of warming. All temperatures shown here use the 2-meter air temperature variable output, and temperature anomalies are calculated with respect to each ensemble member's 1850–1920 average. . . . . 19
- 2.7 Time evolution of Arctic sea ice area from January to June (a–f) in the observations (red), the CESM2(CAM6) (orange), the CESM2(WACCM6) (blue) and the CESM-LE (grey). . . . . 21
- 2.8 Ensemble mean, decadal mean March ice concentration during the 2070s (left), 2080s (center) and 2090s (right) in the CESM2(CAM6) (top), the CESM2(WACCM6) (middle) and the CESM-LE (bottom). . . . . 22
- 2.9 March sea ice area as a function of (a) annual global atmospheric CO<sub>2</sub> concentration, (b) annual Arctic temperature and (c) annual Arctic temperature anomaly over the historical period and the different future simulations for the CESM2(CAM6) (orange circles), the CESM2(WACCM6) (blue diamonds) and the CESM-LE (grey squares). Arctic temperatures are calculated over the region north of 70°N, and temperature anomalies are calculated with respect to each ensemble member's 1850–1920 average. All temperatures shown here use the 2-meter air temperature variable output. . . . . 23

- 2.10 Ensemble mean net surface ocean heat flux from 2080 to 2099 for the months of October (left), November (center) and December (right) in the CESM2(CAM6) (top), the CESM2(WACCM6) (middle) and the CESM-LE (bottom). Negative values indicate heat loss from the ocean to the atmosphere. The cyan lines indicate the monthly mean 15% sea ice concentration contour averaged over the same years and all ensemble members. No cyan line in a panel indicates that if there is any sea ice, sea ice concentration is below 15% everywhere. . . . . 25
- 2.11 Ensemble mean, decadal mean length of the open-water period during the 2070s (left), 2080s (center) and 2090s (right) in the CESM2(CAM6) (top), the CESM2(WACCM6) (middle) and the CESM-LE (bottom). . . . . 27
- 2.12 20-year linear trends in September ice area in the CESM2(CAM6) (a–d) and the CESM2(WACCM6) (e–h) under the historical forcing (black) and different future emissions scenarios (colors). (g) also includes 20-year linear trends in September ice area in three AerChemMIP experiments (Collins et al., 2017). The range of trends in September ice area across all ensemble members of the CESM-LE (grey shading) is shown for the historical period in all panels and additionally for the RCP8.5 scenario in (d) and (h). Values on the x-axis represent the end year of the 20-year period over which linear trends are calculated. The horizontal dashed lines indicate no trend, and the vertical double-dashed lines indicate the transition year between historical and future simulations in the CESM2. . . . . 29
- S2.1 Ensemble mean sea surface temperature averaged over 2080 to 2099 for the months of September (a, e, i), October (b, f, j), November (c, g, k) and December (d, h, l) in the CESM2(CAM6) (a–d), the CESM2(WACCM6) (e–h) and the CESM-LE (i–l). The cyan line indicates the monthly mean 15% sea ice concentration contour averaged over the same years and all ensemble members. No cyan line in a panel indicates that if there is any sea ice, sea ice concentration is below 15% everywhere. 34

S2.2 Ensemble mean, decadal mean day of the year of sea ice break-up during the 2070s (a, d, g), 2080s (b, e, h) and 2090s (c, f, i) in the CESM2(CAM6) (a–c), the CESM2(WACCM6) (d–f) and the CESM-LE (g–i). Regions of the ocean that are not colored (i.e., white) do not experience break-up because sea ice concentration was already below 15% on March 1st. . . . .	35
S2.3 Ensemble mean, decadal mean day of the year of sea ice freeze-up during the 2070s (a, d, g), 2080s (b, e, h) and 2090s (c, f, i) in the CESM2(CAM6) (a–c), the CESM2(WACCM6) (d–f) and the CESM-LE (g–i). Regions of the ocean that are not colored (i.e., white) do not experience freeze-up because the sea ice concentration never exceeds 15% before March 1st of the following year. . . . .	36
S2.4 As in Figure 2.12, but for September ice volume. . . . .	37
<b>3.1 Differences in the rate of Arctic sea ice loss.</b> Time evolution of (a) September sea ice area (SIA), (b) SIA anomalies relative to the 1940–1969 average, and (c) 20-year linear SIA trends in the CESM1-LE and the CESM2-LE. The ensemble mean is shown by the solid line, the full ensemble range is shown by the shading, the horizontal dashed line indicates ice-free conditions in (a), no anomalies in (b) and no trend in (c), and the two vertical double-dashed lines indicate the GFED period. Years when the CESM1-LE and the CESM2-LE are statistically different at the 95% significance level are indicated with a thicker ensemble mean line and are determined using a two-sample Welch’s t-test. In (c), values on the x-axis indicate the end year of the 20-year period over which the linear trend is computed. . . . .	41

- 3.2 Changes in BB forcing.** Prescribed total black carbon emissions from BB (a) between 40–70°N and (b) globally in CMIP5, CMIP6 and the CESM2-BB, smoothed with a 12-month running mean. The two vertical double-dashed lines indicate the GFED period. Note that the range of values on the y-axis is different between the two panels, with higher values of total black carbon emissions globally. Here we used black carbon emissions to represent BB emissions as it is the most radiatively important one, but all other prescribed BB emissions (dimethyl sulfide, primary organic matter, sulfur dioxide, sulfate aerosols and secondary organic aerosols) follow a similar time evolution as black carbon (not shown). . . . . 42
- 3.3 BB emissions impact on Arctic climate.** Annual Arctic (70–90°N) surface air temperature (a) anomalies relative to the 1940–1969 average and (b) 20-year linear trends, and September sea ice area (SIA) (c) anomalies relative to the 1940–1969 average and (d) 20-year linear trends in the CESM2-LE and the CESM2-BB. The ensemble mean is shown by the solid line, the full ensemble range is shown by the shading, the horizontal dashed line indicates no anomalies in (a, c) and no trend in (b, d), and the two vertical double-dashed lines indicate the GFED period. Years when the CESM2-LE and the CESM2-BB are statistically different at the 95% significance level are indicated with a thicker ensemble mean line and are determined using a two-sample Welch’s t-test. Note that while the CESM2-BB has a smaller ensemble size than the CESM2-LE (10 versus 50 ensemble members), its ensemble size is sufficient to detect a forced sea ice response to the modified BB emissions (Figure S3.5c, d). In (b, d), values on the x-axis indicate the end year of the 20-year period over which the linear trend is computed. . . . . 43

- 3.4 **BB emissions impact on sea ice sensitivity.** Sea ice sensitivity to (a) cumulative anthropogenic CO<sub>2</sub> emissions (defined as the change in Arctic September sea ice area per change in cumulative anthropogenic CO<sub>2</sub> emissions in m<sup>2</sup> per tonne of CO<sub>2</sub>) and (b) global annual mean surface air temperature (defined as the change in Arctic September sea ice area per change in global mean surface temperature in million km<sup>2</sup> per °C) from 1979–2014 in the CESM1-LE, the CESM2-BB and the CESM2-LE, with the red dashed line showing the observed sensitivity. For the two large ensembles, the box shows the inter-quartile range, the line inside the box shows the median, and the whiskers show the minimum and maximum across all ensemble members, and for the CESM2-BB the green circles indicate the sea ice sensitivity for each of the 10 ensemble members. Histograms of sea ice sensitivity to (c) cumulative anthropogenic CO<sub>2</sub> emissions and (d) global annual mean surface air temperature obtained by bootstrapping CESM1-LE and CESM2-LE ensemble means with 10 members 10,000 times, with the dotted lines showing the 95% confidence range for each distribution and the green line indicating the ensemble mean sensitivity of the CESM2-BB. . . . . 45
- 3.5 **Potential impact of BB emissions on observed Arctic sea ice decline.** 20-year linear trends in September sea ice area in each individual ensemble member of the (a) CESM2-LE and the (b) CESM2-BB compared to observations. The horizontal dashed line indicates no trend, and the two vertical double-dashed lines indicate the GFED period. Values on the x-axis indicate the end year of the 20-year period over which the linear trend is computed. . . . . 47

- S3.1 BB emissions impact on sea ice area in all months.** Sea ice area (SIA) anomalies relative to the 1940–1969 average in each month of the year in the CESM2-LE and the CESM2-BB. The ensemble mean is shown by the solid line, the full ensemble range is shown by the shading, the horizontal dashed line indicates no anomalies, and the two vertical double-dashed lines indicate the GFED period. Years when the CESM2-LE and the CESM2-BB are statistically different at the 95% significance level are indicated with a thicker ensemble mean line and are determined using a two-sample Welch’s t-test. Note that the range of values on the y-axis varies across all panels. . . . . 58
- S3.2 September sea ice evolution in CMIP6 models.** September sea ice area (SIA) anomalies relative to the 1940–1969 average for each CMIP6 model. The models in the sensitive category are shown in purple and the ones in the not sensitive category are shown in turquoise. For each model, the first three ensemble members are shown as thin lines and the ensemble mean is shown by the thick line. The light gray shaded region corresponds to the reference period 1978–1990 and the dark grey shaded region corresponds to the acceleration period 1997–2009 (see section 3.5.5 for more details). The horizontal dashed line indicates no anomalies and the two vertical double-dashed lines indicate the GFED period. The last row shows the CESM2-LE, the CESM2-WACCM and the CESM2-BB for comparison, only using the first three ensemble members. . . . . 59
- S3.3 September sea ice area trends in CMIP6 models.** As in Figure S3.2, but for 20-year linear trends in September sea ice area (SIA). The horizontal dashed line indicates no trend. Values on the x-axis indicate the end year of the 20-year period over which the linear trend is computed. . . . . 60
- S3.4 Spatial patterns of BB impacts.** Spatial distribution of the linear trend in (a, b) annual surface air temperature and (c, d) September sea ice concentration over the GFED period (1997–2014) in (a, c) the CESM2-LE and (b, d) the CESM2-BB. . . 61

- S3.5 Minimum number of ensemble members needed to detect a forced response to the homogenized BB emissions.** September sea ice area (SIA) (a) anomalies relative to the 1940–1969 average and (b) 20-year linear trends in the first and last 50 members of the CESM2-LE. Minimum number of ensemble members needed for the September SIA (c) anomalies relative to the 1940–1969 average and (d) 20-year linear trends between the first 50 member and last 50 member ensembles to be statistically different at the 95% significance level. This is done by bootstrapping the two ensembles 10,000 times with a sub-sample size varying from 2 to 49. The ensemble mean is shown by the solid line, the full ensemble range is shown by the shading, the horizontal dashed line indicates no anomalies in (a), no trend in (b), and 10 ensemble members in (c, d), and the two vertical double-dashed lines indicate the GFED period. In (a, b), years when the first 50 member and last 50 member ensembles are statistically different at the 95% significance level are indicated with a thicker ensemble mean line and are determined using a two-sample Welch’s t-test. In (b), values on the x-axis indicate the end year of the 20-year period over which the linear trend is computed. . . . . 62
- 4.1 Map of the exclusive economic zones (EEZs) of the Arctic based on the definition from the United Nations Convention on the Law of the Sea (Nordquist, 2011): Canada (purple), the United States (dark blue), Russia (light blue), Norway (turquoise), Iceland (green) and Greenland (orange). The region in the middle of the Arctic Ocean that is not included within an EEZ is referred to as the Central Arctic (CNT) for the context of this study. . . . . 67

- 4.2 Time evolution of (a) the total CO<sub>2</sub> emissions in GtC/yr, (b) the atmospheric CO<sub>2</sub> concentration in ppm, (c) the September Arctic sea ice extent in million square kilometers for all ensemble members with the threshold for a nearly ice-free Arctic shown by the grey dashed line, (d) the 20-year running mean annual-mean global temperature anomalies for all ensemble members (relative to pre-industrial levels, taken as 1850–1920 here) and (e) the 20-year running mean annual-mean Arctic temperature anomalies for all ensemble members. All panels cover the historical period of the CESM-LE (black), the future RCP8.5 scenario of the CESM-LE (blue) and the future low warming scenario of the CESM-LW (orange). Note the different range of the y-axis for (d) the global temperature anomalies and (e) the Arctic temperature anomalies. The grey shaded areas highlight the three different time periods our analysis focuses on (adapted from Figure S1 of Jahn, 2018). . . . . 69
- 4.3 Average September sea ice concentration for the CESM-LE over the period of (a) 1981–2000 as well as for (b, d) the CESM-LE and (c, e) the CESM-LW over the periods of (b, c) 2031–2050 and (d, e) 2081–2100. The borders of the EEZs are indicated by red lines. The cyan line shows the 15% sea ice concentration contour. . . . . 71
- 4.4 Annual mean average areal flux of transnational ice for the CESM-LE over the period of 1981–2000 (a) and for the CESM-LE (b, d) and the CESM-LW (c, e) over the periods of 2031–2050 (b, c) and 2081–2100 (d, e). The height of each colored portion within one bar represents the annual mean areal flux of ice between the EEZ of formation ( $x$  axis) and the EEZ of melt (color). Note that domestic ice is not included in this figure in order to focus on the features of transnational ice exchange. The average amount of ice area exchanged between all EEZs, including domestic ice, for both experiments as well as a statistical assessment of the pathways that are significantly different between the CESM-LE and the CESM-LW can be found in Tables S4.1 and S4.2 in the supporting information. . . . . 75

4.5	Average number of ice formation events per year in fall (SON) and winter (DJF) for the CESM-LE over the period of 1981–2000 (a, b) and for the CESM-LE (c, d, g, and h)] and the CESM-LW (e, f, i, and j)] over the periods of 2031–2050 (c–f)] and 2081–2100 (g–j)]. Only grid cells that are ice covered for at least one month during the specified season and time period and for a least one ensemble member are colored. The borders of the EEZs are indicated by red lines. Only ice floes that formed and melted between the specified time periods are considered. . . . .	76
4.6	As in Figure 4.5, but for the average number of ice melt events per year in summer (JJA) and fall (SON). . . . .	77
4.7	Annual cycle of areal ice formation [ <i>left</i> ] and melt [ <i>right</i> ] for the periods of 1981–2000 (a,b), 2031–2050 (c,d) and 2081–2100 (e,f) in the CESM-LE [ <i>blue</i> ] and the CESM-LW [ <i>orange</i> ]. The error bars show the 95% confidence intervals of the 20-year averaged ice formation/melt area for each month across the 40 ensemble members of the CESM-LE and the 11 ensemble members of the CESM-LW. Only ice floes that formed and melted between the specified time periods are considered. . . . .	79
4.8	Average transit time in years for the 15 pathways exchanging the largest areal flux of transnational ice throughout all three time periods and both experiments. The error bars show the 95% confidence bounds of the 20-year averaged transit time for the 40 ensemble members of the CESM-LE and the 11 ensemble members of the CESM-LW.	81
S4.1	Annual cycle of ice formation (a, c, e) and melt (b, d, f) over the periods of 1990–2005 (a, b), 2026–2035 (c, d) and 2071–2080 (e, f) for the first 35 members of the CESM-LE using a monthly (burgundy) and weekly (light blue) time resolutions. Only ice floes that formed and melted between the specified time periods are considered. Note that some of the differences between the weekly and monthly time resolution can be attributed to the way weeks are distributed into months as every month contains either 29, 30 or 31 days and thus always includes part of a week. . . . .	92

S4.2	Annual mean average areal flux of transnational ice for the CESM-LE over the periods of 1990–2005 (a, b), 2026–2035 (c, d) and 2071–2080 (e, f) using a monthly (a, c, e) and weekly (b, d, f) time resolutions. The height of each colored portion within one bar represents the annual mean areal flux of ice between the EEZ of formation ( $x$ axis) and the EEZ of melt (color). Note that domestic ice is not included in this figure in order to focus on the features of transnational ice exchange.	93
S4.3	Annual cycle of mean areal ice formation (a) and melt (b) in the observations (green) and the CESM-LE (blue) for the period of 1989–2008. The error bars show the maximum and minimum 20-year averaged formation/melt area for each month across the 40 ensemble members of the CESM-LE, showing the range of internal variability for this ensemble. Only ice floes that formed and melted between 1989–2008 are considered. Note that the values shown here are not meant to represent the actual amount of ice that forms and melts in the Arctic every year, but rather the area of ice formation and melt we obtain from SITU (see section 2.2).	94
S4.4	Average number of ice formation events per year in fall (SON) (a, c) and winter (DJF) (b, d) over the period of 1989–2008 for both observations (a, b) and the CESM-LE (c, d). The borders of the EEZs are indicated by red lines. Only ice floes that formed and melted between 1989–2008 are considered.	95
S4.5	As in Figure S4.4, but for the average number of ice melt events per year in summer (JJA) (a, c) and fall (SON) (b, d).	96

- S4.6 Annual mean areal transnational ice flux for the observations (wide bar) and annual mean minimum (left narrow bar), average (middle narrow bar) and maximum (right narrow bar) areal transnational ice flux for the 40 members of the CESM-LE for the period of 1989–2008. The height of each colored portion within one bar represents the annual mean areal flux of ice between the EEZ of formation ( $x$  axis) and the EEZ of melt (color). The CESM-LE is consistent with the observations when the observed value for each pathway lies between the range of the CESM-LE (minimum to maximum). Note that domestic ice is not included in this figure in order to focus on the features of transnational ice exchange. . . . . 97
- S4.7 Probability of transnational ice promotion for observations (a), the ensemble mean of the CESM-LE (b) as well as the ensemble mean  $\pm$  one standard deviation for the CESM-LE (c, d) over the period of 1989–2008. The color represents the probability that an ice parcel forming at each grid cell gets promoted from domestic ice to transnational ice. The borders of the EEZs are indicated by red lines. Note that the probability is calculated for each grid cell in which at least one ice parcel forms and thus gives no indication of how many ice parcels are considered in the calculation. . . 98

## CHAPTER 1

### INTRODUCTION

Global warming is occurring at a faster rate in the Arctic than anywhere else in the world (Post et al., 2019), and the rapid loss of Arctic sea ice in the last few decades has been one of the most iconic emblems of anthropogenic climate change (Serreze and Barry, 2011; IPCC, 2014; Koenigk et al., 2020). Sea ice plays a critical role in Arctic climate by increasing the reflectivity of the surface relative to open ocean (Perovich and Polashenski, 2012) and by regulating the exchanges of heat, momentum and moisture between the atmosphere and the polar oceans. Since the start of polar-orbiting satellites in 1979, the Arctic sea ice extent in September has decreased by about 45%, with large decreases also observed across all months (Stroeve and Notz, 2018). In addition, the Arctic sea ice cover has experienced considerable thinning with a substantial decline in multi-year ice extent and area (Comiso, 2012; Kwok, 2018) associated with a lengthening of the melt season (Markus et al., 2009; Stroeve et al., 2014b). Nearly all climate models project that the loss of Arctic sea ice will continue throughout the 21<sup>st</sup> century in response to increasing atmospheric greenhouse gas (Davy and Outten, 2020; SIMIP Community, 2020; Long et al., 2021). Recent studies suggest that the Arctic Ocean will become seasonally ice free by the end of the century (e.g., SIMIP Community, 2020), but projections of when, how frequently, and for how long still exhibit large uncertainties (Jahn, 2018; Niederdrenk and Notz, 2018; Sigmund et al., 2018).

There are three main sources of uncertainty that explain the range of possible climate projections in models (Cox and Stephenson, 2007; Hawkins and Sutton, 2009; Lehner et al., 2020). The first is the internal variability of the climate system, which refers to natural fluctuations in climate that occur even in the absence of any radiative forcing. These natural fluctuations have the

potential to reverse the long-term trends associated with anthropogenic climate change for about a decade or so, and their importance increases at smaller spatial scales and shorter time scales. The second is model uncertainty (also known as climate response uncertainty), which relates to the parameters used to specify climate processes in models. These structural differences between models explain why they simulate different climate responses under the same external forcing. The third is scenario uncertainty (also known as radiative forcing uncertainty), which represents the lack of knowledge of future radiative forcing associated with unknown future societal choices. In CMIP, this uncertainty is represented by scenarios of possible future emissions of greenhouse gases and aerosols generated by socioeconomic models that take into account a range of “story lines” covering global population growth, economic development, energy use, land use change, and a variable mix of future energy sources (e.g., O’Neill et al., 2016). To better interpret climate projections of Arctic sea ice, the relative importance of the contributing sources of uncertainty needs to be considered.

Internal variability is known as an important source of uncertainty in projections of future climate (Hawkins and Sutton, 2009; Deser et al., 2012; Lehner et al., 2020). Several studies suggest that internal variability has contributed to about 50% of the observed trend in September sea ice extent since 1979 (Stroeve et al., 2007, 2012a; Kay et al., 2011; Zhang, 2015; Ding et al., 2017, 2019), although the imprint of internal variability has been found to be highly nonuniform both in time and in space (England et al., 2019). A recent study demonstrates that the uncertainty in short-term projections of Arctic sea ice change will continue to be dominated by internal variability, regardless of the season, while for long-term projections both model and scenario uncertainty become important (Bonan et al., 2021).

The ongoing rapid loss of Arctic sea ice has far-reaching consequences for the global climate system, as well as Arctic’s ecology, economy and human activities. These include amplified warming of the Arctic (Screen and Simmonds, 2010; Screen et al., 2012; Stuecker et al., 2018; Dai et al., 2019; Previdi et al., 2020), changing habitat for polar ecosystems and prospects for human activities in the high north (Post et al., 2013; Meier et al., 2014; Macias-Fauria and Post, 2018; Ng et al., 2018; Huserbråten et al., 2019; Huntington et al., 2020), increased frequency of extreme events in

Arctic climate (Kirchmeier-Young et al., 2017; Rinke et al., 2017; Landrum and Holland, 2020), and possible linkages of sea ice loss to mid-latitude weather patterns (Francis and Vavrus, 2012, 2015; Vihma, 2014; Coumou et al., 2018), although this last point is still actively debated within the science community (Cohen et al., 2014; Barnes and Screen, 2015; Francis, 2017; Francis et al., 2017; Vavrus, 2018; Blackport and Screen, 2020). The considerable uncertainty in climate projections is particularly problematic for decision makers, who require reliable predictions of regional and local changes in climate that will impact people, economies and ecosystems. Initial-value predictability of Arctic sea ice extent has been shown to be regionally and seasonally dependent (Blanchard-Wrigglesworth et al., 2011b; Bushuk et al., 2019), often only lasting a few years at most for total Arctic sea ice extent (Blanchard-Wrigglesworth et al., 2011a; Guemas et al., 2016). This means that the predictability of future Arctic sea ice extent at decadal timescales could remain heavily influenced by internal variability. Even if the range of internal variability cannot be reduced, understanding its magnitude will allow for better decision making in light of this uncertainty.

Here we evaluate climate projections of Arctic sea ice in multiple versions of the Community Earth System Model (CESM) and CMIP6 models, with a focus on the dynamical and thermodynamic processes that leads to sea ice retreat on decadal to multi-decadal time scales. **The guiding science question of this dissertation is how to best interpret the processes that lead to Arctic sea ice retreat in the context of the different sources of uncertainty in climate change projections, as well as the implications of a diminishing Arctic sea ice cover.** The results of this dissertation are divided into three chapters: an assessment of the current and future states of Arctic sea ice in two different configurations of the CESM2 and analysis of the impact of internal variability and model uncertainty on the timing and probability of first ice-free conditions (Chapter 2); evidence that forcing uncertainty associated with increased inter-annual variability in boreal biomass burning emissions in CMIP6 leads to a strong acceleration in sea ice decline in the early 21<sup>st</sup> century in the CESM2 Large Ensemble (Chapter 3); and the impact of scenario uncertainty on the amount of sea ice exchanged between the different regions of the Arctic as it transitions towards a thinner, less extensive, more mobile sea ice cover (Chapter 4).

## CHAPTER 2

# ARCTIC SEA ICE IN TWO CONFIGURATIONS OF THE CESM2 DURING THE 20TH AND 21ST CENTURIES

### Preface

This chapter is published as cited below, and is reproduced here based on the last author version. It is identical in content to the published version, except for formatting and copy editing:

DeRepentigny, P., Jahn, A., Holland, M. M. and Smith, A.: Arctic sea ice in two configurations of the CESM2 during the 20th and 21st centuries, *Journal of Geophysical Research: Oceans*, 125(9), e2020JC016133, <https://doi.org/10.1029/2020JC016133>, 2020.

### Abstract

We provide an assessment of the current and future states of Arctic sea ice simulated by the Community Earth System Model version 2 (CESM2). The CESM2 is the version of the CESM contributed to the sixth phase of the Coupled Model Intercomparison Project (CMIP6). We analyze changes in Arctic sea ice cover in two CESM2 configurations with differing atmospheric components: the CESM2(CAM6) and the CESM2(WACCM6). Over the historical period, the CESM2(CAM6) winter ice thickness distribution is biased thin, which leads to lower summer ice area compared to CESM2(WACCM6) and observations. In both CESM2 configurations, the timing of first ice-free conditions is insensitive to the choice of CMIP6 future emissions scenario. In fact, the probability of an ice-free Arctic summer remains low only if global warming stays below 1.5°C, which none of the CMIP6 scenarios achieve. By the end of the 21<sup>st</sup> century, the CESM2 simulates less ocean heat loss during the fall months compared to its previous version, delaying sea ice formation and leading

to ice-free conditions for up to 8 months under the high emissions scenario. As a result, both CESM2 configurations exhibit an accelerated decline in winter and spring ice area under the high emissions scenario, a behavior that had not been previously seen in CESM simulations. Differences in climate sensitivity and higher levels of atmospheric CO<sub>2</sub> by 2100 in the CMIP6 high emissions scenario compared to its CMIP5 analog could explain why this winter ice loss was not previously simulated by the CESM.

### Plain Language Summary

We provide a first look at the current and future states of Arctic sea ice as simulated by the Community Earth System Model version 2 (CESM2), which is part of the newest generation of large-scale climate models. The CESM2 model has two configurations that differ in their representation of atmospheric processes: the CESM2(CAM6) and the CESM2(WACCM6). We find several differences in the simulated Arctic sea ice cover between the two CESM2 configurations, as well as compared to the previous generation of the CESM model. Over the historical period, the CESM2(CAM6) model simulates a winter ice cover that is too thin, which leads to lower summer ice coverage compared to the CESM2(WACCM6) model and observations. In both CESM2 configurations, the probability of the Arctic becoming nearly ice free at the end of the summer only remains low if global warming stays below 1.5°C. In addition, the specific year a first ice-free Arctic is reached is not sensitive to the future greenhouse gas emissions trajectories considered here. In contrast to the previous generation of the CESM, both CESM2 configurations project an accelerated decline in winter and spring ice area by the end of the 21<sup>st</sup> century if greenhouse gases emissions remain high.

## 2.1 Introduction

In recent decades, the Arctic sea ice cover has changed dramatically, with negative linear trends in sea ice extent in all months (Stroeve and Notz, 2018). The loss of summer sea ice has been particularly striking, with decreases of roughly 50% and 66% in September ice extent and thickness since 1979, respectively (Comiso et al., 2017; Kwok, 2018; Stroeve and Notz, 2018). Newly

available climate model simulations from the sixth phase of the Coupled Model Intercomparison Project (CMIP6; Eyring et al., 2016) represent a powerful tool for advancing our understanding of present and future changes in the Arctic climate system. The Sea-Ice Model Intercomparison Project (SIMIP; Notz et al., 2016) community has recently found that CMIP6 model performance in simulating Arctic sea ice is similar to CMIP5 and CMIP3 in many aspects, but that the sensitivity of Arctic sea ice to changes in the forcing is generally better captured by CMIP6 models (SIMIP Community, 2020).

The Community Earth System Model version 2 (CESM2; Danabasoglu et al., 2020) is the contribution of the National Center for Atmospheric Research (NCAR) to CMIP6. Two separate CESM2 configurations that differ only in their atmosphere model have been contributed to CMIP6. The Community Earth System Model (CESM) and its various iterations have been widely used in the past to understand the changing Arctic and have performed well in capturing the Arctic mean sea ice state, trends and variability (e.g., Barnhart et al., 2016; DeRepentigny et al., 2016; England et al., 2019; Jahn et al., 2016; Labe et al., 2018). The goal of this paper is to provide an overview of the major Arctic sea ice features during the 20<sup>th</sup> and 21<sup>st</sup> centuries in the CESM2 that are of interest to the Arctic and global climate change communities. Specifically, we assess the performance of the two CESM2 configurations over the historical period in comparison with both the previous CESM version and available observations (section 2.3). This is followed by an analysis of the future evolution of the Arctic sea ice cover in the two configurations, including determining when an ice-free Arctic may occur (section 2.4) and documenting a dramatic winter and spring ice loss in the late 21<sup>st</sup> century due to a reduction in oceanic heat loss in fall (section 2.5), something that had not been previously seen in the CESM model over the 21<sup>st</sup> century. Finally, we present some initial analysis of a reduction in the simulated negative trends of Arctic sea ice cover at the historical-scenario transition (section 2.6). The source of the differences in Arctic sea ice simulations between the two CESM2 configurations in the pre-industrial simulations is analyzed in a companion paper by DuVivier et al. (2020).

## 2.2 Data and Methods

### 2.2.1 The Community Earth System Model Version 2 (CESM2)

The CESM2 is a community-developed, fully-coupled earth system model publicly available at <http://www.cesm.ucar.edu/models/cesm2/>. It is the latest generation of the CESM and NCAR’s contribution to CMIP6. Two separate CESM2 configurations have been contributed to the CMIP6 effort, differing only in their atmosphere component: the “low-top” (40 km, with limited chemistry) Community Atmosphere Model version 6 (CAM6; Danabasoglu et al., 2020) and the “high-top” (140 km, with interactive chemistry) Whole Atmosphere Community Climate Model version 6 (WACCM6; Gettelman et al., 2019b). The CESM2 presents several science and infrastructure changes that have been fully documented in Danabasoglu et al. (2020). In particular, the CESM2 shows large reductions in low latitude precipitation and short-wave cloud radiative forcing biases, resulting in improved historical simulations with respect to the available observations compared to its previous major release, the CESM1.1 (Hurrell et al., 2013). As a result of an improved cloud distribution compared to the CESM1.1, increased cloud feedbacks in the CESM2 lead to a higher equilibrium climate sensitivity (ECS; Gettelman et al., 2019a) that is more than 1°C above the ECS of the CESM1.1 (Danabasoglu et al., 2020) and at the upper end of the range of CMIP6 models (Meehl et al., 2020).

The CESM2 uses a nominal 1° (1.25° longitude x 0.9° latitude) horizontal resolution configuration, with the Parallel Ocean Program version 2 (POP2; Smith et al., 2010) as its ocean component and the Community Land Model version 5 (CLM5; Lawrence et al., 2019) as its land component. The “low-top” CAM6 atmosphere model has 32 vertical levels and the model top reaches into the stratosphere at 3.6 hPa. The “high-top” WACCM6 model has 70 vertical levels and a model top in the lower thermosphere at  $6 \times 10^{-6}$  hPa. The vertical levels in CAM6 and WACCM6 are identical up to 87 hPa. A major difference between the two atmosphere models is that WACCM6 has interactive chemistry with 228 prognostic chemical species, including an extensive representation of secondary organic aerosols (Tilmes et al., 2019). WACCM6 simulations

were used to force the CAM6 simulations at the model top, so that both model configurations use the same forcing. The two CESM2 configurations will be referred to as CESM2(CAM6) and CESM2(WACCM6) hereafter.

For its sea ice component, the CESM2 uses the Los Alamos Sea Ice Model version 5.1.2 (CICE5; Hunke et al., 2015), which has the same horizontal grid as the ocean component POP2 (as described in Danabasoglu et al., 2012). CICE5 uses the mushy-layer thermodynamics scheme (Turner and Hunke, 2015) rather than that of Bitz and Lipscomb (1999) which was used in CICE4, the sea ice component of CESM1. Further changes in CICE5 include a salinity-dependent freezing point for seawater (Assur, 1960), a prognostic vertical profile of ice salinity, and an updated melt pond parameterization (Hunke et al., 2013). In order to better represent salinity and temperature profiles in sea ice, the vertical sea ice resolution has been increased from four layers in CICE4 to eight layers in CICE5 and from one to three layers for the vertical snow resolution.

The CESM2 historical simulations extend from 1850 to 2014, with 11 ensemble members for CESM2(CAM6) (Danabasoglu, 2019a) and three for CESM2(WACCM6) (Danabasoglu, 2019i) (Table 2.1). Each ensemble member is branched from a random year in its respective pre-industrial control simulation. The future simulations extend from 2015 to 2100 and follow the Shared Socioeconomic Pathways (SSPs; O’Neill et al., 2014), a new scenario framework designed to account for future socioeconomic development in addition to climate change resulting from increasing greenhouse gas emissions. Currently, CESM2 simulations following four different SSPs are available (Danabasoglu, 2019b,c,d,e,j,k,l,m), and the number of ensemble members in each of these different simulations is given in Table 2.1. Most of the analysis presented in this paper is done using the historical and SSP5-8.5 simulations (high challenges for mitigation and low challenges for adaptation, as described in O’Neill et al., 2016), unless noted otherwise. Note that even though the CMIP5 Representative Concentration Pathway 8.5 (RCP8.5; Van Vuuren et al., 2011) and the CMIP6 SSP5-8.5 scenarios are designed to result in the same radiative forcing when applied in a simple climate model (O’Neill et al., 2016), the prescribed concentration of greenhouse gases, land use change and other external forcings differ substantially between the two. Notably, the SSP5-8.5

Table 2.1: Number of Ensemble Members for the Different CESM2 Simulations and the CESM-LE.

	CESM2(CAM6)	CESM2(WACCM6)	CESM-LE
Historical	11	3	40
SSP1-2.6	3	1	—
SSP2-4.5	3	3	—
SSP3-7.0	3	3 <sup>a</sup>	—
SSP5-8.5	3	3	—
RCP8.5	—	—	40

<sup>a</sup>Members #2 and #3 only extend to the end of 2055.

scenario reaches higher atmospheric CO<sub>2</sub> concentration by the end of the century (see Figure 3 of O’Neill et al., 2016). The different transient nature of the forcings and different radiative feedbacks in the models will influence the radiative imbalance at the top of the atmosphere that results by 2100. Hence, some combination of differences in the forcing and the higher ECS in CESM2 compared to CESM1 (Gettelman et al., 2019a) leads to an additional 1°C of warming in the CESM2 compared to the CESM1 by the end of the 21<sup>st</sup> century (Meehl et al., 2020).

Note that here we use the CESM2(CAM6) future scenario simulations contributed to the CMIP6 archive in May 2020. The initial CESM2(CAM6) future scenario simulations submitted to the CMIP6 archive had to be retracted in April 2020 because both anthropogenic and biomass burning secondary organic aerosol emissions were set to zero starting in 2015 in error, and have been replaced by the new runs analyzed here. For Arctic sea ice, no impact of this erroneous forcing in the future scenario simulations is detectable within the limits of internal variability, so any results based on the previous CESM2(CAM6) Arctic sea ice output remain valid (e.g., SIMIP Community, 2020), but will differ in their internal variability from the new set of runs shown here.

We use sea ice area as our primary variable to describe sea ice coverage instead of sea ice extent since sea ice extent is a strongly grid-dependent, non-linear quantity, making model comparisons less accurate (Notz, 2014). Note however that we use sea ice extent in section 2.4 where we discuss ice-free conditions in the Arctic to allow for comparison with previous studies that all define ice-free conditions in terms of ice extent. An assessment of the effect of using extent rather than area to define ice-free conditions is provided in section 2.4.

### **2.2.2 The Community Earth System Model Large Ensemble (CESM-LE)**

Results from the CESM2 simulations are compared to the previous version of the CESM, the CESM1.1-CAM5 (Hurrell et al., 2013). In particular, we use the CESM Large Ensemble (CESM-LE; Kay et al., 2015), a 40-member ensemble experiment (Table 2.1) that has been widely used for Arctic sea ice studies and generally performs well when compared to observations (e.g., Barnhart et al., 2016; DeRepentigny et al., 2016; England et al., 2019; Jahn et al., 2016; Kirchmeier-Young et al., 2017; Smith and Jahn, 2019; Swart et al., 2015). It follows the RCP8.5 scenario with the same radiative imbalance by 2100 as the SSP5-8.5 scenario used to force the CESM2. The CESM-LE historical simulations span 1920 to 2005, while the RCP8.5 scenario simulations cover 2006 to 2100.

### **2.2.3 Observational Datasets for Comparison**

To assess how realistic the CESM2 simulations are in terms of northern hemisphere monthly sea ice area over the satellite era, we use the National Snow and Ice Data Center (NSIDC) Sea Ice Index version 3 (Fetterer et al., 2017) between 1979 and 2020, with the observational pole hole filled assuming sea ice concentration of 100%. We also use sea ice concentration data derived from passive microwave brightness temperature from the National Oceanic and Atmospheric Administration (NOAA)/NSIDC Climate Data Record (Meier et al., 2017; Peng et al., 2013) to obtain the location of the observed sea ice edge (defined as the 15% sea ice concentration contour). For the analysis of sea ice thickness, we do not compare model results to reanalyzed or observational estimates as those still exhibit substantial uncertainties (Bunzel et al., 2018; Chevallier et al., 2017).

## **2.3 Historical Arctic Sea Ice**

### **2.3.1 September – Arctic Sea Ice Minimum**

Over the historical period, the simulated September pan-Arctic sea ice cover differs greatly between the CESM2(CAM6) and the CESM2(WACCM6) (Figures 2.1a and 2.2a–f). The September

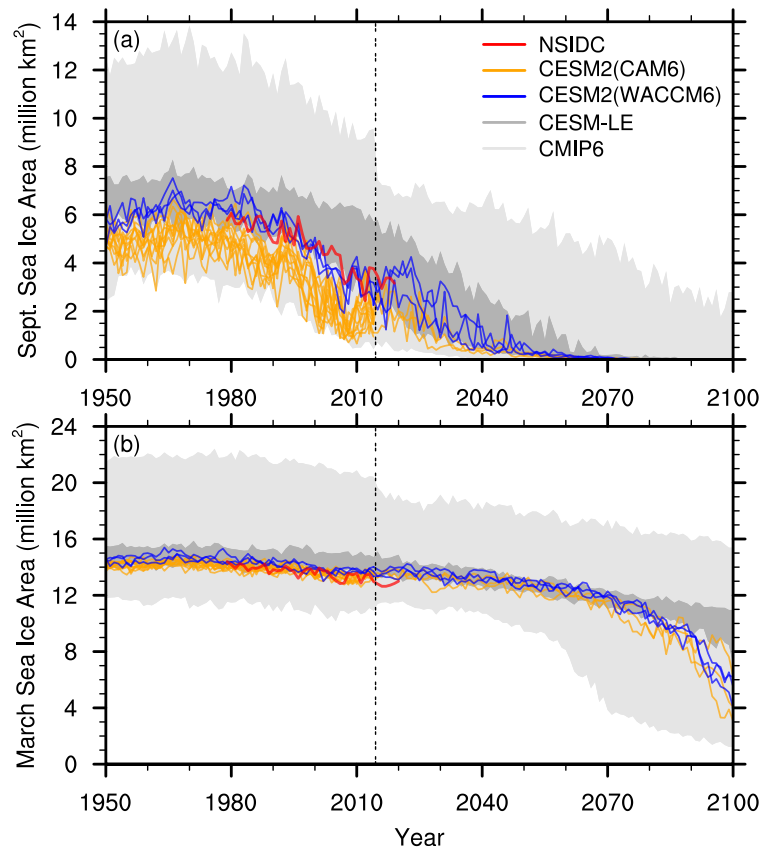


Figure 2.1: Time evolution of (a) September and (b) March Arctic sea ice area in the observations (red), the CESM2(CAM6) (orange), the CESM2(WACCM6) (blue), the CESM-LE (dark grey) and the CMIP6 model spread (light grey). The vertical double-dashed lines indicate the transition year between historical and future simulations in CMIP6. Note that the reduction in the spread of CMIP6 models at the historical-scenario transition is due to a lower number of available simulations under the SSP5-8.5 scenario compared to historical simulations. The CMIP6 range shown here is the same as in SIMIP Community (2020).

ice area in CESM2(WACCM6) compares well with observations over the satellite era (Figures 2.1a and 2.2d–f). Conversely, the CESM2(CAM6) September ice area is consistently lower than observed (Figure 2.1a), with too little ice in the Pacific and Eurasian sectors of the Arctic (Figure 2.2a–c). Compared to the spread of the CESM-LE, the CESM2(CAM6) September sea ice area is consistently less extensive, while the CESM2(WACCM6) sea ice area falls at the low end of the range of internal variability of the CESM-LE (Figure 2.1a). Compared to the available CMIP6 simulations (SIMIP Community, 2020), the CESM2(CAM6) falls at the low end of the spread while the CESM2(WACCM6) is found in the lowest one third of the CMIP6 model spread (Figure 2.1a).

DuVivier et al. (2020) found that differences in ice area already exist between CESM2(CAM6) and CESM2(WACCM6) in their pre-industrial control simulations, with the largest differences in the summer months. These discrepancies in ice area and volume can be attributed to thinner early spring clouds in the CESM2(CAM6), which drive a strong ice-albedo feedback and result in a lower ice area in September and significantly thinner ice year-round (DuVivier et al., 2020).

The decline in summer ice area at the end of the 20<sup>th</sup> century occurs more rapidly in the CESM2 (Figure 2.2a–f) than in the CESM-LE (Figure 2.2g–i), and results in a northern hemisphere September sea ice area for the CESM2(WACCM6) that compares more favorably to observations at the start of the 21<sup>st</sup> century (Figure 2.1a). The CESM2(CAM6) sea ice coverage (Figure 2.2a–c) is consistently less extensive than the CESM2(WACCM6) and the CESM-LE almost everywhere in the Arctic, with no ice left in the peripheral seas. By the 2000s, sea ice is confined to the Central Arctic in the CESM2(CAM6), with open-water conditions over a large area of the Pacific, Eurasian and Atlantic sectors of the Arctic Ocean.

### 2.3.2 March – Arctic Sea Ice Maximum

At the Arctic sea ice maximum in March, sea ice area is comparable to observations for both CESM2 configurations whereas it is generally too extensive in the CESM-LE (Figure 2.1b). The lower March sea ice area in the CESM2 compared to the CESM-LE is mainly due to less ice coverage in the Pacific Ocean south of the Bering Strait (not shown), and these differences in winter ice coverage between the two model versions get larger toward the end of the historical period (Figure 2.1b).

In addition to ice area, an accurate representation of winter ice thickness is important to effectively characterize the sea ice state in light of the inverse relationship between sea ice volume and the efficiency of thermodynamic processes such as sea ice growth and melt (Bitz and Roe, 2004). This relationship impacts the simulated Arctic sea ice volume variability on long timescales and thus the projected evolution of Arctic sea ice (Massonnet et al., 2018). Compared to five years of gridded ICESat satellite sea ice thickness data in February and March (2003–2007), DuVivier

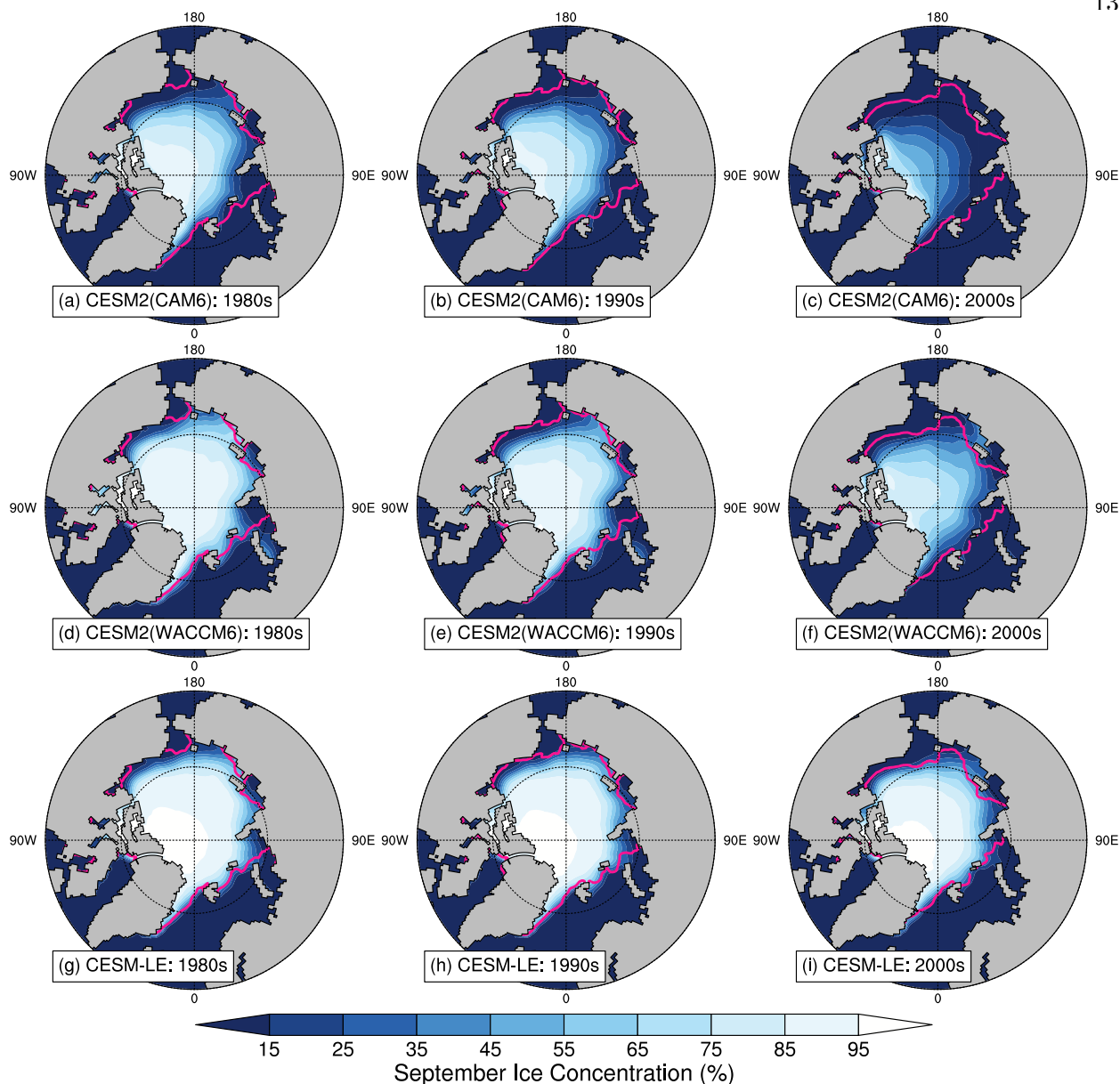


Figure 2.2: Ensemble mean, decadal mean September sea ice concentration during the 1980s (left), 1990s (center) and 2000s (right) in the CESM2(CAM6) (top), the CESM2(WACCM6) (middle) and the CESM-LE (bottom). The decadal-averaged observed sea ice edge (defined as the 15% sea ice concentration contour) is indicated by the pink line.

et al. (2020) found better agreement between observations and the CESM2(WACCM6) than with the CESM2(CAM6), despite ICESat observations showing a higher fraction of thick ice ( $> 2$  m) than in either CESM2 configuration. We find that during the 1980s, the CESM2(CAM6) March ice thickness distribution is biased thin compared to the CESM2(WACCM6) and the CESM-LE (Figure

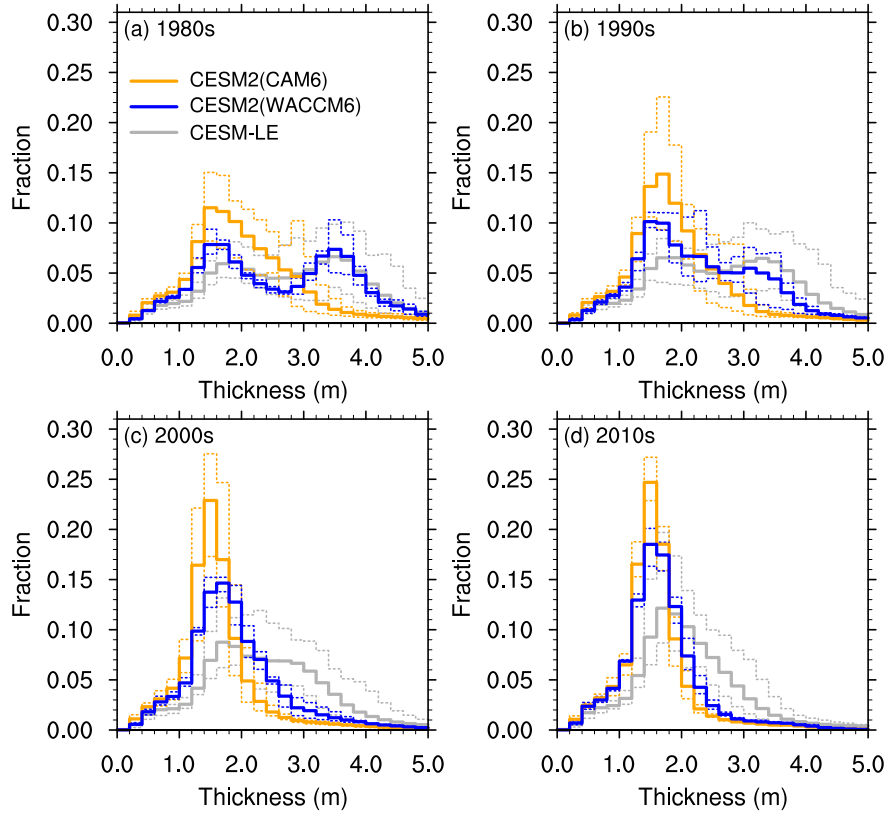


Figure 2.3: Fraction of total March ice area (where ice concentration is greater or equal to 15%) for different ice thickness categories during the (a) 1980s, (b) 1990s, (c) 2000s and (d) 2010s in the CESM2(CAM6) (orange), the CESM2(WACCM6) (blue) and the CESM-LE (grey). The solid line and the lower/upper dotted lines show the mean and the minimum/maximum across all ensemble members, respectively. In (d), given the different number of ensemble members in the CESM2(CAM6) between the historical (2010–2014) and the SSP5-8.5 (2015–2019) simulations, only ensemble members that cover the full decade are used.

2.3a). In particular, the CESM2(CAM6) distribution is unimodal, with a peak in ice thickness at  $\sim 1.5$  m and an asymmetric tail towards thicker ice. This unimodal structure is also present during the early 20<sup>th</sup> century of the CESM2(CAM6) historical simulations (not shown). On the other hand, the CESM2(WACCM6) and the CESM-LE have similar, bimodal ice thickness distributions (Figure 2.3a) with a high percentage of thin ice (ranging from 1.2–2.0 m) and a similarly high percentage of thick ice (ranging from 3.0–4.0 m). The shape of the ice thickness distribution in the CESM2(CAM6) is associated with a low winter mean sea ice thickness, with a sea ice cover up to 1.5 m thinner over most of the Arctic Ocean compared to the CESM2(WACCM6) and the

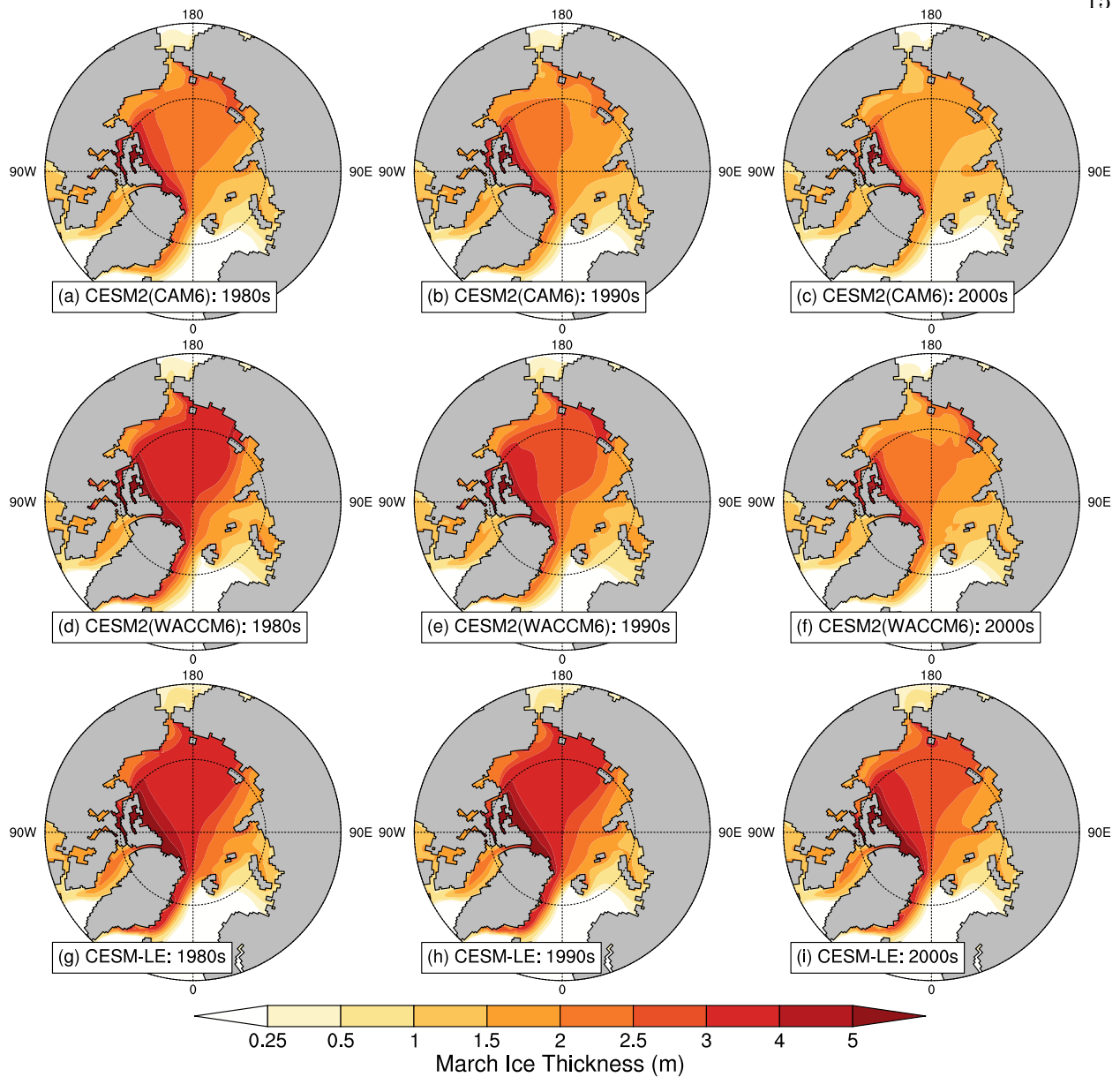


Figure 2.4: Ensemble mean, decadal mean March ice thickness during the 1980s (left), 1990s (center) and 2000s (right) in the CESM2(CAM6) (top), the CESM2(WACCM6) (middle) and the CESM-LE (bottom). Note that the spacing of the color shading is uneven to highlight the thinner ice categories.

CESM-LE (Figure 2.4a, d, g).

During the 1990s, the CESM2(WACCM6) gains ice in the thinner categories at the expense of the thicker categories, whereas the CESM-LE retains its characteristic bimodal shape with similar fractions of ice across the two modes (Figure 2.3b). The loss of thick ice ( $> 3$  m) in the

CESM2(WACCM6) occurs mainly over the Central Arctic (Figure 2.4e). For the CESM-LE, the loss of thick ice over the Central Arctic begins in the 2000s, reaching a similar winter state as the CESM2(WACCM6) a decade later on average (Figures 2.3b, c and 2.4e, i). At the start of the 21<sup>st</sup> century, the CESM2(WACCM6) exhibits a unimodal shape similar to the CESM2(CAM6), but with the peak of the distribution slightly shifted toward thicker ice categories (Figure 2.3c). By the 2010s, all three model simulations show substantially reduced fractions of ice thicker than 3 m, with the peak of each distribution centered around ice thicknesses of 1–2 m (Figure 2.3d).

## 2.4 Ice-Free Conditions

In both CESM2 configurations, we find that the timing of first summer ice-free conditions (defined as pan-Arctic monthly sea ice extent below 1 million km<sup>2</sup>) is insensitive to the choice of future emissions scenario considered here (i.e., SSP1-2.6, SSP2-4.5, SSP3-7.0 and SSP5-8.5; Figure 2.5a). The absence of a relationship between the year of first September ice-free conditions and the different SSPs in the CESM2 implies that internal variability, not differences in future anthropogenic emissions as represented by the CMIP6 future scenarios, ultimately determines the year of first ice-free conditions in the Arctic. This is in agreement with an earlier study using the CESM1.1 (Jahn, 2018), as well as with the CMIP6 models overall (SIMIP Community, 2020). The lack of a scenario impact on the timing of a first ice-free Arctic can be explained by the fact that the atmospheric CO<sub>2</sub> concentration and resulting global mean temperature change from the different SSPs only start to substantially diverge between 2040 and 2060 (see Figure 3 of O’Neill et al., 2016), after the Arctic has already become ice free in September in the CESM2 and most CMIP6 models (SIMIP Community, 2020). Furthermore, as the mean sea ice state approaches ice-free conditions, the importance of internal variability has been shown to increase relative to the forced change necessary to melt the remaining sea ice cover in September (Jahn et al., 2016).

Given that we find no CMIP6 scenario impact on the timing of first ice-free conditions in September, the CESM2 simulations from each configuration can be combined to obtain a distribution of the year of first September ice-free conditions (Figure 2.5b). Consistent with a

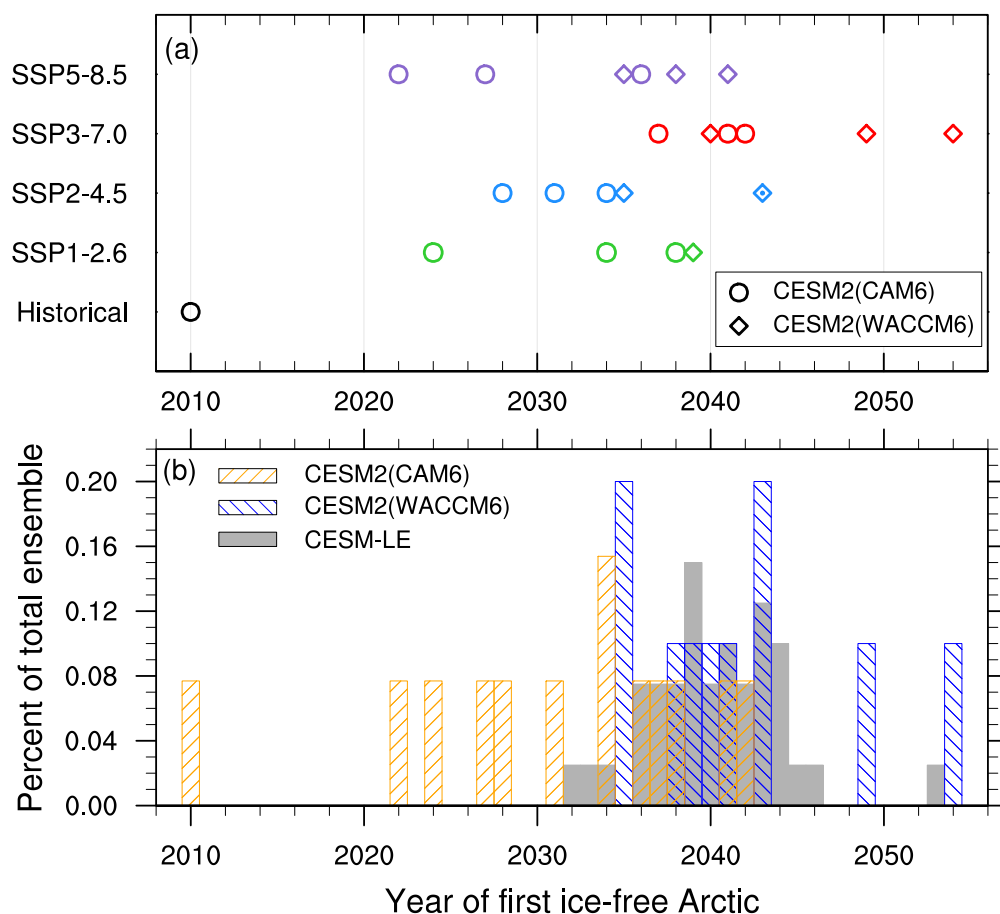


Figure 2.5: **Timing of first ice-free Arctic:** (a) Year of first September ice-free conditions in the CSM2(CAM6) (circles) and the CSM2(WACCM6) (diamonds) over the historical period (black) and the different future simulations (colors). The symbols with a dot in the middle indicate that two ensemble members reach first ice-free conditions in the same year. (b) Percentage of the total number of ensemble members reaching first September ice-free conditions in a given year in the CSM2(CAM6) (orange; total of 13 ensemble members), the CSM2(WACCM6) (blue; total of 10 ensemble members) and the CSM-LE (grey; total of 40 ensemble members). For the CSM2(CAM6) and the CSM2(WACCM6), this is done by combining the historical and all future simulations into one single distribution.

lower mean sea ice state, the CSM2(CAM6) generally reaches ice-free conditions earlier than the CSM2(WACCM6), with the first ice-free year occurring in 2010 for one of the CSM2(CAM6) ensemble members and in 2035 for two CSM2(WACCM6) ensemble members (Figure 2.5b). However, the distributions of years of first September ice-free conditions for both CSM2 configurations overlap with each other, as well as with the range of the CSM-LE. The internal variability uncertainty on the year of first September ice-free conditions spans 32 and 19 years for the

CESM2(CAM6) and the CESM2(WACCM6) ensembles, respectively, compared to 21 years of internal variability prediction uncertainty for the CESM-LE (Figure 2.5b; see also Jahn et al., 2016).

Despite seeing no impact of the choice of CMIP6 future emissions scenario on the first year of an ice-free Arctic, we still find a relatively low probability of a September ice-free Arctic in a given year in the CESM2 if global warming is limited to 1.5°C rather than 2.0°C (Figure 2.6b), in agreement with previous studies (Jahn, 2018; Sanderson et al., 2017; Sigmond et al., 2018). In the CESM2(CAM6), the probability of September ice-free conditions in a given year for an annual mean global temperature anomaly of 1.5°C is 6.1%, compared to 0% in the CESM2(WACCM6) and the CESM-LE (Figure 2.6b). For a global warming of 2.0°C, the probability of ice-free conditions in a given year increases to 83% in the CESM2(CAM6), compared to 7.0% in the CESM2(WACCM6) and 22% in the CESM-LE. These ice-free probabilities for 2.0°C of warming in the two CESM2 configurations bracket the probabilities found in previous studies for warming limited to 2.0°C, which vary between 16% and 34% (Jahn, 2018; Sanderson et al., 2017; Sigmond et al., 2018). All model simulations predict a nearly 100% chance of September ice-free conditions in a given year for 3.0°C of global warming (Figure 2.6b), similar to the probability of 90–100% found by Sigmond et al. (2018) using indirectly constrained 3°C stabilized warming simulations. The higher probabilities of ice-free conditions in the CESM2(CAM6) can be explained by generally lower September sea ice extent for any 5-year annual mean global temperature anomaly in this configuration compared to all other model simulations analyzed here (Figure 2.6a), a result of the lower winter ice thickness at the end of the historical period (see Figure 2.4a–c and section 2.3.2).

Note that here we calculate the probability of ice-free conditions in September for 5-year annual mean global temperature anomalies within  $\pm 0.1^\circ\text{C}$  of different levels of warming using every year of the historical and future simulations. This method differs from previous studies (Jahn, 2018; Sanderson et al., 2017; Screen and Williamson, 2017; Sigmond et al., 2018), which themselves all differ in their methodology. To quantify the effect of the method choice on the probabilities found, we apply our methodology to the same set of CESM1.1 stabilization experiments previously used in Jahn (2018) and Sanderson et al. (2017). We find that the probabilities are comparable but slightly

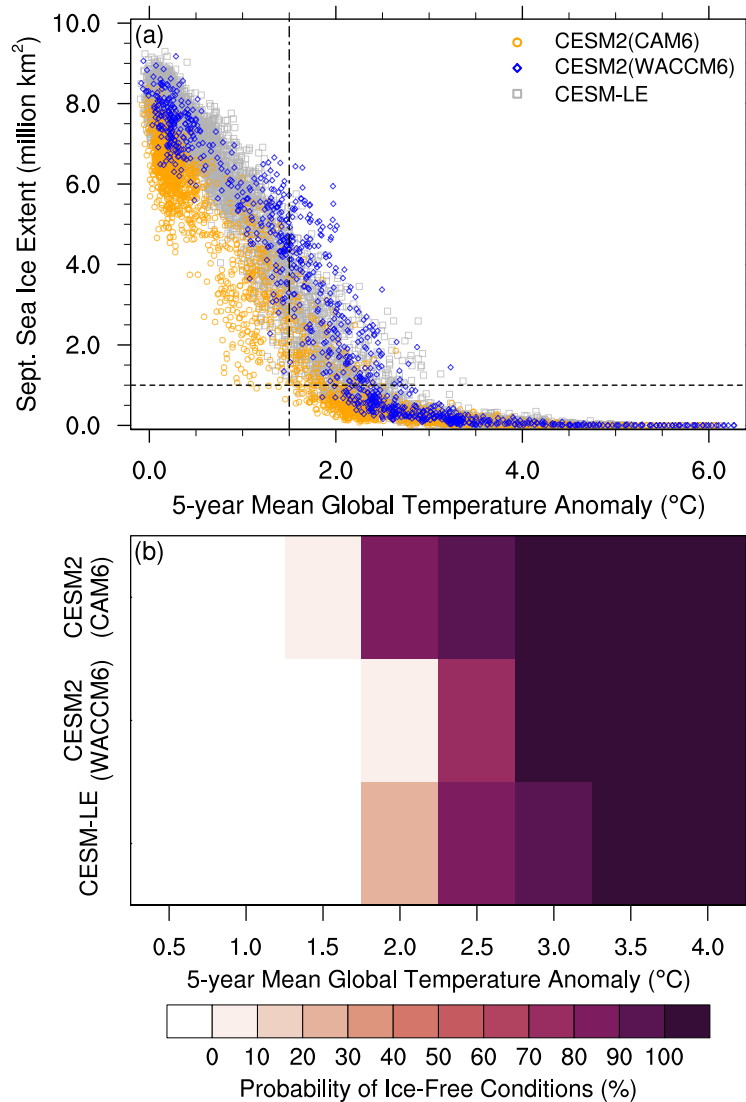


Figure 2.6: **Ice-free Arctic as a function of global warming:** (a) September sea ice extent as a function of 5-year annual mean global temperature anomaly in the CESM2(CAM6) (orange circles), the CESM2(WACCM6) (blue diamonds) and the CESM-LE (grey squares) over the historical period and the different future simulations. The horizontal dashed line indicates ice-free conditions of 1 million km<sup>2</sup> and the vertical dash-dotted line indicates 1.5°C of global warming. (b) Probability of September ice-free conditions for different values of 5-year annual mean global temperature anomaly in the CESM2(CAM6) (top), the CESM2(WACCM6) (middle) and the CESM-LE (bottom). The probability is calculated for temperature anomalies within  $\pm 0.1^\circ\text{C}$  of each target level of warming. All temperatures shown here use the 2-meter air temperature variable output, and temperature anomalies are calculated with respect to each ensemble member's 1850–1920 average.

lower when using our method: 0.7% versus 2.5% for 1.5°C of warming and 30% versus 34% for 2.0°C of warming. Furthermore, we find that our method yields comparable though slightly lower ice-free

probabilities in a given year for transient versus stabilization simulations using the same model (the CESM1.1): 0% versus 0.7% for 1.5°C of warming and 22% versus 30% for 2.0°C of warming, respectively. This is consistent with the expectation that transient simulations likely underestimate the true probability of ice-free conditions for a climate around a specific value of global warming, due to an inadequate sampling of internal variability (Jahn, 2018; Screen, 2018; Sigmond et al., 2018) and the potential impact of a delayed oceanic response to atmospheric warming on sea ice (Gillett et al., 2011; Sigmond et al., 2018). At the same time, these comparisons show that our method to assess ice-free conditions provides probabilities within 10% of previously used methods and between transient and stabilization experiments. As such, our method may be a useful technique to assess ice-free probabilities in a given year in transient simulations, in particular in the absence of stabilization experiments.

When using sea ice area rather than extent to define ice-free conditions (as done in SIMIP Community, 2020), the 1 million km<sup>2</sup> threshold is crossed earlier. As a result, the probabilities of ice-free conditions in a given year using sea ice area are about twice what we show here for a warming up to 2.0°C, with smaller differences between an extent-based and area-based threshold as the probabilities increase for larger warming. Hence, despite differences in methodology, the CESM2 results are overall consistent with previous studies that showed that by limiting global warming to 1.5°C, the probability of Arctic ice-free conditions in a given year is low, increases for a warming of 2.0°C, and can be expected every year for warming of 3.0°C or more (Jahn, 2018; Sigmond et al., 2018).

## 2.5 Accelerated Decline in Winter and Spring Ice Cover

Toward the end of the 21<sup>st</sup> century, both CESM2 configurations simulate an accelerated decline in sea ice area during the winter and spring months (Figure 2.7). This winter and spring ice loss is not seen in the previous version of the CESM, and results in monthly ice area values that fall significantly below the range of internal variability of the CESM-LE (Figure 2.7). Both CESM2 configurations even simulate ice-free conditions for up to eight months per year by 2100,

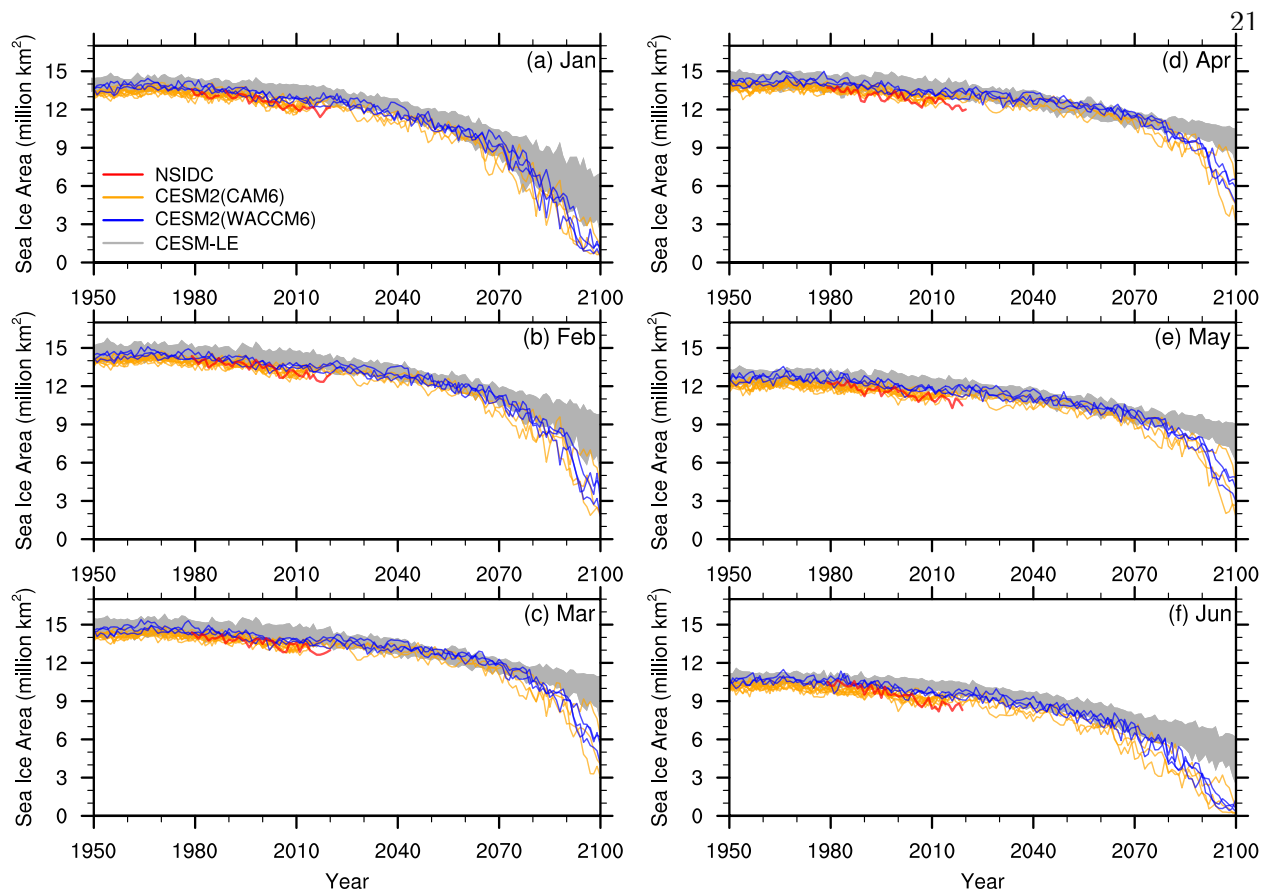


Figure 2.7: Time evolution of Arctic sea ice area from January to June (a–f) in the observations (red), the CESM2(CAM6) (orange), the CESM2(WACCM6) (blue) and the CESM-LE (grey).

with only the months of February to May showing a pan-Arctic ice extent larger than 1 million  $\text{km}^2$  (not shown) compared to a maximum of five months of ice-free conditions for the CESM-LE (Jahn, 2018). Some other CMIP6 models show a similar acceleration of the March sea ice area decline over the last 20–30 years of the 21<sup>st</sup> century (see Figure 2c of SIMIP Community, 2020). The retreat of March ice area originates in the Chukchi Sea in the 2070s in the CESM2(CAM6) and the 2080s in the CESM2(WACCM6), leaving a large portion of the Pacific sector of the Arctic ice free by the 2090s (Figure 2.8a–f). The CESM-LE only starts to show a similar winter ice loss in the Chukchi Sea at the end of the century, lagging the CESM2(CAM6) by two decades and the CESM2(WACCM6) by one decade (Figure 2.8g–i). This lag between the different model versions is consistent with a similarly delayed response of winter ice thickness over the historical period

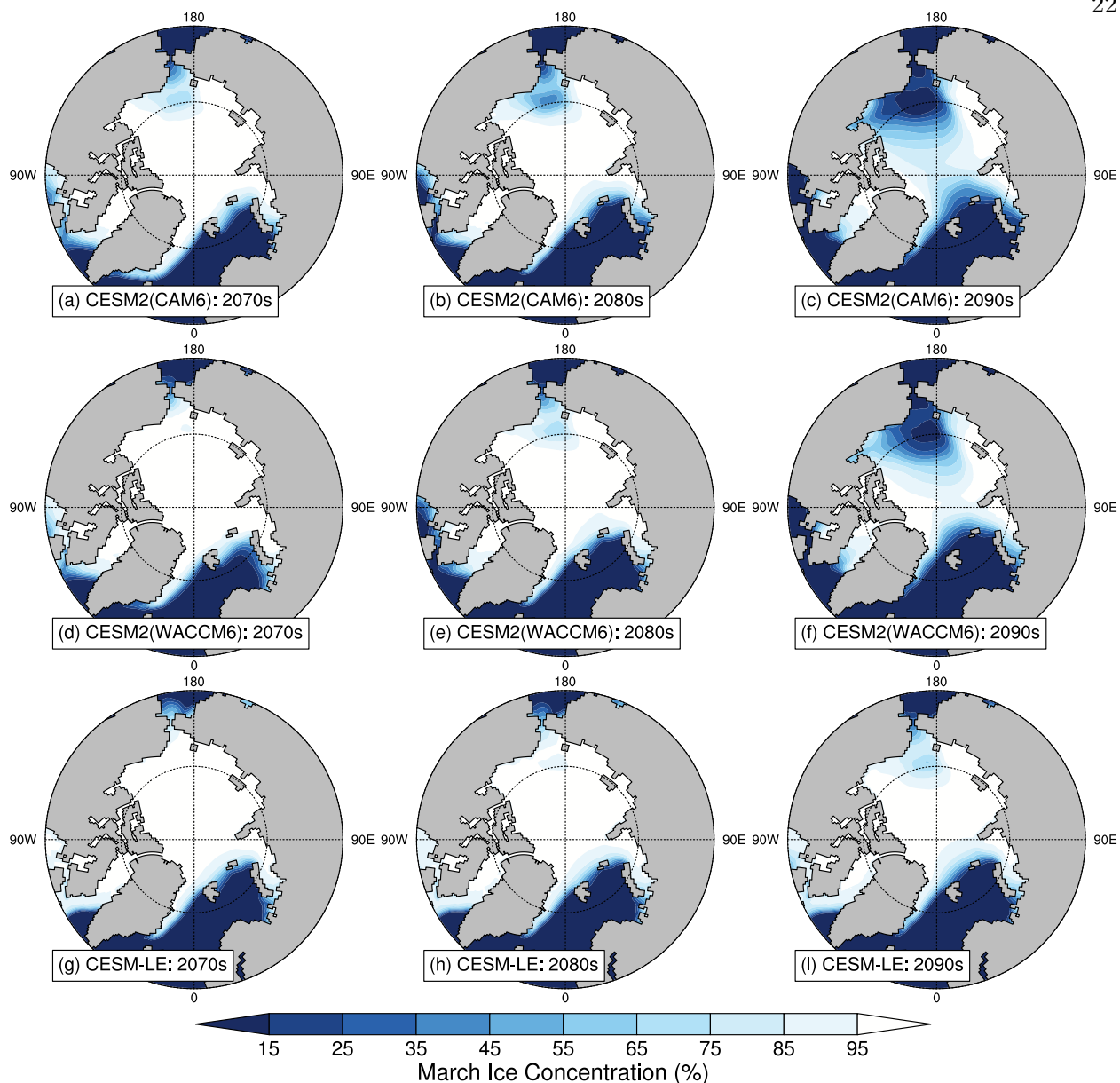


Figure 2.8: Ensemble mean, decadal mean March ice concentration during the 2070s (left), 2080s (center) and 2090s (right) in the CESM2(CAM6) (top), the CESM2(WACCM6) (middle) and the CESM-LE (bottom).

(Figure 2.4).

The discrepancies in the time evolution of winter and spring ice area between the two CESM versions (Figure 2.7) arise as the CESM2 reaches a very different climate at the end of the 21<sup>st</sup> century compared to the CESM-LE. Despite the same top-of-atmosphere radiative forcing in the

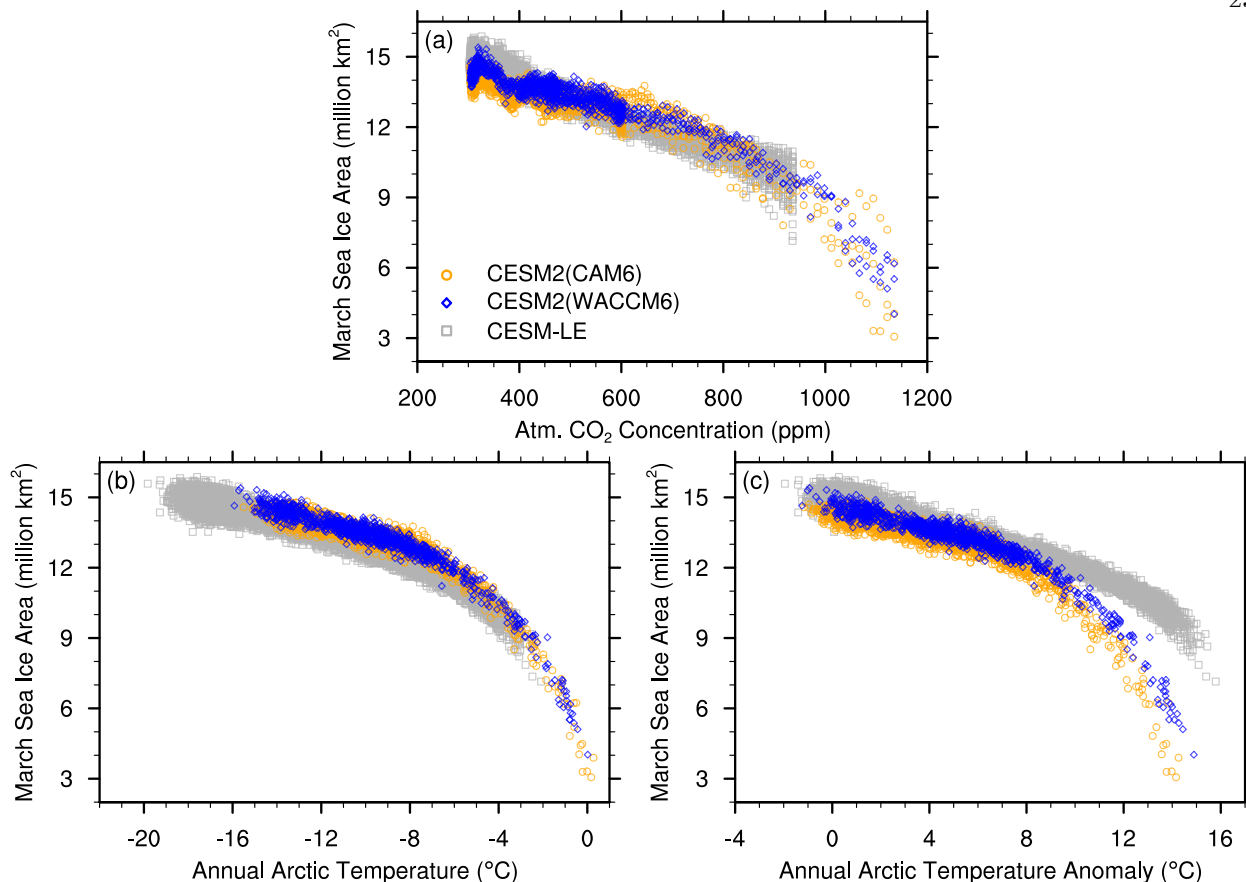


Figure 2.9: March sea ice area as a function of (a) annual global atmospheric CO<sub>2</sub> concentration, (b) annual Arctic temperature and (c) annual Arctic temperature anomaly over the historical period and the different future simulations for the CESM2(CAM6) (orange circles), the CESM2(WACCM6) (blue diamonds) and the CESM-LE (grey squares). Arctic temperatures are calculated over the region north of 70°N, and temperature anomalies are calculated with respect to each ensemble member’s 1850–1920 average. All temperatures shown here use the 2-meter air temperature variable output.

SSP5-8.5 and RCP8.5 scenarios in 2100, the SSP5-8.5-forced CESM2 simulates higher annual Arctic (and global) temperatures by 2100 compared to the RCP8.5-forced CESM-LE (Figure 2.9b). These higher temperatures are likely a result of the higher ECS in the CESM2 compared to the CESM-LE (Gettelman et al., 2019a; Meehl et al., 2020) and differences in the applied forcing. When considering the evolution of March ice area as a function of CO<sub>2</sub> concentration, the CESM2 largely falls within the range of internal variability of the CESM-LE (Figure 2.9a). Similar results are found for the evolution of March sea ice area as a function of annual Arctic temperatures (Figure

2.9b). However, toward the end of the CESM-LE simulations (i.e., around  $\text{CO}_2$  concentrations of 900 ppm and annual mean Arctic temperatures of  $-4^\circ\text{C}$ ), the approximately linear relationship between March sea ice area and atmospheric  $\text{CO}_2$  and Arctic temperatures breaks down as the CESM2 reaches a considerably warmer climate than the CESM-LE (Figure 2.9a, b). This points to a non-linear behavior of the winter Arctic sea ice area that was not sampled in the CESM-LE. Due to the differences in greenhouse gas trajectories and climate sensitivities between CMIP5 and CMIP6, comparing simulated sea ice properties as a function of  $\text{CO}_2$  concentration or temperature rather than time is found to be a more appropriate way to assess differences in sea ice evolution. However, care should be taken when comparing model versions with different climate base states in terms of temperature anomalies rather than absolute temperatures. We find that while the evolution of March sea ice area as a function of Arctic temperature is consistent across the three CESM simulations (Figure 2.9b), it is not consistent when assessed in terms of Arctic temperature anomalies (Figure 2.9c). The evolution of March sea ice area as a function of annual Arctic temperature anomalies generally only overlaps with the lower end of the range of the CESM-LE, which means that the CESM2 simulates a less extensive winter ice cover for the same annual Arctic temperature anomaly (Figure 2.9c). This is due to the fact that the annual Arctic mean temperature of the reference period 1850–1920 used to calculate temperature anomalies is higher by about  $3^\circ\text{C}$  in the CESM2 compared to the CESM-LE (McIlhatten et al., 2020). As such, a smaller temperature anomaly in the CESM2 compared to the CESM-LE for the same March ice area does not correspond to a smaller absolute temperature in the CESM2 if the difference between the two temperature anomalies is smaller than the difference between the mean temperatures of the reference period.

The accelerated decline in winter and spring ice cover in the CESM2 compared to the CESM-LE is driven in large part by changes in ocean heat loss during the preceding fall. As the Arctic goes ice free every summer in all three CESM simulations, differences in winter ice area are related to the amount of ice formed during fall and winter. Before ice formation can commence in the fall, all of the mixed layer heat accumulated over the summer must be released to the atmosphere

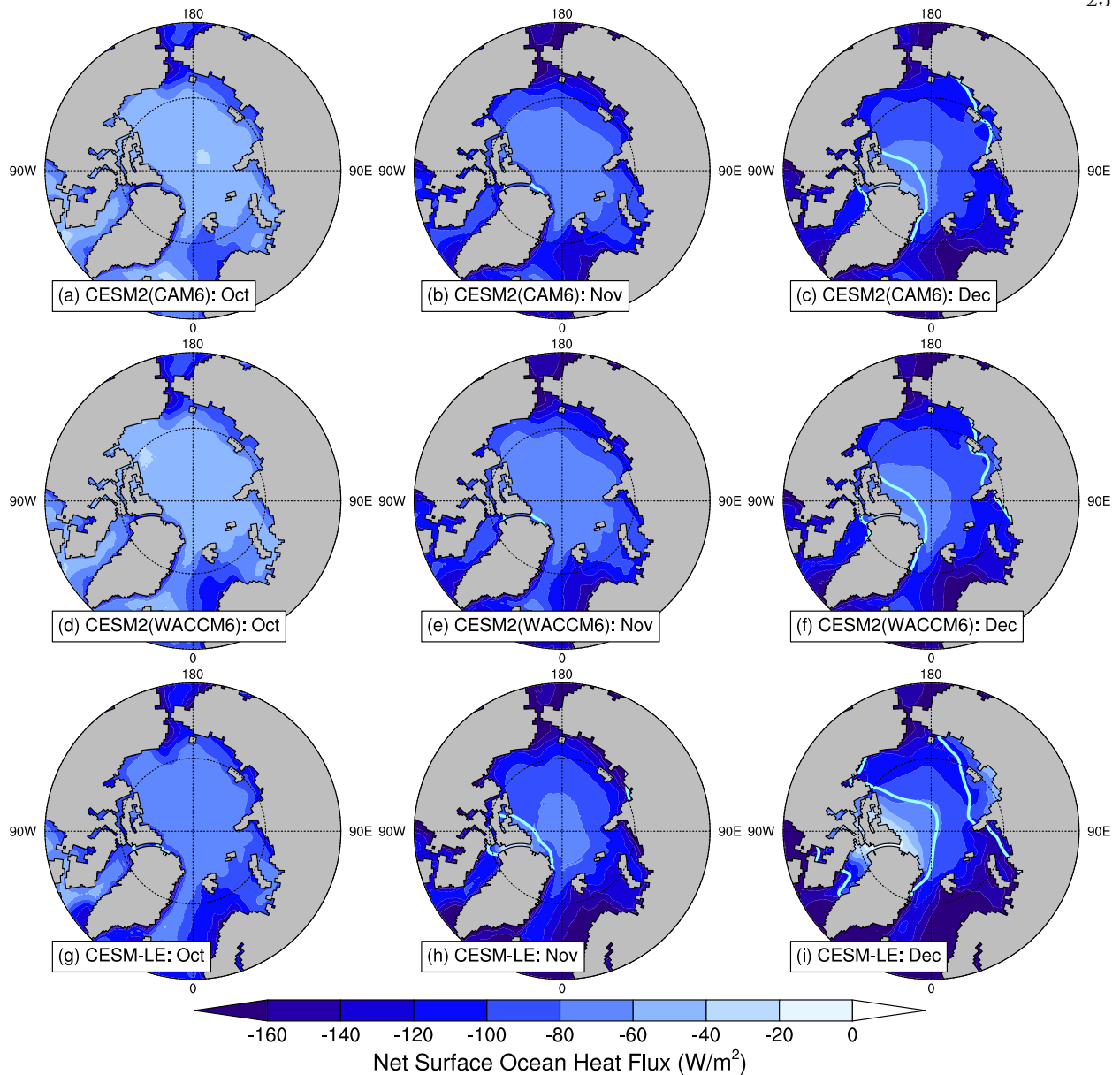


Figure 2.10: Ensemble mean net surface ocean heat flux from 2080 to 2099 for the months of October (left), November (center) and December (right) in the CESM2(CAM6) (top), the CESM2(WACCM6) (middle) and the CESM-LE (bottom). Negative values indicate heat loss from the ocean to the atmosphere. The cyan lines indicate the monthly mean 15% sea ice concentration contour averaged over the same years and all ensemble members. No cyan line in a panel indicates that if there is any sea ice, sea ice concentration is below 15% everywhere.

for the surface temperature of the ocean to drop below the freezing point of seawater. Similar sea surface temperatures at the sea ice minimum (Figure S2.1a, e, i) and no significant differences in volume and heat transports through the Bering Strait between the CESM2 and the CESM-LE in

the late 21<sup>st</sup> century (not shown) suggest that the mixed layer heat accumulated over the summer is similar across the simulations. Hence, differences in ice formation result mainly from differences in the rate of oceanic heat loss in the fall. Indeed, we find that the ocean loses less heat to the atmosphere during the fall months in the CESM2 compared to the CESM-LE over the last two decades of the 21<sup>st</sup> century (Figure 2.10), preventing the formation of sea ice in the CESM2 by keeping most of the Arctic Ocean at temperatures above freezing (Figure S2.1). The reduced ocean heat loss in CESM2 is related to warmer Arctic air temperatures and a reduced air-sea temperature difference relative to the CESM-LE (Figure 2.9b).

As a result of the late 21<sup>st</sup> century reduction in winter and spring ice area in the CESM2, the pan-Arctic open-water period is about one to two months longer than in the CESM-LE (Figure 2.11). Compared to monthly mean sea ice area, the open-water period is a more practical metric for stakeholders who rely on predicted ice-free conditions (Barnhart et al., 2016; Parkinson, 2014). The open-water period is defined as the total number of days at each grid point between March 1st and February 28th of the next year when sea ice is not present, using a 15% sea ice concentration threshold to define the presence or absence of sea ice (Bliss et al., 2019). Over most of the Arctic basin, the CESM2 open-water period varies between 200 and 365 days in the 2090s (Figure 2.11c, f), in contrast to an open-water period of 140 to 240 days in the CESM-LE for the same period (Figure 2.11i). A later sea ice freeze-up in the CESM2 is found to contribute more to the overall lengthening of the open-water period than an earlier sea ice break-up (Figures S2.2 and S2.3), consistent with previous work (Wang et al., 2018) and with the reduced ocean heat loss found during the fall (Figure 2.10). Indeed, sea ice break-up occurs about 15 days earlier across the whole Arctic basin in the CESM2 compared to the CESM-LE over the last three decades of the 21<sup>st</sup> century (Figure S2.2), whereas sea ice freeze-up occurs up to one month later (Figure S2.3). Such a lengthening of the open-water period would have a tremendous impact on the Arctic climate system, from changes in regional oceanic heat budgets to modification of the timing of phytoplankton blooms and a shortening of the primary hunting season of large animals such as walruses, seals and polar bears (Fernández-Méndez et al., 2015; Moore and Huntington, 2008; Perovich et al., 2007; Post

et al., 2013; Stroeve et al., 2014b).

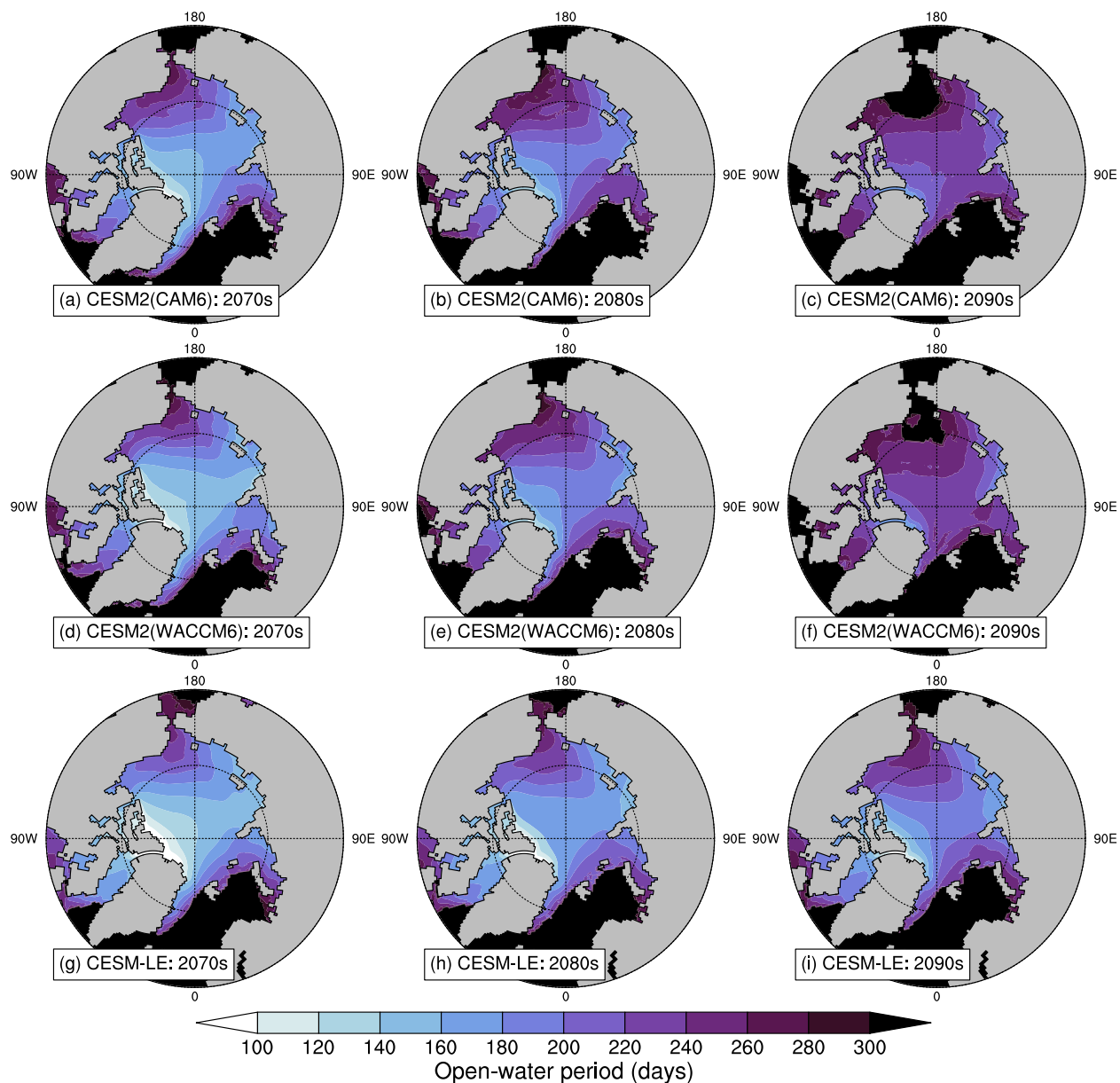


Figure 2.11: Ensemble mean, decadal mean length of the open-water period during the 2070s (left), 2080s (center) and 2090s (right) in the CESM2(CAM6) (top), the CESM2(WACCM6) (middle) and the CESM-LE (bottom).

## 2.6 Sea Ice Trends at the Historical-Scenario Transition

Around the transition between historical and future simulations, we find that the 20-year linear trends in September sea ice area in the CESM2 change abruptly from strongly negative to zero or even slightly positive (Figure 2.12; end years 2010–2025). This behavior is present in all ensemble members of both the CESM2(CAM6) and the CESM2(WACCM6) and across all future emissions scenarios (Figure 2.12), but not in the CESM-LE (Figure 2.12d, h). It also appears in all months of the year, although it is most pronounced in the months surrounding the sea ice minimum (August–October) when negative trends are largest (not shown). September sea ice volume trends also show a similar pattern as sea ice area (Figure S2.4). This implies that the Arctic sea ice cover is also not thinning over this period, in addition to no loss in ice area. The cause of the reduced negative trends in ice area and volume is currently unknown and requires further work beyond the scope of this paper. Nevertheless, it is important to highlight this feature of the CESM2 simulations here, as it may impact other aspects of the Arctic and global climate in the CESM2. While we do not currently know the cause of this pattern, we have been able to rule out a few possible explanations.

Although natural climate variability can cause positive 20-year trends in Arctic sea ice (Kay et al., 2011), we find that the change in the CESM2 trends is likely not the result of internal variability, given that all ensemble members from all CMIP6 scenarios show such a pattern (Figure 2.12). We have also ruled out a number of forcings as the cause of the pattern in the trends. In particular, we calculated the same 20-year linear trends in September sea ice area and volume using the AerChemMIP hist-piNTCF (Danabasoglu, 2019g), hist-1950HC (Danabasoglu, 2019f) and SSP3-7.0-lowNTCF (Danabasoglu, 2019h) simulations and found similar results (Figures 2.12g and S2.4g). The AerChemMIP simulations use WACCM6 as their atmospheric component and are meant to quantify the effect of chemistry and aerosols in CMIP6 (as described in Collins et al., 2017). The hist-piNTCF simulation covers the historical period 1850–2014, with emissions of near-term climate forcings (NTCFs: methane, tropospheric ozone and aerosols, and their precursors)

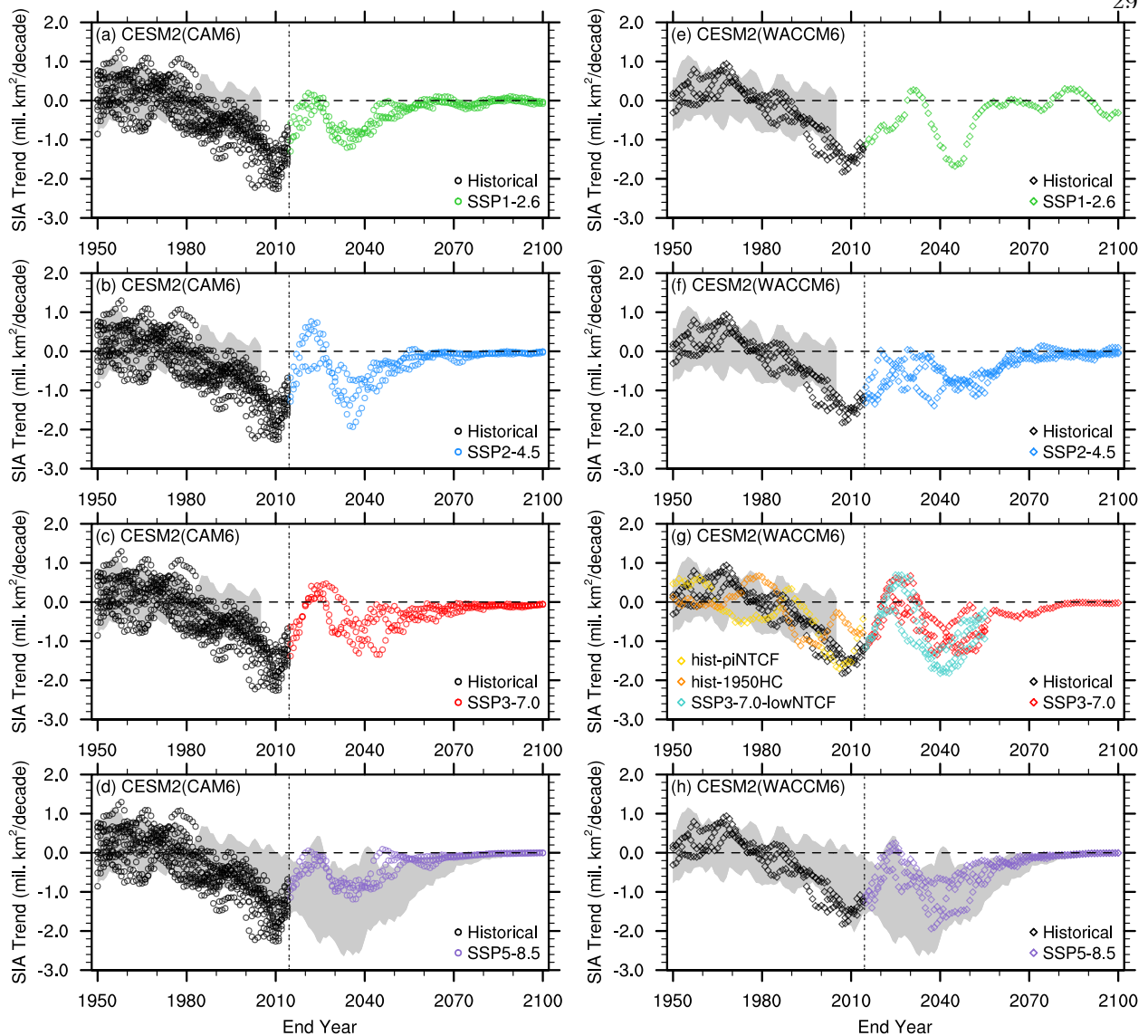


Figure 2.12: 20-year linear trends in September ice area in the CESM2(CAM6) (a–d) and the CESM2(WACCM6) (e–h) under the historical forcing (black) and different future emissions scenarios (colors). (g) also includes 20-year linear trends in September ice area in three AerChemMIP experiments (Collins et al., 2017). The range of trends in September ice area across all ensemble members of the CESM-LE (grey shading) is shown for the historical period in all panels and additionally for the RCP8.5 scenario in (d) and (h). Values on the x-axis represent the end year of the 20-year period over which linear trends are calculated. The horizontal dashed lines indicate no trend, and the vertical double-dashed lines indicate the transition year between historical and future simulations in the CESM2.

fixed at pre-industrial levels at the start of the simulation. The hist-1950HC simulation also covers the historical period 1850–2014 and branches from the CMIP6 historical simulation at year 1950

with chlorofluorocarbon (CFC) and hydrochlorofluorocarbon (HCFC) concentrations fixed at 1950 conditions, resulting in a 20<sup>th</sup> century climate without an ozone hole. The two AerChemMIP historical simulations show a stabilization of the trends in ice area toward the end of the historical period, similar to the CESM2(WACCM6) historical simulations (Figure 2.12g). Therefore, these particular forcings are likely not the cause for the stabilization of the trends in ice area at the end of the historical period. The SSP3-7.0-lowNTCF simulations start at the end of the historical simulations and are branched from the three CESM2(WACCM6) historical ensemble members. They are run for 41 years following the SSP3-7.0-lowNTCF scenario, a version of the SSP3-7.0 scenario with cleaner air quality policies. All three ensemble members show a similar behavior during the first 10-15 years of the future simulations as the three CESM2(WACCM6) SSP3-7.0 ensemble members (Figure 2.12g), indicating that the specific aerosol and ozone precursors that are kept at a “clean” level are likely not the cause of the change in trends either. Finally, given that the anthropogenic and biomass burning secondary organic aerosol emissions were set to zero from 2015 onward in the initial CESM2(CAM6) future scenario simulations (see section 2.2.1 for more details) and that these simulations also showed this trend behavior (not shown), the anthropogenic and biomass burning secondary organic aerosol emissions can also be ruled out as a possible explanation for this pattern in the trends.

## 2.7 Conclusions

In this contribution, we presented an analysis of some key metrics of the historical and future simulations from two configurations of the CESM2 compared to its previous version, the CESM-LE, as well as observations. We found that the winter ice thickness distribution of the CESM2(CAM6) configuration is biased thin over the historical period, which leads to lower September sea ice area compared to the CESM2(WACCM6), the CESM-LE and observations. As a result, the CESM2(CAM6) generally reaches first September ice-free conditions earlier than the CESM2(WACCM6) and the CESM-LE. The timing of first September ice-free conditions in the Arctic is found to be insensitive to the choice of CMIP6 future emissions scenario in both CESM2

configurations. Instead, the first year of an ice-free September is determined by internal variability, with the CESM2 showing a two to three decade uncertainty range, similar to the two decades found in the CESM-LE (Jahn et al., 2016). Regarding the response of Arctic sea ice to global warming, the CESM2 simulates a low probability of ice-free conditions in September if warming is limited to 1.5°C but increases for any additional warming, consistent with previous studies (Jahn, 2018; Sanderson et al., 2017; Screen and Williamson, 2017; Sigmond et al., 2018). By the late 21<sup>st</sup> century, the CESM2 exhibits an accelerated decline in winter and spring ice area that was not sampled in the CESM-LE simulations. However, when looking at the evolution of March ice area as a function of atmospheric CO<sub>2</sub> or Arctic temperature rather than time, the two versions of the CESM model are consistent and the differences in their time evolution arise as the CESM2 reaches higher CO<sub>2</sub> concentrations and Arctic temperatures than those in the CESM-LE. Our results suggest that reaching CO<sub>2</sub> concentration higher than 900 ppm and annual mean Arctic temperatures higher than -4°C could lead to an accelerated loss of winter and spring sea ice in the Arctic. The different simulated climate by 2100 between the CESM1 simulations with CMIP5 forcing versus the CESM2 simulations with CMIP6 forcing results in less ocean heat loss during the fall months in the CESM2. This strongly delays the formation of sea ice by keeping the surface temperature of the ocean above freezing point longer and leads to ice-free conditions for up to eight months of the year in the CESM2 and an open-water period more than 30 days longer than in the CESM-LE. It is important to note that the evolution of March ice area is not as consistent between the CESM-LE and the CESM2 when analyzed as a function of temperature anomalies rather than temperatures due to differences in the mean global temperature of the reference period (McIlhattan et al., 2020). This highlights the need for caution when comparing model versions in terms of temperature anomalies, something that is widely done when analyzing the potential impacts of global warming.

We also document a large reduction in the simulated 20-year linear trends in September ice conditions, indicating less rapid ice loss and thinning, around the transition between historical and future simulations. This feature is consistent across both CESM2 configurations, all ensemble members, all future scenarios considered here, and is also present in all months of the year. Based on

preliminary analysis in section 2.6, we have ruled out the following explanations for this behavior: internal variability, NTCFs and their precursors, CFCs and HCFCs as well as anthropogenic and biomass burning secondary organic aerosol emissions. More analysis is needed to understand the causes and implications of this pattern in the Arctic sea ice trends.

To conclude, our analysis provides the first overview of the major features of the evolution of Arctic sea ice in the CESM2 over the 20<sup>th</sup> and 21<sup>st</sup> centuries. Overall, the CESM2 reasonably simulates the important properties of Arctic sea ice, with CESM2(WACCM6) generally performing better than CESM2(CAM6) over the historical period. Differences in the simulated sea ice between the two CESM2 configurations, and differences compared to the previous version (CESM-LE), are important to consider when analyzing other aspects of these new CMIP6 simulations, in particular in the Arctic. An important bias to keep in mind for future work involving the CESM2 is the lower-than-observed mean state of Arctic sea ice in the CESM2(CAM6) during the historical period, which results in simulated September ice-free conditions as early as 2010. Biased simulations of present-day sea ice properties, especially Arctic sea ice volume, have been shown to bias future projections of summer sea ice conditions (Massonnet et al., 2018). This suggests that the CESM2(WACCM6), with its present-day Arctic sea ice mean state closer to observations, is the more appropriate CESM2 configuration contributed to CMIP6 to use for in-depth studies of future sea ice changes in the Arctic.

## 2.8 Acknowledgements

P. DeRepentigny is supported by the Natural Sciences and Engineering Council of Canada (NSERC), the Fonds de recherche du Québec – Nature et Technologies (FRQNT) and the Canadian Meteorological and Oceanographic Society (CMOS) through PhD scholarships and by NSF-OPP award 1847398. A. Jahn’s contribution is supported by NSF-OPP award 1847398. M. Holland is supported by NSF-OPP award 1724748. A. Smith is supported by the Future Investigators in Earth System Science Grant No. 80NSSC19K1324 and NSF-OPP award 1847398.

P. DeRepentigny and A. Jahn designed the study. P. DeRepentigny performed the analysis

and wrote the manuscript under the supervision of A. Jahn. A. Smith contributed the analysis of the open-water period, break-up and freeze-up. M. Holland provided CESM2 specific expertise. All authors provided critical feedback and collaborated in shaping the research, analysis and final version of the manuscript. We thank Hannah Zanowski for valuable feedback on the manuscript. We also thank Jakob Dörr for providing the range of sea ice area across CMIP6 models as well as two anonymous reviewers and the editor for providing constructive feedback on an earlier version of the manuscript.

Previous and current versions of the CESM are freely available at [cesm.ucar.edu/models/?ref=hp](https://cesm.ucar.edu/models/?ref=hp). The CESM2 data analyzed in this study have been contributed to CMIP6 and are freely available from the Earth System Grid Federation (ESGF) at [esgf-node.llnl.gov/search/cmip6/](https://esgf-node.llnl.gov/search/cmip6/), from the NCAR Digital Asset Services Hub (DASH) at [data.ucar.edu](https://data.ucar.edu) and from the links provided on the CESM website at [cesm.ucar.edu/models/cesm2/](https://cesm.ucar.edu/models/cesm2/). Note that we here use the corrected CESM2(CAM6) future scenario simulations, uploaded to the CMIP6 archive in May 2020. The CESM-LE data can be found at [cesm.ucar.edu/projects/community-projects/LENS/](https://cesm.ucar.edu/projects/community-projects/LENS/).

The CESM project is supported primarily by the National Science Foundation (NSF). This material is based upon work supported by the National Center for Atmospheric Research (NCAR), which is a major facility sponsored by the NSF under Cooperative Agreement No. 1852977. Computing and data storage resources, including the Cheyenne supercomputer (doi:10.5065/D6RX99HX), were provided by the Computational and Information Systems Laboratory (CISL) at NCAR. We thank all the scientists, software engineers, and administrators who contributed to the development of CESM2.

## 2.9 Supplementary Material

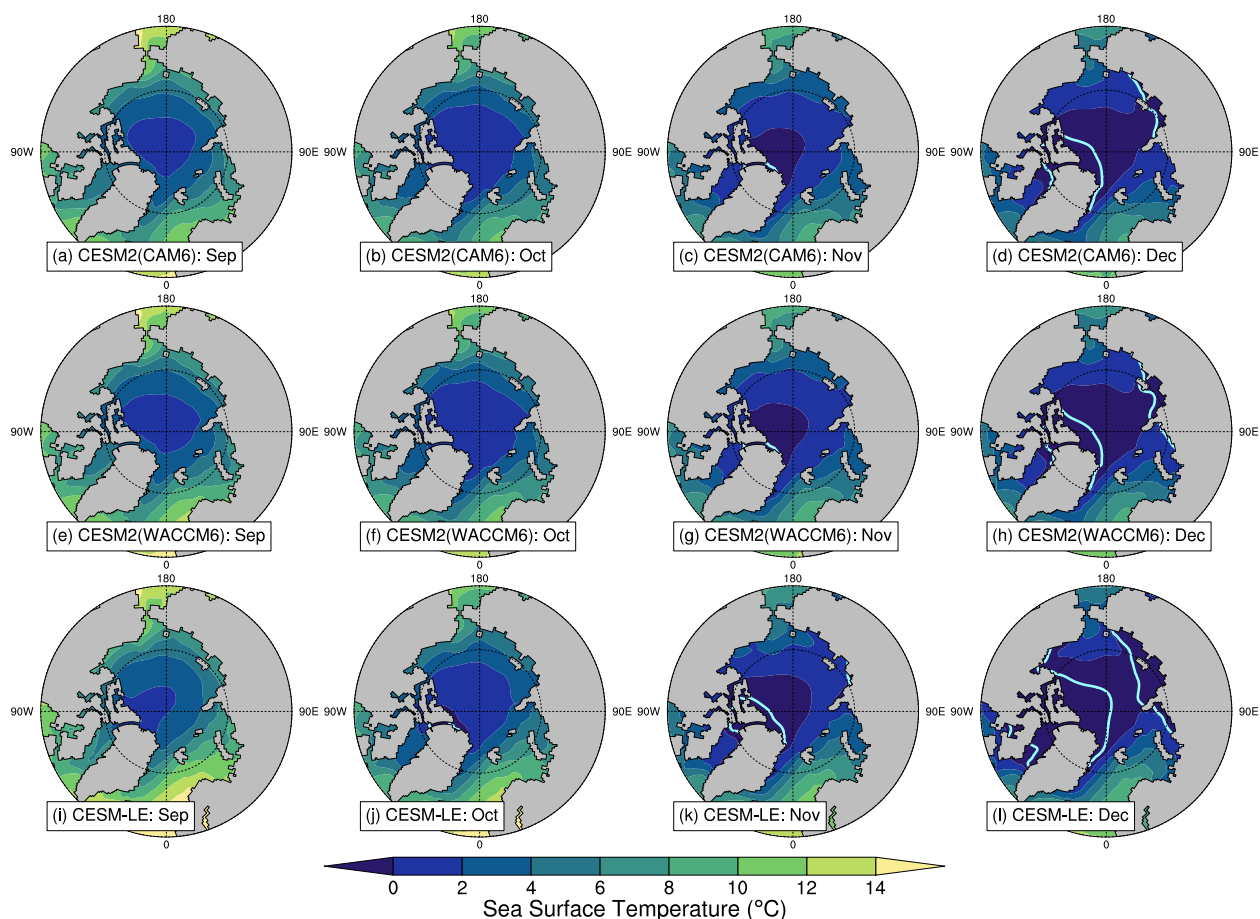


Figure S2.1: Ensemble mean sea surface temperature averaged over 2080 to 2099 for the months of September (a, e, i), October (b, f, j), November (c, g, k) and December (d, h, l) in the CESM2(CAM6) (a–d), the CESM2(WACCM6) (e–h) and the CESM-LE (i–l). The cyan line indicates the monthly mean 15% sea ice concentration contour averaged over the same years and all ensemble members. No cyan line in a panel indicates that if there is any sea ice, sea ice concentration is below 15% everywhere.

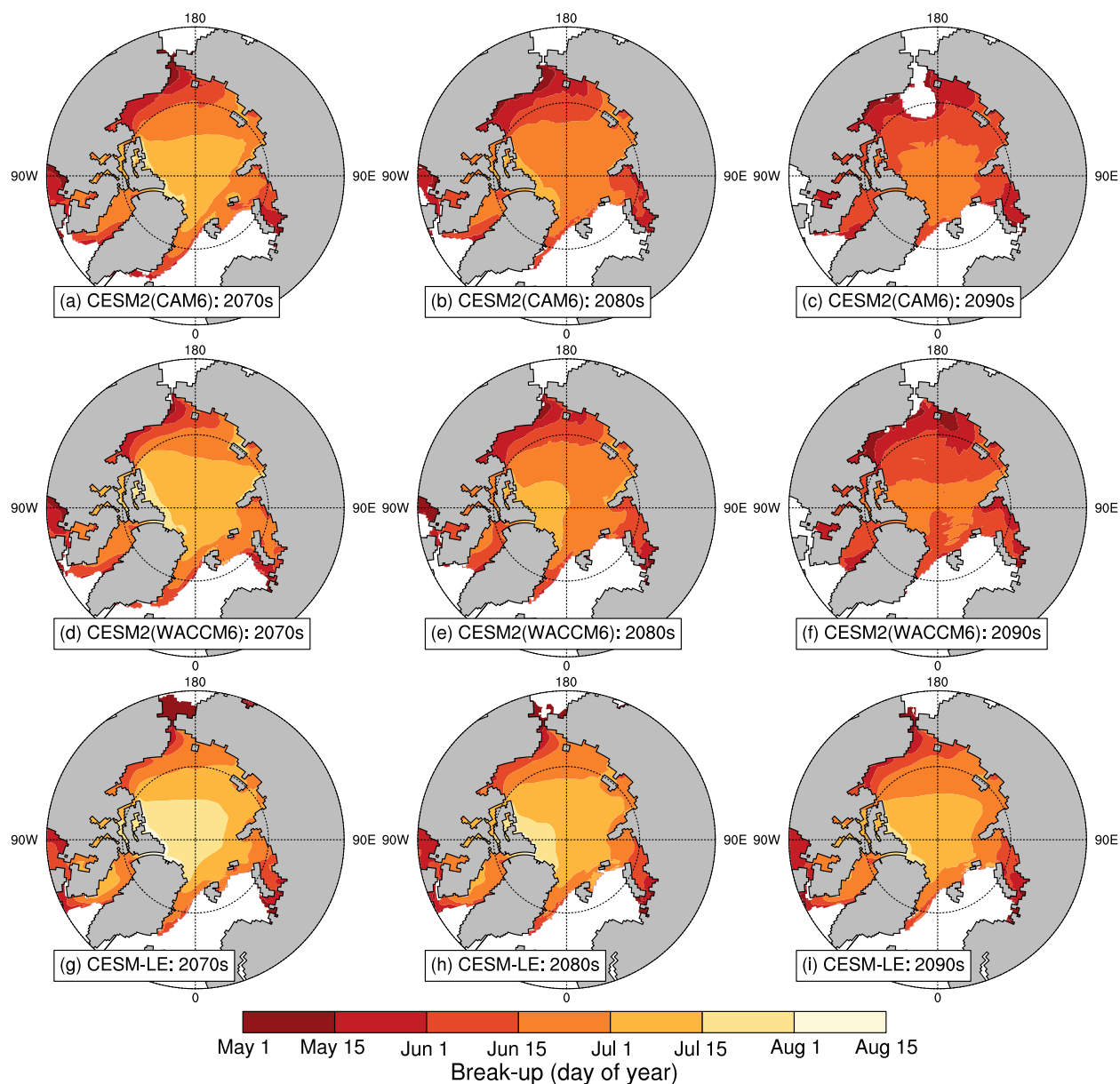


Figure S2.2: Ensemble mean, decadal mean day of the year of sea ice break-up during the 2070s (a, d, g), 2080s (b, e, h) and 2090s (c, f, i) in the CESM2(CAM6) (a–c), the CESM2(WACCM6) (d–f) and the CESM-LE (g–i). Regions of the ocean that are not colored (i.e., white) do not experience break-up because sea ice concentration was already below 15% on March 1st.

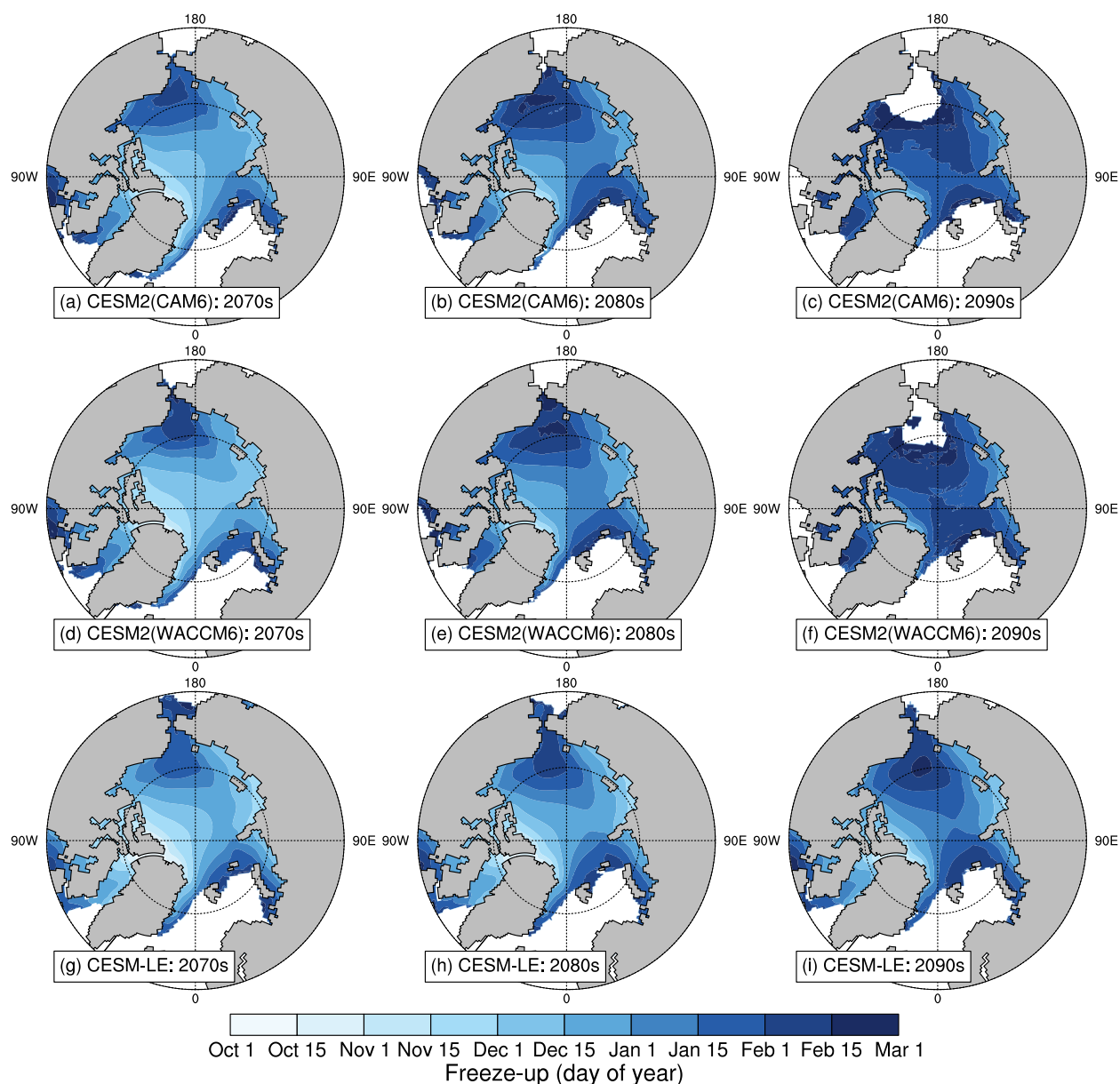


Figure S2.3: Ensemble mean, decadal mean day of the year of sea ice freeze-up during the 2070s (a, d, g), 2080s (b, e, h) and 2090s (c, f, i) in the CESM2(CAM6) (a–c), the CESM2(WACCM6) (d–f) and the CESM-LE (g–i). Regions of the ocean that are not colored (i.e., white) do not experience freeze-up because the sea ice concentration never exceeds 15% before March 1st of the following year.

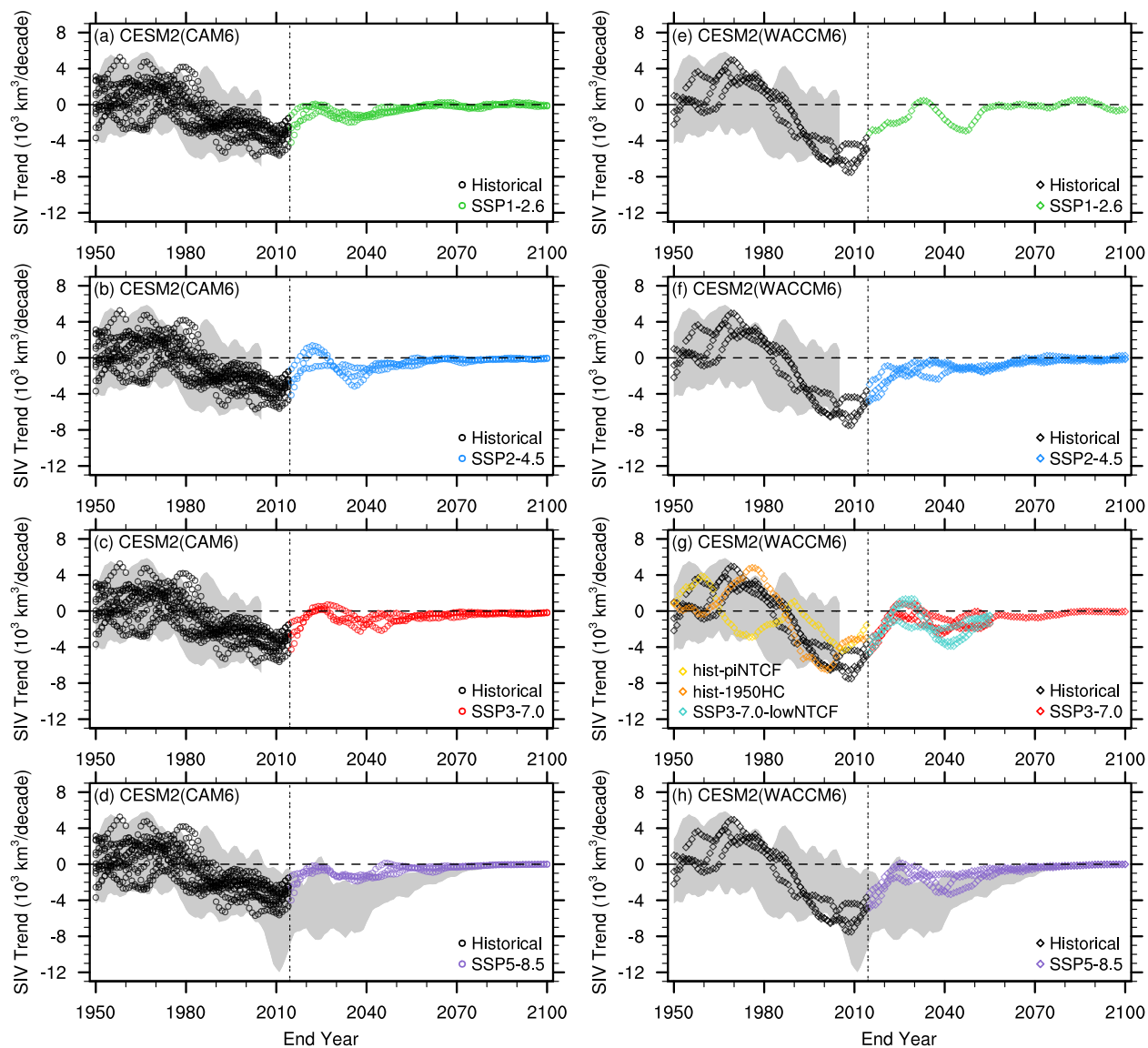


Figure S2.4: As in Figure 2.12, but for September ice volume.

## CHAPTER 3

# ENHANCED EARLY 21<sup>ST</sup> CENTURY ARCTIC SEA ICE LOSS DUE TO CMIP6 BIOMASS BURNING EMISSIONS

### Preface

This chapter is a manuscript being revised for Nature Climate Change (manuscript number: NCLIM-21030586). The authors are P. DeRepentigny, A. Jahn, M. M. Holland, J. E. Kay, J. Fasullo, J.-F. Lamarque, C. Hannay, M. J. Mills, D. A. Bailey, S. Tilmes and A. Barrett.

### Abstract

The mechanisms underlying decadal variability in Arctic sea ice remain an active area of research. Here we show that a strong acceleration in Arctic sea ice decline in the early 21<sup>st</sup> century in the Community Earth System Model version 2 (CESM2) is caused by increased variability in prescribed boreal biomass burning (BB) emissions after 1997 based on new satellite data. Furthermore, we find that the previously reported improvement in sea ice sensitivity to cumulative anthropogenic CO<sub>2</sub> emissions and global warming from CMIP5 to CMIP6 can be attributed in large part to the imposed increased BB emission variability, at least in the CESM. These results highlight the importance of avoiding temporal discontinuities in prescribed aerosol emissions and raise the question of a BB-forced contribution to the observed accelerated early 21<sup>st</sup> century Arctic sea ice loss.

### 3.1 Introduction

Arctic sea ice has experienced drastic reductions in extent, thickness and volume in recent decades, making it one of the most striking manifestations of anthropogenic climate change. Sea

ice loss has been observed during all months of the year (Stroeve and Notz, 2018), but particularly striking is the loss of late-summer sea ice, with reductions in September ice extent and thickness since 1979 of roughly 45% and 66%, respectively (Kwok, 2018; Stroeve and Notz, 2018). The September sea ice extent loss was largest in the early 21<sup>st</sup> century, reaching  $-13.3\%$  per decade over the 14-year period of 1993–2006 (Perovich et al., 2020). In contrast, the last 14 years have seen a slowdown of the rate of sea ice decline (Baxter et al., 2019), with the 2007–2020 sea ice loss trend decreasing to  $-4.0\%$  per decade (Perovich et al., 2020).

The fact that internal climate variability can produce periods of up to two decades featuring enhanced or negligible sea ice loss in the 21<sup>st</sup> century is well documented in the scientific literature (Holland et al., 2006; Kay et al., 2011; Day et al., 2012; Swart et al., 2015). It is thus possible that the current period of reduced September sea ice trends is due solely to internal climate variability masking the anthropogenically-induced decline (Swart et al., 2015). For example, recent work suggested that the inter-decadal variability of Arctic atmospheric circulation related to teleconnections from the eastern-central tropical Pacific contributed to abrupt warming and Arctic sea ice loss from 2007 to 2012, followed by a much slower decline in recent years (Baxter et al., 2019). However, it is also possible that there is a previously unidentified forced contribution to the observed changes in sea ice loss trends. For example, recent model-based analysis has raised the possibility that Arctic warming and sea ice loss in the second half of the 20<sup>th</sup> century has been enhanced by emissions of ozone depleting substances (Polvani et al., 2020). Here we show that increased inter-annual variability in prescribed CMIP6 biomass burning (BB) emissions after 1997 leads to an acceleration of simulated early 21<sup>st</sup> century Arctic sea ice loss in the CESM2 Large Ensemble (CESM2-LE; Danabasoglu et al., 2020; Rodgers et al., 2021). We identify this link by performing sensitivity experiments that remove the increased BB variability from the CMIP6 historical forcing while conserving the total integrated amount of BB emissions from 1997–2014. We further show how this affects simulated sea ice sensitivities in the CESM, before discussing how the BB-forced simulated sea ice loss acceleration compares to the observed evolution of Arctic sea ice.

## 3.2 Results

### 3.2.1 Accelerated sea ice loss in the CESM2-LE compared to the CESM1-LE

Internal variability has been shown to have a large impact on Arctic sea ice evolution (Kay et al., 2011; Notz, 2015; Swart et al., 2015; Jahn et al., 2016; England et al., 2019) and can lead to large differences between individual model simulations from the same model. Hence, in order to isolate forced contributions to the Arctic sea ice evolution, we primarily focus on ensemble means (see section 3.5.2 for more details), which reflect the model response to external forcing.

The evolution of Arctic sea ice area in September throughout the 20<sup>th</sup> and 21<sup>st</sup> centuries differs greatly between the CMIP5-forced version of the CESM, the CESM1-LE (Kay et al., 2015), and the CMIP6-forced version, the CESM2-LE (Rodgers et al., 2021, Figure 3.1a). Even before the start of the decline in Arctic sea ice in the later part of the 20<sup>th</sup> century, the two CESM simulations have a large mean state difference, with the CESM1-LE simulating a thicker and more extensive sea ice cover compared to the CESM2-LE (DeRepentigny et al., 2020). In addition to this mean state difference, there is a statistically significant difference in the rate of Arctic sea ice loss starting in the mid-1990s (Figure 3.1b, c). The CESM1-LE September sea ice area anomaly and trend get gradually more negative with time until the Arctic reaches ice-free conditions every year (Jahn, 2018). In contrast, the sea ice cover in the CESM2-LE experiences a sharp decline in area starting in the mid-1990s up until the end of the first decade of the 21<sup>st</sup> century (Figure 3.1b), with the ensemble mean ice loss trend reaching its highest value of about  $-1.8$  million  $\text{km}^2/\text{decade}$  around end year 2010 (Figure 3.1c). This is followed by a decade-long sea ice recovery in the CESM2-LE ensemble mean until  $\sim 2025$  characterized by neutral or even positive trends, after which the ensemble mean area anomaly and trend continue to become more negative until the anomaly stabilizes and the trend gets smaller again as the sea ice cover melts out completely every summer (DeRepentigny et al., 2020). Note that this is present regardless of the choice of future CMIP6 emissions scenario (DeRepentigny et al., 2020), in all months of the year (Figure S3.1), as well as in the version of the CESM2 that uses a high-top atmosphere model, WACCM6, instead of

the standard CESM2 atmosphere model, CAM6 (DeRepentigny et al., 2020).

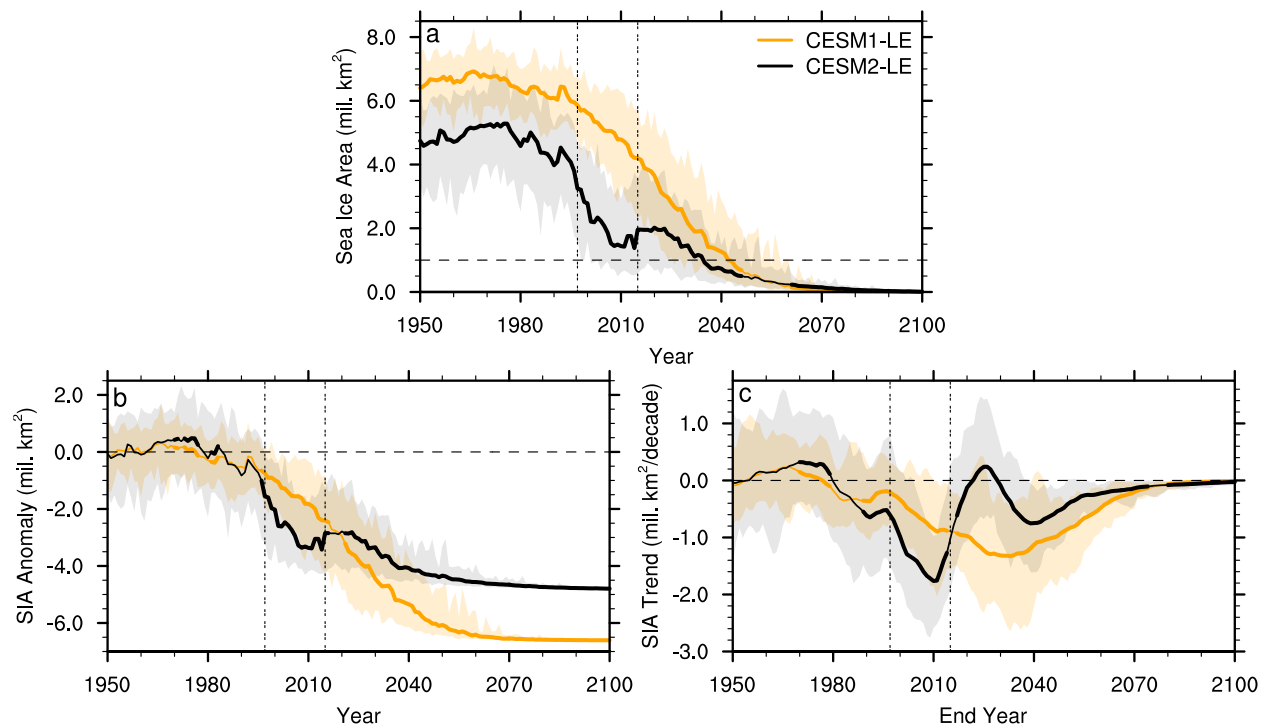


Figure 3.1: **Differences in the rate of Arctic sea ice loss.** Time evolution of (a) September sea ice area (SIA), (b) SIA anomalies relative to the 1940–1969 average, and (c) 20-year linear SIA trends in the CESM1-LE and the CESM2-LE. The ensemble mean is shown by the solid line, the full ensemble range is shown by the shading, the horizontal dashed line indicates ice-free conditions in (a), no anomalies in (b) and no trend in (c), and the two vertical double-dashed lines indicate the GFED period. Years when the CESM1-LE and the CESM2-LE are statistically different at the 95% significance level are indicated with a thicker ensemble mean line and are determined using a two-sample Welch’s t-test. In (c), values on the x-axis indicate the end year of the 20-year period over which the linear trend is computed.

### 3.2.2 Impact of BB emissions on simulated Arctic climate

We find that the change in prescribed BB emissions from CMIP5 to CMIP6 can explain the difference in Arctic sea ice evolution between the CESM1-LE and the CESM2-LE. In CMIP6, BB emissions were updated to include inter-annual variability, rather than using decadal means (Figure 3.2; Van Marle et al., 2017). Although this decision allows for a more realistic depiction of BB emissions over the historical period, it also results in a sudden increase of the inter-annual variability in BB emissions in 1997 (Figure 3.2), when the Global Fire Emissions Database (GFED)

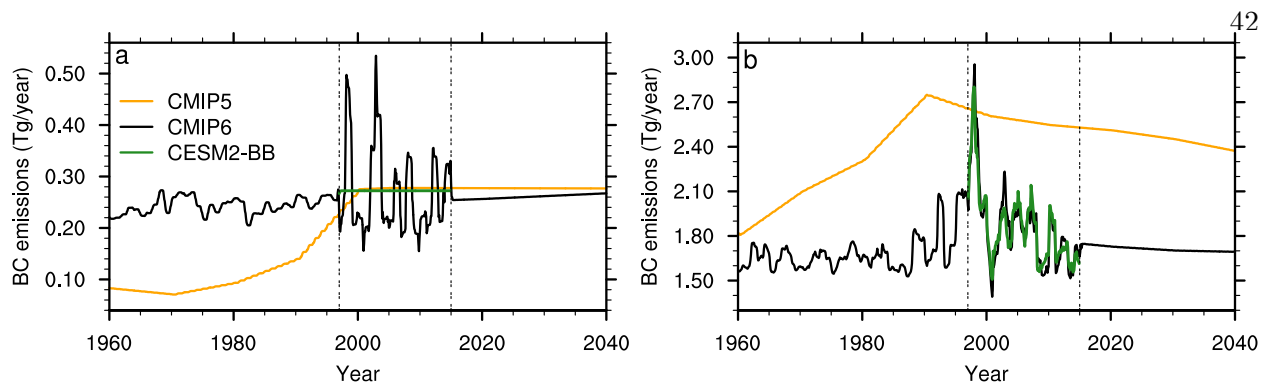
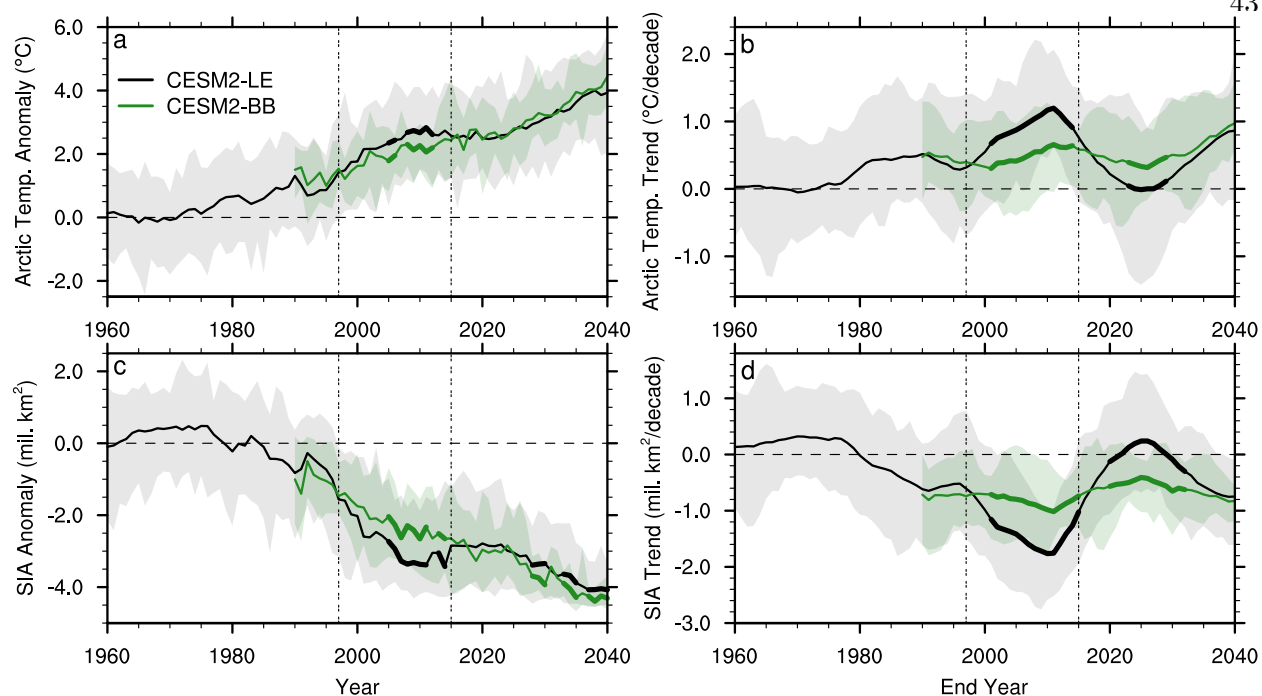


Figure 3.2: **Changes in BB forcing.** Prescribed total black carbon emissions from BB (a) between 40–70°N and (b) globally in CMIP5, CMIP6 and the CESM2-BB, smoothed with a 12-month running mean. The two vertical double-dashed lines indicate the GFED period. Note that the range of values on the y-axis is different between the two panels, with higher values of total black carbon emissions globally. Here we used black carbon emissions to represent BB emissions as it is the most radiatively important one, but all other prescribed BB emissions (dimethyl sulfide, primary organic matter, sulfur dioxide, sulfate aerosols and secondary organic aerosols) follow a similar time evolution as black carbon (not shown).

starts (Werf et al., 2017). This increase in variability is especially pronounced in the Northern Hemisphere (NH) mid-latitudes, where the range of inter-annual variability increases by a factor of five compared to pre-GFED years (defined here as 1950–1996; Figure 3.2a). The inter-annual variability in global BB emissions increases as well, but only by a factor of two (Figure 3.2b).

To isolate the impact of increased variability in NH mid-latitude BB emissions over the GFED era on Arctic sea ice, we conducted sensitivity ensemble simulations (referred to as CESM2-BB thereafter) in which the inter-annual variability in NH mid-latitude BB emissions from 1997–2014 was removed but the integrated amount of emissions over that same period is retained (Figure 3.2a; see section 3.5.3 for details). As a result, the CESM2-BB has prescribed BB emissions over the NH mid-latitudes that are similar to CMIP5 during the GFED period, with the emissions pre- and post-GFED being the same as in CMIP6 (Figure 3.2a). Since NH mid-latitude BB emissions make up only  $\sim 14\%$  of the global BB emissions, the variability of global BB emissions is almost unchanged in the CESM2-BB compared to CMIP6 values (Figure 3.2b).

The sensitivity experiments show that the increased NH mid-latitude variability in BB emissions after 1997 leads to an enhanced NH extratropical warming rate, particularly over land and



**Figure 3.3: BB emissions impact on Arctic climate.** Annual Arctic ( $70\text{--}90^\circ\text{N}$ ) surface air temperature (a) anomalies relative to the 1940–1969 average and (b) 20-year linear trends, and September sea ice area (SIA) (c) anomalies relative to the 1940–1969 average and (d) 20-year linear trends in the CESM2-LE and the CESM2-BB. The ensemble mean is shown by the solid line, the full ensemble range is shown by the shading, the horizontal dashed line indicates no anomalies in (a, c) and no trend in (b, d), and the two vertical double-dashed lines indicate the GFED period. Years when the CESM2-LE and the CESM2-BB are statistically different at the 95% significance level are indicated with a thicker ensemble mean line and are determined using a two-sample Welch’s t-test. Note that while the CESM2-BB has a smaller ensemble size than the CESM2-LE (10 versus 50 ensemble members), its ensemble size is sufficient to detect a forced sea ice response to the modified BB emissions (Figure S3.5c, d). In (b, d), values on the x-axis indicate the end year of the 20-year period over which the linear trend is computed.

north of  $30^\circ\text{N}$ , as shown in a companion paper (Fasullo et al., 2021). This warming is caused by disproportionate reductions in cloud drop number and cloud liquid water path over Siberia, Alaska and Canada, leading to a larger downwelling shortwave flux at the surface (Fasullo et al., 2021). Over the Arctic ( $70\text{--}90^\circ\text{N}$ ), the warming is more pronounced in the CESM2-LE compared to the CESM2-BB over the GFED period (Figure 3.3a), with the largest difference over the central and Pacific sectors of the Arctic Ocean (Figure S3.4a, b). Specifically, the 20-year linear trend in Arctic surface air temperature in the CESM2-LE is significantly larger than the CESM2-BB over most of

the GFED period (Figure 3.3b), after which the trend reduces to neutral values in the ensemble mean until around end year 2025.

Consistent with the impact on Arctic surface air temperature, the September Arctic sea ice area anomaly and trends are reduced (i.e., less negative) in the CESM2-BB compared to the CESM2-LE over the GFED period, in particular between 1997–2010 (Figure 3.3c, d). Furthermore, the magnitude of the sea ice recovery after 2010 is reduced in the CESM2-BB (Figure 3.3d). Similar results are found not just at the sea ice minimum but also from July to November (Figure S3.1). This reduction in the rate of Arctic sea ice decline over the GFED era is not limited to a specific region, but is present everywhere in the central Arctic Ocean and particularly over the Pacific sector of the Arctic (Figure S3.4c, d). As only the inter-annual variability in BB emissions over the GFED period differs between the two ensembles, these results allow us to conclude that the increased BB variability in CMIP6 over the GFED period is causing enhanced Arctic warming and sea ice decline since the late 1990s in the CESM2-LE, as a result of changes in clouds and shortwave radiative fluxes over Russia and North America (Fasullo et al., 2021).

### **3.2.3 Impact of BB emissions on sea ice sensitivity**

The observed loss of Arctic sea ice has been shown to be tightly coupled to increasing global mean surface air temperature (Winton, 2011; Mahlstein and Knutti, 2012; Stroeve and Notz, 2015) and cumulative anthropogenic CO<sub>2</sub> emissions (Notz and Stroeve, 2016). This metric of sea ice sensitivity to CO<sub>2</sub> and global warming is commonly used by the sea ice community and has even been proposed as a way to reduce the uncertainty range of future sea ice evolution (Notz and Stroeve, 2016; Niederdrenk and Notz, 2018). Previous literature has shown that model simulations usually simulate a lower sensitivity of Arctic sea ice loss per degree of global warming than has been observed (Mahlstein and Knutti, 2012; Notz and Stroeve, 2016; Rosenblum and Eisenman, 2017) and simulated Arctic sea ice retreat has been found to be accurate only in runs that have far too much global warming, which suggests that models may be getting the right Arctic sea ice retreat for the wrong reasons (Rosenblum and Eisenman, 2017). More recently, the CMIP6 multi-model

ensemble mean was shown to provide a more realistic estimate of the sensitivity of September Arctic

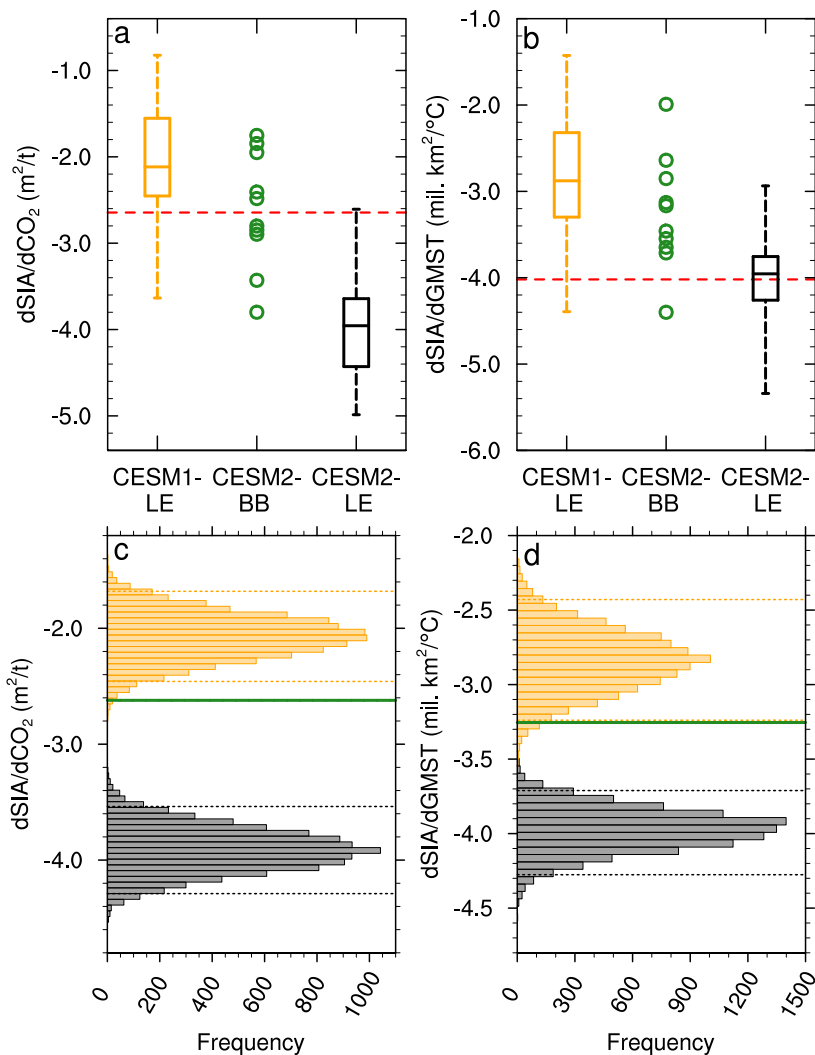


**Figure 3.4: BB emissions impact on sea ice sensitivity.** Sea ice sensitivity to (a) cumulative anthropogenic CO<sub>2</sub> emissions (defined as the change in Arctic September sea ice area per change in cumulative anthropogenic CO<sub>2</sub> emissions in m<sup>2</sup> per tonne of CO<sub>2</sub>) and (b) global annual mean surface air temperature (defined as the change in Arctic September sea ice area per change in global mean surface temperature in million km<sup>2</sup> per °C) from 1979–2014 in the CESM1-LE, the CESM2-BB and the CESM2-LE, with the red dashed line showing the observed sensitivity. For the two large ensembles, the box shows the inter-quartile range, the line inside the box shows the median, and the whiskers show the minimum and maximum across all ensemble members, and for the CESM2-BB the green circles indicate the sea ice sensitivity for each of the 10 ensemble members. Histograms of sea ice sensitivity to (c) cumulative anthropogenic CO<sub>2</sub> emissions and (d) global annual mean surface air temperature obtained by bootstrapping CESM1-LE and CESM2-LE ensemble means with 10 members 10,000 times, with the dotted lines showing the 95% confidence range for each distribution and the green line indicating the ensemble mean sensitivity of the CESM2-BB.

sea ice area to a given amount of anthropogenic CO<sub>2</sub> emissions and global warming, compared with earlier CMIP experiments (SIMIP Community, 2020). It was, however, unclear whether this reflects an improvement of model physics or primarily arises from the change in historical forcing in CMIP6 relative to CMIP5, in particular differences in BB emissions and ozone (SIMIP Community, 2020).

In agreement with what was reported for CMIP6 models as a group (SIMIP Community, 2020), we find that the sea ice sensitivity to cumulative anthropogenic CO<sub>2</sub> emissions and global mean surface air temperature is generally higher in the CMIP6-forced version of the CESM, the CESM2-LE, compared to the CMIP5-forced version, the CESM1-LE (Figure 3.4a, b). In contrast, the sea ice sensitivities of the CESM2-BB fall somewhere in between the range of sea ice sensitivities of the CESM1-LE and CESM2-LE, although all 10 ensemble members of the CESM2-BB overlap with the range of at least one of the large ensemble distributions if not both. Using bootstrapping, we show that the sea ice sensitivity of the CESM2-BB ensemble is statistically distinct from the CESM1-LE and the CESM2-LE at the 95% confidence level when accounting for the different ensemble size of the three CESM simulations (Figure 3.4c, d). Note that bootstrapping, or randomly resampling with replacement to generate statistics, requires no distribution assumptions and is only possible with sufficiently large ensembles. Hence, based on results from the CESM model, the increased variability in BB emissions from CMIP6 to CMIP5 is responsible in large part for the increased sea ice sensitivity to CO<sub>2</sub> and global warming from CMIP6 to CMIP5 recently reported by the SIMIP Community (SIMIP Community, 2020), with the rest related to others changes in historical forcing and/or improvement of model physics. This is especially true for the sea ice sensitivity to CO<sub>2</sub>, as temperature is also affected by the change in BB emissions but CO<sub>2</sub> concentrations are the same across all CESM simulations.

### 3.3 Discussion

Our analysis shows that the way short-lived climate forcings like BB emissions are prescribed in models can have unexpected remote effects in vulnerable regions such as the Arctic. In addition, we show that changes in the variability, not just changes in the mean, can have large effects on

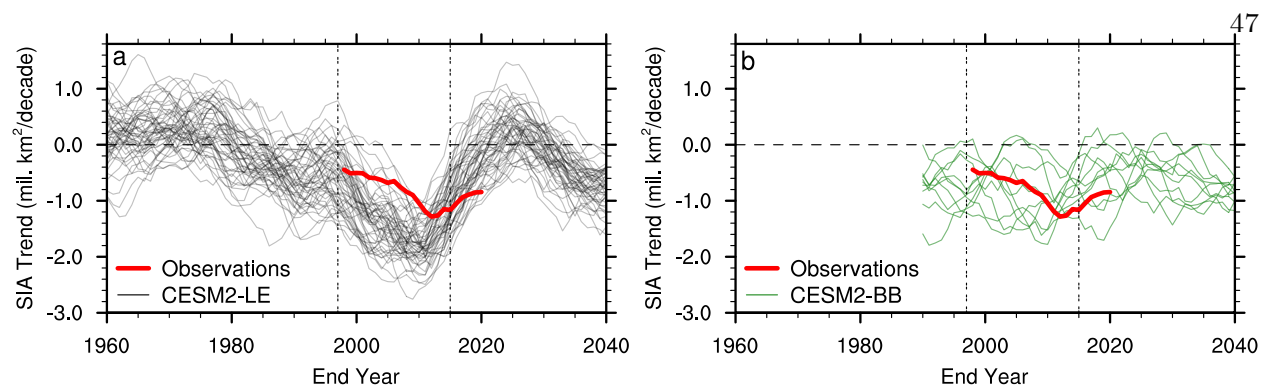


Figure 3.5: **Potential impact of BB emissions on observed Arctic sea ice decline.** 20-year linear trends in September sea ice area in each individual ensemble member of the (a) CESM2-LE and the (b) CESM2-BB compared to observations. The horizontal dashed line indicates no trend, and the two vertical double-dashed lines indicate the GFED period. Values on the x-axis indicate the end year of the 20-year period over which the linear trend is computed.

climate. This highlights the challenges associated with incorporating newly available observations into climate forcing datasets and the importance of avoiding temporal discontinuities, which may help guide decisions in future phases of CMIP. In particular, we find that an increase in the variability of BB emissions in CMIP6 leads to enhanced Arctic warming and rapid sea ice loss in the CESM2-LE in the early 21<sup>st</sup> century (Figure 3.3). Importantly, it is not just the CESM2 that shows an increase of the rate of Arctic sea ice decline over the GFED period, but some other CMIP6 models do as well (Figures S3.2 and S3.3). From the 12 additional CMIP6 models assessed here (see section 3.5.4), four (ACCESS-ESM1.5, FGOALS-g3, MIROC6 and MPI-ESM1.2-HR) show an accelerated ensemble mean sea ice loss over the GFED period, although none of them simulate an acceleration in sea ice decline as large as the CESM2. The fact that some CMIP6 models show a similar sea ice loss acceleration as the one attributed to the new BB emissions in the CESM2 while others do not calls for a better understanding of inter-model differences in light of their sensitivity to aerosol emissions. Furthermore, the sensitivity of the CESM2 to changes in BB variability raises the question as to whether the lack of inter-annual variability in aerosol forcing in the pre-industrial control and future runs could be problematic.

What do our results mean for understanding the evolution of the observed Arctic sea ice loss? As discussed earlier, several studies have documented a steepening of the trend of Arctic sea

ice decline since the mid-1990s (Stroeve et al., 2012b; Serreze and Stroeve, 2015) and a smaller trend since 2007 (Swart et al., 2015; Perovich et al., 2020). This qualitatively matches the behavior simulated by most of the individual ensemble members of the CESM2-LE (Figure 3.5a) and some other CMIP6 models (Figure S3.3). In contrast, only a few ensemble members of the CESM2-BB simulate a similar increase in negative sea ice area trend over the GFED period as seen in the observations with no clear coherent response across the full ensemble (Figure 3.5b). Moreover, the sea ice recovery that follows is also not clearly present in the CESM2-BB compared to the CESM2-LE. This raises the question as to whether the BB forcing has affected the observed Arctic sea ice loss since the late 1990s. Of course, the real world most likely did not experience an increase in inter-annual variability of BB emissions as drastic as the one prescribed in the CMIP6 forcing after 1997 (Figure 3.2), which we have shown causes accelerated Arctic sea ice loss in the CESM2-LE (Figure 3.3c). However, the high BB variability in the early GFED period may nonetheless have represented an increase of the variability of NH mid-latitude BB emissions compared to pre-GFED years (Hanes et al., 2019), and could hence have contributed to the observed accelerated sea ice loss as a non-greenhouse gas forcing. This should be further investigated, as a better understanding of the impact of BB variability on Arctic sea ice is especially timely given the record northern fire year in 2020 (Witze, 2020), the recent observed positive trend in burned area and severity of NH wildfires (Hanes et al., 2019; Huang et al., 2020), and the projected increase in wildfires in the future (de Groot et al., 2013; Sherstyukov and Sherstyukov, 2014; Tang et al., 2021).

### 3.4 Conclusions

New satellite-based estimates of historical BB emissions exhibit large inter-annual variability, and their usage as prescribed forcing in CMIP6 in the early 21<sup>st</sup> century results in discontinuities prior to and after the range of years covered by the GFED dataset. This increase in variability is especially pronounced north of 40°N, where the variability increases by a factor of five compared to previous decades. Using sensitivity ensemble simulations with homogenized BB emissions over the GFED period but leaving all other forcings unchanged, we are able to attribute the excessive

early 21<sup>st</sup> century Arctic surface warming and strong decline in September Arctic sea ice area in the CESM2-LE compared to the CESM1-LE to the increased BB variability. Specifically, the sensitivity experiments clearly show a reduced warming and sea ice loss in the early 21<sup>st</sup> century, isolating the role of the BB emissions forcing over the GFED era and showing that the increased BB variability leads to an additional forced sea ice loss beyond the sea ice loss driven by increases in greenhouse gases (Notz and Marotzke, 2012) and internal variability (Kay et al., 2011; Ding et al., 2019; England et al., 2019). Enhanced sea ice loss over the GFED period is also present in some, but not all, CMIP6 models. This indicates that the impact of BB emissions is not just limited to the CESM2 but may affect other CMIP6 models, in agreement with results from a companion paper that also finds increased surface downwelling shortwave radiation during the GFED period in several other CMIP6 models (Fasullo et al., 2021). Overall, our results call attention to the challenges related to incorporating new observations into forcing data without causing unintended effects in climate simulations by introducing temporal discontinuities.

The presence of this non-greenhouse gas forced sea ice loss in the early 21<sup>st</sup> century in models also affects the sea ice sensitivity often used to evaluate model performance (Stroeve and Notz, 2015; Notz and Stroeve, 2016; Jahn, 2018; SIMIP Community, 2020). Specifically, we find that the increased inter-annual variability in BB emissions during the GFED era explains about half of the increase in sea ice sensitivity to CO<sub>2</sub> and global warming from the CMIP5-forced to the CMIP6-forced versions of the CESM. This is the second time that aerosol-related forcing changes have been shown to impact Arctic sea ice trends between CMIP generations (Rosenblum and Eisenman, 2016), highlighting how sensitive sea ice is to the effects of aerosol emissions.

Finally, the early GFED period stands out as particularly variable in BB emissions north of 40°N (Van Marle et al., 2017), in the real world and in the CMIP6 forcing. The good alignment of the simulated and observed accelerated Arctic sea ice loss in the early 21<sup>st</sup> century, and the reduced ice loss that follows, raises the question as to whether there could be a forced signal driven by BB emissions and/or other non-CO<sub>2</sub> forcings not just in CMIP6 models, but also in the observed Arctic sea ice loss.

## 3.5 Methods

### 3.5.1 Observational data

Observed estimates of NH monthly sea ice area since the beginning of the continuous satellite record in 1979 are from the National Snow and Ice Data Center (NSIDC) Sea Ice Index version 3 (Fetterer et al., 2017), with the observational pole hole filled assuming sea ice concentration of 100%. Historical anthropogenic CO<sub>2</sub> emissions are taken from the historical budget of the Global Carbon Project (Global Carbon Project, 2019). For global mean surface temperature, we use estimates from GISTemp v4 (GISTEMP Team, 2021; Lenssen et al., 2019) and calculate anomalies relative to the period 1850–1900.

### 3.5.2 CESM simulations

The CESM Large Ensemble (CESM1-LE; Kay et al., 2015) is a 40-member ensemble of the CESM1.1 model (Hurrell et al., 2013) that has been widely used for Arctic sea ice studies and generally performs well when compared to observations (Barnhart et al., 2016; DeRepentigny et al., 2016; Jahn et al., 2016; Kirchmeier-Young et al., 2017; England et al., 2019; Smith and Jahn, 2019). The historical simulations span 1920 to 2005, while the RCP8.5 scenario simulations cover 2006 to 2100. The CESM1-LE uses the Community Atmosphere Model version 5 (CAM5; Hurrell et al., 2013) along with a 3-mode version of the Modal Aerosol Module (MAM3; Liu et al., 2012), and cloud-aerosol interactions are represented by the MG1 cloud microphysics scheme (Morrison and Gettelman, 2008).

With several science and infrastructure improvements, the CESM2 model (Danabasoglu et al., 2020) is the latest generation of the CESM and NCAR’s contribution to CMIP6. Specifically, aerosols are simulated through the use of the MAM4 approach (Liu et al., 2016) and cloud-aerosol interactions are represented by the updated Morrison and Gettelman scheme (MG2; Gettelman and Morrison, 2015). The CAM5 shallow convection, planetary boundary layer and cloud macrophysics schemes are replaced in CESM2 with an unified turbulence scheme, the Cloud Layers Unified By Bi-

normals (CLUBB; Bogenschutz et al., 2013). As a result of these improvements, the CESM2 shows large reductions in low-latitude precipitation and short-wave cloud radiative forcing biases, leading to improved historical simulations with respect to available observations compared to its previous major release, the CESM1.1 used in the CESM1-LE (Danabasoglu et al., 2020). Two separate CESM2 configurations have been contributed to the CMIP6 effort, differing only in their atmosphere component: the “low-top” (40 km, with limited chemistry) Community Atmosphere Model version 6 (CAM6; Danabasoglu et al., 2020, referred to as CESM2) and the “high-top” (140 km, with interactive chemistry) Whole Atmosphere Community Climate Model version 6 (WACCM6; Gettelman et al., 2019b, referred to as CESM2-WACCM). Most of the analysis presented here focuses on a recently released large initial-condition ensemble (referred to as CESM2-LE) that uses the version of the CESM2 with CAM6 as the atmosphere component (Rodgers et al., 2021), but results from the CESM2-WACCM are also included in the comparison with other CMIP6 models (Figures S3.2 and S3.3).

The CESM2-LE (Rodgers et al., 2021) is a 100-member large ensemble suite that was run from 1850 to 2014 under historical forcing and from 2015 to 2100 following the medium-to-high SSP3-7.0 scenario (O’Neill et al., 2016). The CESM2-LE initialization procedure was designed to include a mix of macro- and micro-perturbations, where macro-perturbations were initialized from 20 independent restart files at 10-year intervals (total of 20 ensemble members) and micro-initializations involved a small random perturbation in 20 members for 4 different start years of the pre-industrial control simulation meant to represent different AMOC states (total of 80 ensemble members). Note that most of this study focuses on the first 50 members of the CESM2-LE since those follow CMIP6 protocols in terms of BB emissions (Van Marle et al., 2017). For the second set of 50 members, the CMIP6 global BB emissions of all relevant species were smoothed in time from 1990-2020 to remove inter-annual variability based on the climate impacts of the high BB variability over the GFED, as presented in this paper and in a companion paper (Fasullo et al., 2021).

### 3.5.3 CESM2 sensitivity experiments with homogenized forcing

To investigate the impact of the increased inter-annual variability in BB emissions over the GFED period, we ran a set of sensitivity experiments using the CESM2 (referred to as CESM2-BB) in which we averaged BB emissions from 1997–2014, computed on a monthly basis, such that BB emissions have a fixed annual cycle while keeping the same integrated amount of emissions over that same period. This approach is identical in nature to what was used in CMIP5 (Lamarque et al., 2010) and removes any sharp transition with BB emissions over pre-GFED years as well as with the SSP BB emissions since those are homogenized to the averaged GFED emissions. The CESM2-BB simulations are initialized in 1990 from the first 10 members of the CESM2 and only BB emissions over the 40–70°N latitudinal band from 1997–2014 are modified. This region is chosen to target BB emissions from NH mid-latitude wildfires, and similar results are found by removing the variability in BB emissions globally instead of only between 40–70°N (not shown), which highlights the impact of NH mid-latitudes fires on Arctic climate. These sensitivity simulations are the same as the first 10 members used in a companion paper (Fasullo et al., 2021). To look beyond 2014, we extended the 10 members of the CESM2-BB simulations up to 2040 following the same SSP3-7.0 scenario as in CMIP6.

Although the ensemble size of the CESM2-BB is much smaller compared to the CESM2-LE, we find that 10 ensemble members are enough to detect a forced response to the homogenized BB emissions in the CESM2. Specifically, we compare the first 50 members of the CESM2-LE to the last 50 members (Figure S3.5a, b), which also use homogenized BB emissions to avoid the increase in BB variability over the GFED era (Rodgers et al., 2021). With 10 ensemble members, we are able to detect a forced response that is statistically different from 2007–2011 for the September sea ice area and from 2008–2011 and 2025–2027 for the 20-year linear trend in September sea ice area (Figure S3.5c, d). Note, however, that for the last 50 members of the CESM2-LE the chosen smoothing technique and years over which the smoothing is applied differ from what we used in the CESM2-BB experiment. In particular, the smoothing in the CESM2-LE is applied globally over

1990–2020 using an 11-year running mean filter, so that the integrated amount of emissions over the GFED period is not exactly the same as in the CMIP6 forcing (or the CESM2-BB). Nonetheless, the Arctic sea ice response to homogenized BB forcing is similar between the last 50 members of the CESM2-LE and the CESM2-BB.

### 3.5.4 CMIP6 simulations

We also use simulations from a subset of CMIP6 models that provided at least three ensemble members for the historical and SSP3-7.0 scenario simulations. As of December 2<sup>nd</sup> 2020, the models that met this criteria (excluding the CESM2 and CESM2-WACCM described above) are: ACCESS-CM2 (Dix et al., 2019a,b), ACCESS-ESM1.5 (Ziehn et al., 2019a,b), BCC-ESM1 (Zhang et al., 2018, 2019), CanESM5 (Swart et al., 2019a,b), EC-Earth3-Veg (EC-Earth Consortium (EC-Earth), 2019a,b), FGOALS-g3 (Li, 2019a,b), IPSL-CM6A-LR (Boucher et al., 2018, 2019), MIROC6 (Tatebe and Watanabe, 2018; Shiogama et al., 2019), MPI-ESM1.2-HR (Jungclaus et al., 2019; Schupfner et al., 2019), MPI-ESM1.2-LR (Wieners et al., 2019b,a), MRI-ESM2.0 (Yukimoto et al., 2019a,b) and NorESM2-LM (Seland et al., 2019a,b). In cases where the ScenarioMIP SSP3-7.0 simulation was not available, we then used the AerChemMIP SSP3-7.0 simulation that uses the same forcing as the ScenarioMIP SSP3-7.0 but only extends to the end of 2055 (Collins et al., 2017). Even if a modeling center provided more than three ensemble members, only the first three are used to allow for a consistent comparison across all CMIP6 models. Although using only CMIP6 models that provide at least three ensemble members limits the total number of CMIP6 models included in our analysis, it is necessary to choose an ensemble size that is large enough to represent the forced sea ice response to BB emissions, as some individual members of the CESM2-LE show different trajectories despite the identified forced response to the BB forcing (Figure 3.5a). Using an ensemble size of three members was chosen as a compromise since the ensemble mean of the first three ensemble members of the CESM2-LE match the full ensemble mean well while requiring more members would further reduce the number of available CMIP6 models.

### 3.5.5 Criteria for determining sensitive versus not sensitive models

The CMIP6 models are separated into a sensitive and a not sensitive category based on whether they exhibit a similar sensitivity to the increased variability in BB emissions as the CESM2 (Figure S3.2). First, we calculate 20-year linear trends in September sea ice area for each model, and compare the slope of the 20-year linear trends between the reference period of end years 1978–1990 and the acceleration period of end years 1997–2009. Note that we chose the last year of the acceleration period to be 2009 instead of the last year of the GFED era (i.e., 2014) based on when the CESM2 and CESM2-WACCM reach their maximum negative September sea ice area trend (see Figure S3.3). For a model to be characterized as sensitive, the slope of sea ice area trends over the acceleration period needs to be at least 2 times larger (in absolute value) than the slope of sea ice area trends over the reference period. This criteria is defined based on the relative increase in sea ice trend for each model to account for the different magnitudes of sea ice loss across all CMIP6 models (Figure S3.3). We decided to choose two periods of same length and to exclude the years 1991–1996 from the reference period because of the Mount Pinatubo volcanic eruption in 1991 and the global cooling that followed for a few years, which resulted in a peak increase in Arctic sea ice extent about a year and a half after the eruption in some models (Gagné et al., 2017). Note that the classification into the sensitive and not sensitive category is not affected by the choice of reference period or the exact magnitude of the accelerated sea ice loss.

## 3.6 Acknowledgements

P. DeRepentigny is supported by the Natural Sciences and Engineering Council of Canada (NSERC) and the Fonds de recherche du Québec – Nature et Technologies (FRQNT) through PhD scholarships and by NSF-OPP CAREER award 1847398. A. Jahn’s and A. Barrett’s contribution is supported by NSF-OPP CAREER award 1847398. Contributions from M.M. Holland, J.-F. Lamarque, C. Hannay, M.J. Mills, D.A. Bailey and S. Tilmes are supported by the National Center for Atmospheric Research (NCAR), which is a major facility sponsored by the NSF under

Cooperative Agreement No. 1852977. J.E. Kay was supported by NSF CAREER AGS 1554659. The efforts of J. Fasullo were supported by NASA Award 80NSSC17K0565, by NSF Award #AGS-1419571, and by the Regional and Global Model Analysis (RGMA) component of the Earth and Environmental System Modeling Program of the U.S. Department of Energy's Office of Biological & Environmental Research (BER) via National Science Foundation IA 1844590.

The CESM project is supported primarily by the National Science Foundation (NSF). This material is based upon work supported by NCAR, which is a major facility sponsored by the NSF under Cooperative Agreement No. 1852977. Computing and data storage resources, including the Yellowstone (<http://n2t.net/ark:/85065/d7wd3xhc>) and Cheyenne (doi:10.5065/D6RX99HX) supercomputers, were provided by the Computational and Information Systems Laboratory (CISL) at NCAR. We thank all the scientists, software engineers, and administrators who contributed to the development of CESM and the CESM1 and CESM2 Large Ensemble Community Projects. We also acknowledge supercomputing resources provided by the IBS Center for Climate Physics in South Korea for the CESM2 Large Ensemble Project.

We acknowledge the World Climate Research Programme, which, through its Working Group on Coupled Modelling, coordinated and promoted CMIP6. We thank the climate modeling groups for producing and making available their model output, the Earth System Grid Federation (ESGF) for archiving the data and providing access, and the multiple funding agencies who support CMIP6 and ESGF.

We also thank Drs. Clara Deser and Walt N. Meier for useful discussions and three anonymous reviewers for valuable comments on an earlier version of this manuscript. Data analysis and visualization were done using the NCAR Command Language (<http://dx.doi.org/10.5065/D6WD3XH5>).

### **3.7 Author contributions**

P. DeRepentigny and A. Jahn designed the study. P. DeRepentigny performed the analysis and wrote the manuscript under the supervision of A. Jahn. M. M. Holland, J. Fasullo and J.-

F. Lamarque contributed to the experiment design and provided CESM specific expertise. J. E. Kay provided valuable guidance on statistical analysis and revisions to the manuscript. C. Hannay and P. DeRepentigny conducted the sensitivity simulations. M. J. Mills and S. Tilmes provided aerosol emission expertise. D. A. Bailey provided valuable assistance for conducting the sensitivity simulations. A. Barrett compiled CMIP6 data. All authors provided critical feedback and collaborated in shaping the research, analysis and final version of the manuscript.

### **3.8 Competing interests**

The authors declare no competing interests.

### **3.9 Data and materials availability**

Previous and current versions of the CESM are freely available at <https://www.cesm.ucar.edu/models/>. The CESM2-LE data analyzed in this study can be accessed at <https://www.cesm.ucar.edu/projects/community-projects/LENS2/data-sets.html>. The CESM1-LE data can be found at <https://www.cesm.ucar.edu/projects/community-projects/LENS/>. Data from the CMIP6 models analyzed in this study are freely available from the Earth System Grid Federation (ESGF) at [esgf-node.llnl.gov/search/cmip6/](https://esgf-node.llnl.gov/search/cmip6/). Results from the CESM2-BB sensitivity simulations will be made available on NCAR's Earth System Grid while the manuscript is under review.

### 3.10 Supplementary Information

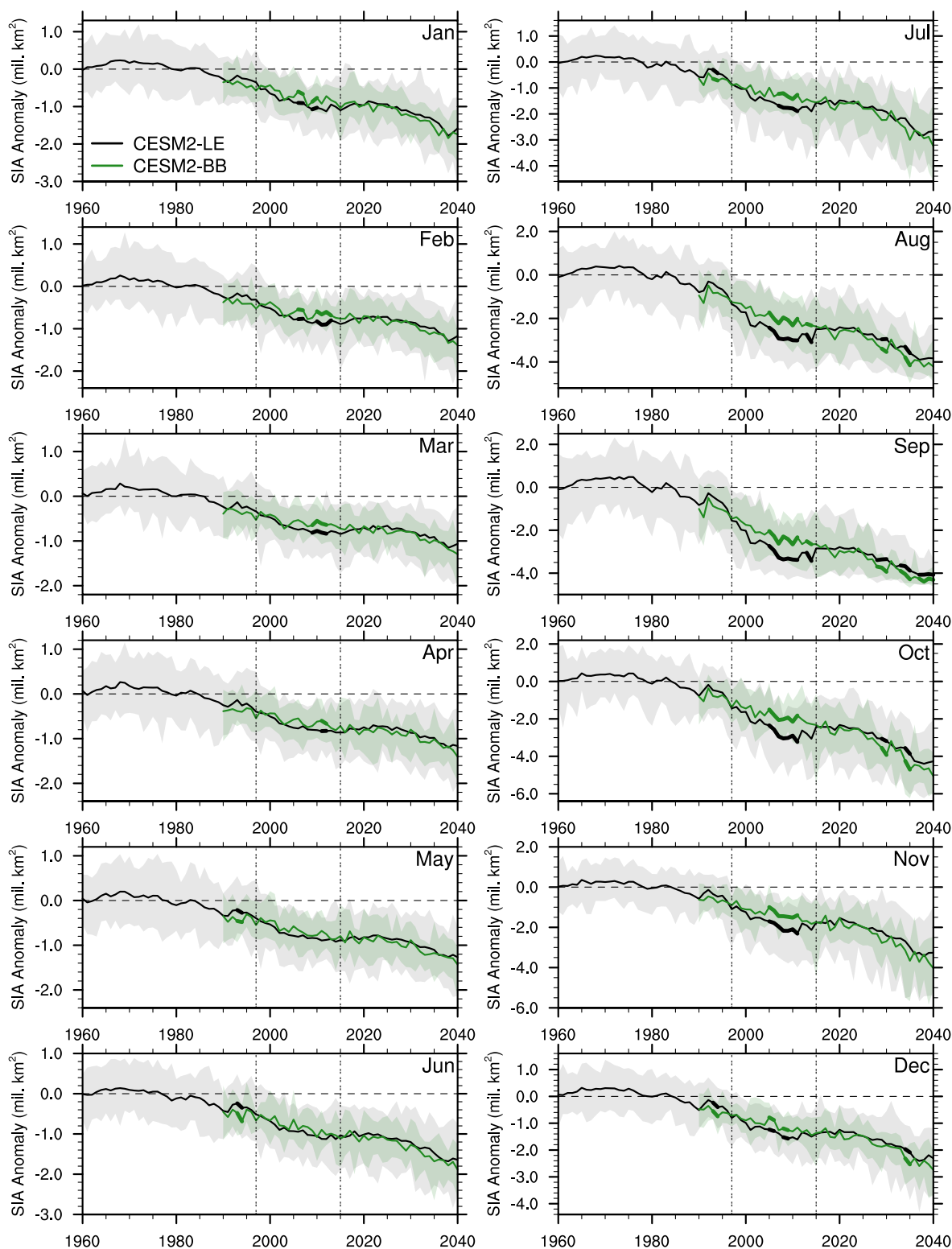


Figure S3.1: **BB emissions impact on sea ice area in all months.** Sea ice area (SIA) anomalies relative to the 1940–1969 average in each month of the year in the CESM2-LE and the CESM2-BB. The ensemble mean is shown by the solid line, the full ensemble range is shown by the shading, the horizontal dashed line indicates no anomalies, and the two vertical double-dashed lines indicate the GFED period. Years when the CESM2-LE and the CESM2-BB are statistically different at the 95% significance level are indicated with a thicker ensemble mean line and are determined using a two-sample Welch’s t-test. Note that the range of values on the y-axis varies across all panels.

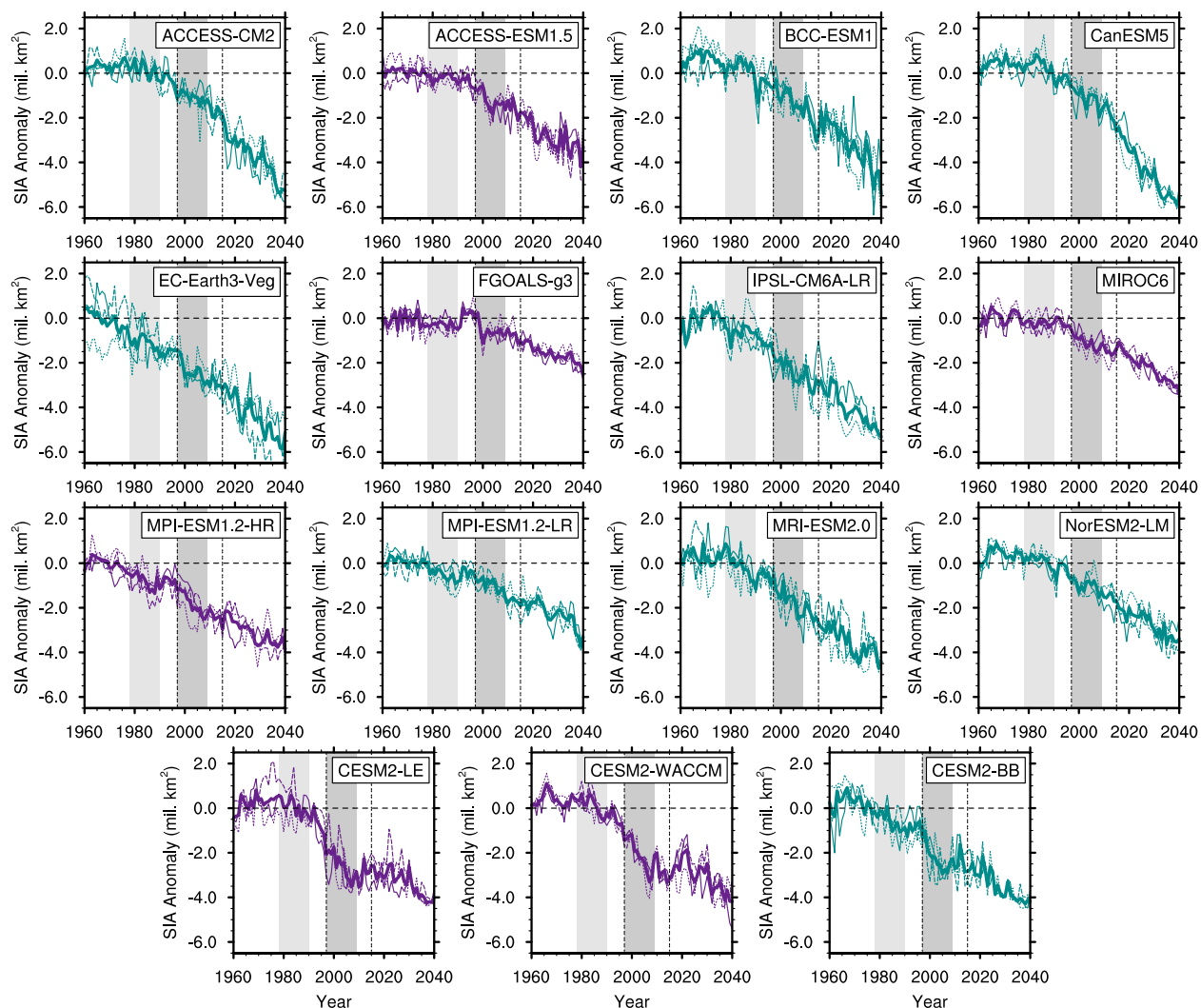


Figure S3.2: **September sea ice evolution in CMIP6 models.** September sea ice area (SIA) anomalies relative to the 1940–1969 average for each CMIP6 model. The models in the sensitive category are shown in purple and the ones in the not sensitive category are shown in turquoise. For each model, the first three ensemble members are shown as thin lines and the ensemble mean is shown by the thick line. The light gray shaded region corresponds to the reference period 1978–1990 and the dark grey shaded region corresponds to the acceleration period 1997–2009 (see section 3.5.5 for more details). The horizontal dashed line indicates no anomalies and the two vertical double-dashed lines indicate the GFED period. The last row shows the CESM2-LE, the CESM2-WACCM and the CESM2-BB for comparison, only using the first three ensemble members.

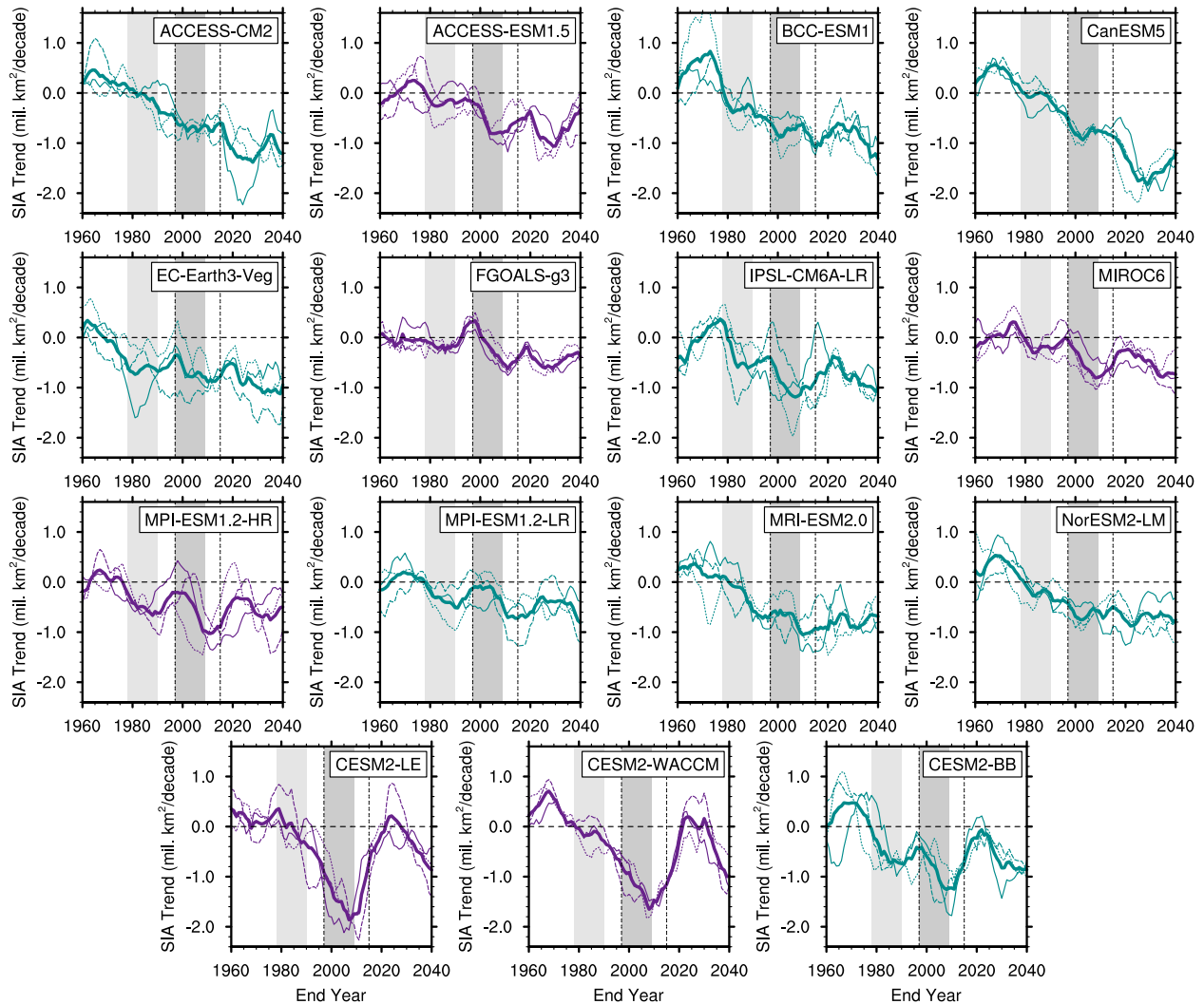


Figure S3.3: **September sea ice area trends in CMIP6 models.** As in Figure S3.2, but for 20-year linear trends in September sea ice area (SIA). The horizontal dashed line indicates no trend. Values on the x-axis indicate the end year of the 20-year period over which the linear trend is computed.

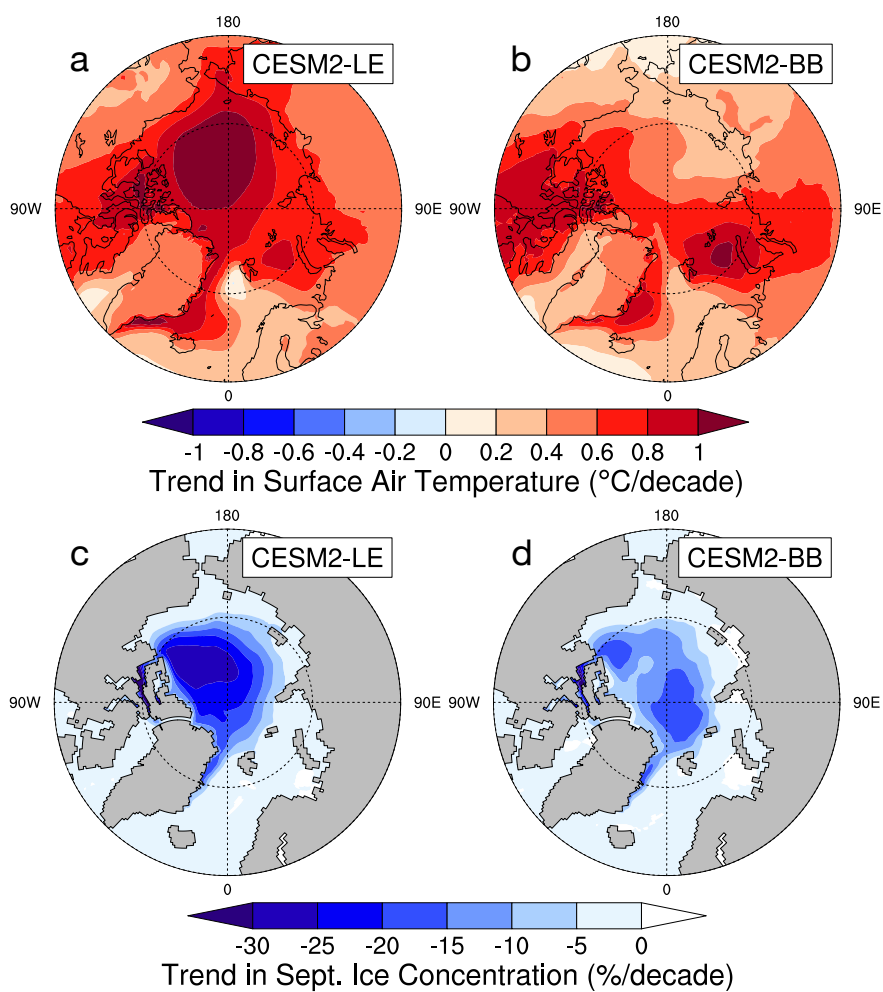


Figure S3.4: **Spatial patterns of BB impacts.** Spatial distribution of the linear trend in (a, b) annual surface air temperature and (c, d) September sea ice concentration over the GFED period (1997–2014) in (a, c) the CESM2-LE and (b, d) the CESM2-BB.

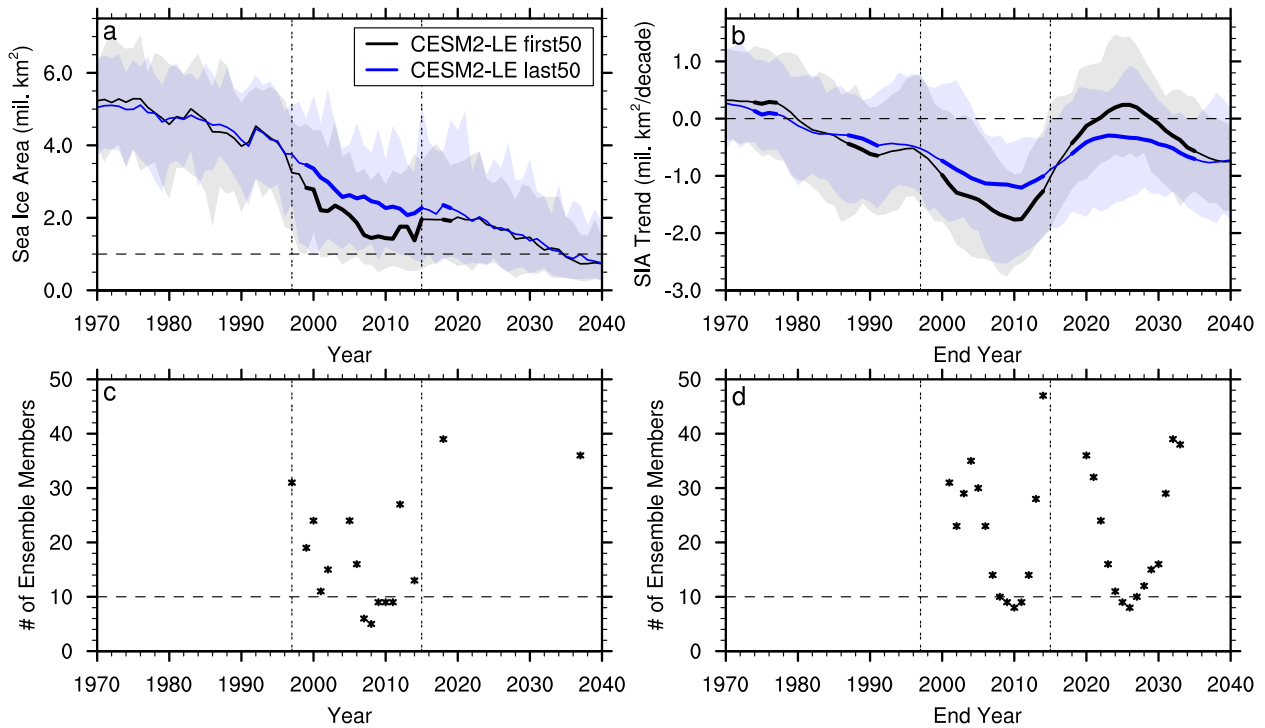


Figure S3.5: **Minimum number of ensemble members needed to detect a forced response to the homogenized BB emissions.** September sea ice area (SIA) (a) anomalies relative to the 1940–1969 average and (b) 20-year linear trends in the first and last 50 members of the CESM2-LE. Minimum number of ensemble members needed for the September SIA (c) anomalies relative to the 1940–1969 average and (d) 20-year linear trends between the first 50 member and last 50 member ensembles to be statistically different at the 95% significance level. This is done by bootstrapping the two ensembles 10,000 times with a sub-sample size varying from 2 to 49. The ensemble mean is shown by the solid line, the full ensemble range is shown by the shading, the horizontal dashed line indicates no anomalies in (a), no trend in (b), and 10 ensemble members in (c, d), and the two vertical double-dashed lines indicate the GFED period. In (a, b), years when the first 50 member and last 50 member ensembles are statistically different at the 95% significance level are indicated with a thicker ensemble mean line and are determined using a two-sample Welch’s t-test. In (b), values on the x-axis indicate the end year of the 20-year period over which the linear trend is computed.

## CHAPTER 4

# INCREASED TRANSNATIONAL SEA ICE TRANSPORT BETWEEN NEIGHBORING ARCTIC STATES IN THE 21<sup>ST</sup> CENTURY

### Preface

This chapter is published as cited below, and is reproduced here based on the last author version. It is identical in content to the published version, except for formatting and copy editing and a requested errata regarding Figures 4.7 and S4.3:

DeRepentigny, P., Jahn, A., Tremblay, L. B., Newton, R. and Pfirman, S.: Increased transnational sea ice transport between neighboring Arctic states in the 21<sup>st</sup> century, *Earth's Future*, 8(3), e2019EF001284, <https://doi.org/10.1029/2019EF001284>, 2020.

### Abstract

The Arctic is undergoing a rapid transition toward a seasonal ice regime, with widespread implications for the polar ecosystem, human activities, as well as the global climate. Here we focus on how the changing ice cover impacts transborder exchange of sea ice between the exclusive economic zones of the Arctic states. We use the Sea Ice Tracking Utility, which follows ice floes from formation to melt, in conjunction with output diagnostics from two ensembles of the Community Earth System Model that follow different future emissions scenarios. The Community Earth System Model projects that by midcentury, transnational ice exchange will more than triple, with the largest increase in the amount of transnational ice originating from Russia and the Central Arctic. However, long-distance ice transport pathways are predicted to diminish in favor of ice exchanged between neighboring countries. By the end of the 21<sup>st</sup> century, we see a large difference between the two future emissions scenarios considered: Consistent nearly ice-free summers under

the high emissions scenario act to reduce the total fraction of transnational ice exchange compared to midcentury, whereas the low emissions scenario continues to see an increase in the proportion of transnational ice. Under both scenarios, transit times are predicted to decrease to less than 2 yr by 2100, compared to a maximum of 6 yr under present-day conditions and 2.5 yr by midcentury. These significant changes in ice exchange and transit time raise important concerns regarding risks associated with ice-rafted contaminants.

### **Plain Language Summary**

The Arctic is undergoing a rapid transition toward a thinner, less extensive, more mobile sea ice cover. This affects the amount of sea ice exchanged between the exclusive economic zones of Arctic states. Here we use an Earth System Model, the Community Earth System Model, to track sea ice from where it forms to where it ultimately melts. By midcentury, the area of sea ice exchanged between the different regions of the Arctic is predicted to more than triple compared to the end of the twentieth century, with the Central Arctic joining Russia as a major ice “exporter.” At the same time, the exchange of sea ice over long distances is predicted to diminish in favor of ice exchanged between neighboring Arctic states. By midcentury, the average time required for ice to travel from one region to another is more than halved; by 2100, nearly all transports take less than a year, with little multiyear ice left in the Arctic. Sea ice provides a transport mechanism for a variety of material, including algae, dust, and a range of pollutants. The acceleration, and then disappearance, of sea ice has important implications for managing contamination in Arctic waters.

#### **4.1 Introduction**

The Arctic sea ice cover has been retreating over the past four decades and is predicted to continue to decline throughout the 21<sup>st</sup> century (e.g., SIMIP Community, 2020; Stroeve et al., 2012a; Stroeve and Notz, 2018). Sea ice loss provides easier marine access to the Arctic and great opportunities for economic activities (Aksenov et al., 2017; Ng et al., 2018; Schøyen and Bråthen, 2011; Stephenson et al., 2013), but is also associated with growing risks and emerging

political tensions (Arctic Council, 2009; Emmerson and Lahn, 2012; Newton et al., 2016). When ice concentrations are high, sea ice can raft various materials, including pollutants, and transport them much farther than ocean currents across the Arctic basin (Blanken et al., 2017). Newton et al. (2017) have shown that the total area of sea ice exchanged across the Arctic Ocean has been increasing over the historical period as a result of sea ice retreat and thinning, with higher ice drift speeds and associated shorter transit times between different regions. However, long-range transport of sea ice and ice-rafted material has started to decrease in recent years due to intensified melt in the marginal ice zones of the Arctic Ocean (Krumpen et al., 2019; Newton et al., 2017). It is currently unclear how transnational ice exchange will evolve in the future as the Arctic continues to transition toward a seasonally ice-free state, in particular when considering the competing effects of increased drift speeds versus shorter periods for sea ice to transit the Arctic as the melt season lengthens. In this study, we investigate how transnational sea ice exchange between the different Arctic states is predicted to change during the 21<sup>st</sup> century using the Community Earth System Model (CESM1; Hurrell et al., 2013).

September sea ice extent has been declining at a rate of roughly 11% per decade since the start of the satellite era in 1979 (Comiso et al., 2017; Stroeve and Notz, 2018) and there is evidence that the rate of decline has accelerated since the beginning of the 21<sup>st</sup> century (Comiso et al., 2008; Ogi and Rigor, 2013; Stroeve et al., 2012b). In addition, there has been an increase in the length of the open-water season in the Arctic over recent decades (Barnhart et al., 2016; Smith and Jahn, 2019; Stroeve et al., 2014b) and the sea ice cover has undergone substantial thinning with a considerable decline in the amount of multi-year ice (Comiso, 2012; Kwok, 2018; Stroeve et al., 2014a; Stroeve and Notz, 2018). The retreat of Arctic sea ice combined with more extensive open-water periods have modified interactions between the different stakeholders of the High North, raising new political issues and heightening potential conflicts among Arctic states (Emmerson and Lahn, 2012; Newton et al., 2016; Wilhelmsen and Gjerde, 2018). Current model projections suggest that nearly ice-free summers, defined as ice extent that falls below  $1 \times 10^6$  km<sup>2</sup>, are very likely unless warming is limited to 1.5°C (Jahn, 2018; Niederdrenk and Notz, 2018; Screen and

Williamson, 2017; Sigmond et al., 2018). It has been shown that if emissions of anthropogenic CO<sub>2</sub> continue on the current trajectory, nearly ice-free conditions will likely occur by the middle of the century (Jahn et al., 2016; Wang and Overland, 2009, 2012). Trends described in Newton et al. (2017) suggest that transnational ice exchange could continue to expand in the near future, increasing political tensions associated with cross-border contaminant transport (Newton et al., 2016). Here we assess how transnational ice exchange will evolve over the 21<sup>st</sup> century, and what impact different future emissions scenarios may have on these projections.

Sea ice acts as a transport medium for materials such as dust, aerosol deposits, sediments, organic matter, macro-nutrients, freshwater, and biological communities growing at the bottom of the ice (Eicken et al., 2000; Eicken, 2004; Melnikov et al., 2002; Newton et al., 2013; Nürnberg et al., 1994). Transport of ice algae and sediments by sea ice has been shown to favor ice-associated phytoplankton blooms when the ice melts in the summer, critically impacting the food web structure (Boetius et al., 2013; Fernández-Méndez et al., 2015; Gradinger et al., 2009; Jin et al., 2007; Olsen et al., 2017). As industrialization of the Arctic continues to expand due to easier marine access, anthropogenic pollutants (e.g., mercury, lead, black carbon, oil, microplastics) may also be transported by sea ice over long distances from where they first enter the ocean (AMAP, 2011, 2015; Blanken et al., 2017; Obbard et al., 2014; Peeken et al., 2018; Pfirman et al., 1995, 1997; Shevchenko et al., 2016; Varotsos and Krapivin, 2018; Venkatesh et al., 1990). This makes assessment of risk, attribution of responsibility for environmental and ecological consequences, as well as containment, recovery, and cleaning operations of contaminants very difficult if not impossible (Glickson et al., 2014; Newton et al., 2016; Peterson et al., 2003; Post et al., 2009; Sørstrøm et al., 2010; Wilkinson et al., 2017).

To explore the connections between future changes in Arctic sea ice and emerging political issues related to long-distance rafting of material, we frame our analysis in the context of exclusive economic zones (EEZs; Flanders Marine Institute, 2018) of the Arctic states (Figure 4.1). This builds on the work by Newton et al. (2017), who used satellite-derived sea ice drifts and analyzed transnational ice transport and change from the years pre to post-2000. An exclusive economic

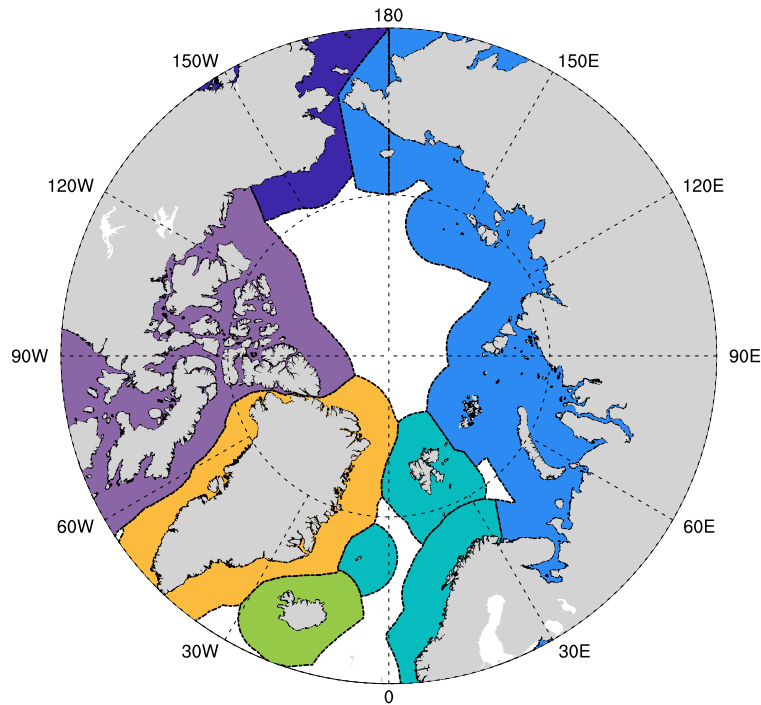


Figure 4.1: Map of the exclusive economic zones (EEZs) of the Arctic based on the definition from the United Nations Convention on the Law of the Sea (Nordquist, 2011): Canada (purple), the United States (dark blue), Russia (light blue), Norway (turquoise), Iceland (green) and Greenland (orange). The region in the middle of the Arctic Ocean that is not included within an EEZ is referred to as the Central Arctic (CNT) for the context of this study.

zone is a sea zone over which a state has special rights regarding the exploration and use of marine resources, including energy production. EEZs extend 200 nautical miles (370.4 km) from the coastline, as prescribed by the United Nations Convention on the Law of the Sea (Nordquist, 2011). There are five Arctic littoral states: Canada, the United States, Russia, Norway (including the Svalbard archipelago and the Jan Mayen island) and Denmark (Greenland). We also consider Iceland as part of our analysis since it receives sea ice exported from the Arctic Ocean through Fram Strait. We define the Central Arctic (CNT) as the region in the middle of the Arctic Ocean over which no country has exclusive economic rights.

## 4.2 Methods

### 4.2.1 Community Earth System Model (CESM)

The CESM1 is a state-of-the-art global Earth System Model characterized by a nominal  $1^\circ$  horizontal resolution in all components (Hurrell et al., 2013). This version of the CESM has been widely used for Arctic sea ice studies and generally performs well in capturing the Arctic mean sea ice state, trend and variability (e.g. Barnhart et al., 2016; DeRepentigny et al., 2016; England et al., 2019; Jahn et al., 2016; Labe et al., 2018; Smith and Jahn, 2019; Swart et al., 2015). Although this study only uses a single Earth System Model, it uses two ensembles from that model, allowing for an assessment of scenario differences while considering internal variability uncertainties. Furthermore, a good representation of present-day sea ice properties has been shown to be critical for future projections of summer sea ice conditions (Massonnet et al., 2012), making the CESM an excellent choice for this type of analysis. Note however that results presented here are closely tied to the simulated atmospheric circulation response to future climate forcing in the Arctic, something that varies across climate models and is still an active area of research (Budikova, 2009; Zappa et al., 2018).

To investigate the impact of different future emissions scenarios on the projections of ice exchange between the different EEZs of the Arctic, we use two ensembles of the fully-coupled climate simulations from the CESM1. The CESM Large Ensemble (CESM-LE; Kay et al., 2015) includes 40 individual ensemble members that differ only by round-off level differences in the initial air temperature field (order of  $10^{-14}$  K). These large ensemble simulations follow the historical forcing from 1920 to 2005 and the business-as-usual Representative Concentration Pathway 8.5 (RCP8.5; Jones et al., 2013) emissions scenario from 2006 to 2100 (Figure 4.2a,b). We also use the CESM ensemble simulations following the  $2^\circ\text{C}$  target low warming scenario (CESM-LW; Sanderson et al., 2017). These  $2^\circ\text{C}$  target low warming simulations, along with similar experiments using a target of  $1.5^\circ\text{C}$  and an overshoot scenario that temporarily exceeds  $1.5^\circ\text{C}$ , were designed to inform assessment of impacts at 1.5 and  $2^\circ\text{C}$  above pre-industrial levels following the Paris Intergovernmental Panel

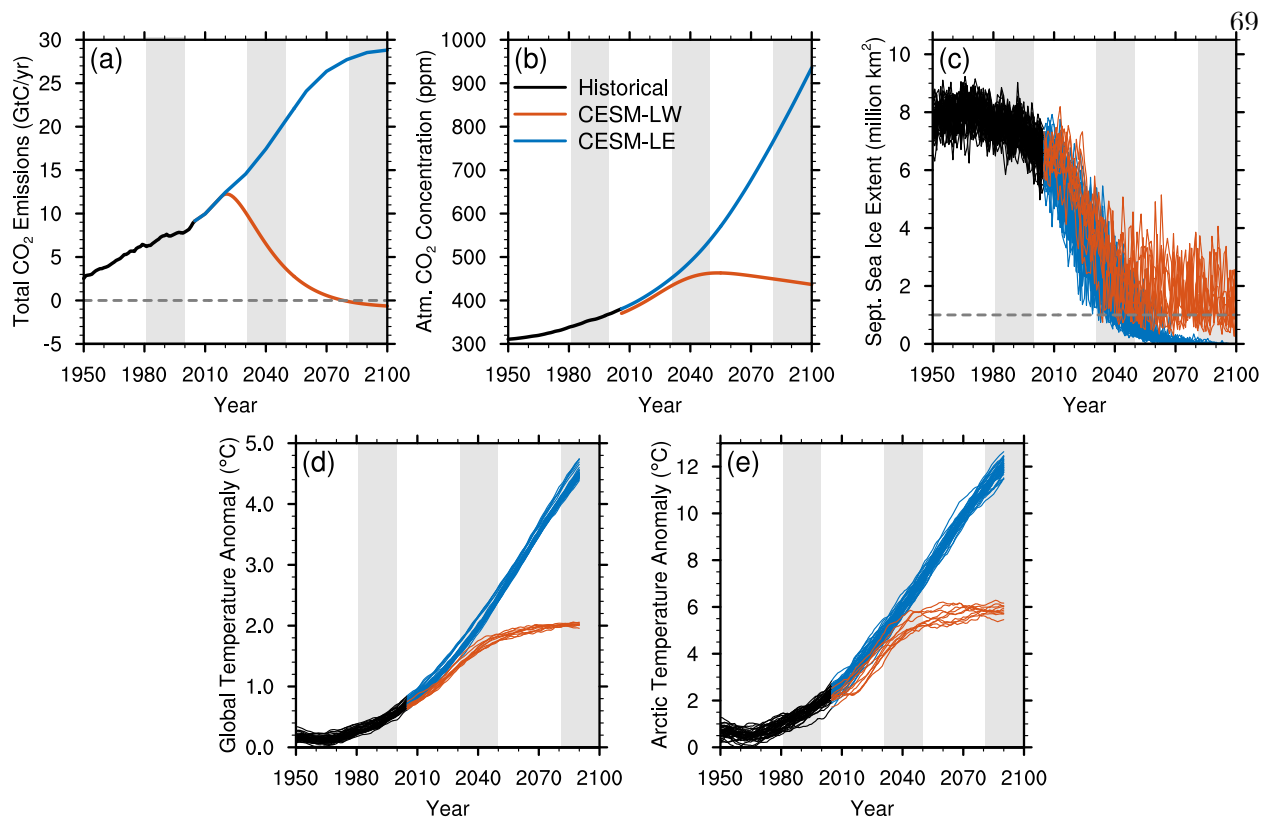


Figure 4.2: Time evolution of (a) the total CO<sub>2</sub> emissions in GtC/yr, (b) the atmospheric CO<sub>2</sub> concentration in ppm, (c) the September Arctic sea ice extent in million square kilometers for all ensemble members with the threshold for a nearly ice-free Arctic shown by the grey dashed line, (d) the 20-year running mean annual-mean global temperature anomalies for all ensemble members (relative to pre-industrial levels, taken as 1850–1920 here) and (e) the 20-year running mean annual-mean Arctic temperature anomalies for all ensemble members. All panels cover the historical period of the CESM-LE (black), the future RCP8.5 scenario of the CESM-LE (blue) and the future low warming scenario of the CESM-LW (orange). Note the different range of the y-axis for (d) the global temperature anomalies and (e) the Arctic temperature anomalies. The grey shaded areas highlight the three different time periods our analysis focuses on (adapted from Figure S1 of Jahn, 2018).

on Climate Change (IPCC) Agreement of December 2015 (Sanderson et al., 2017; UNFCCC, 2015). The simulations are branched from the first 11 ensemble members (001-011) of the CESM-LE in 2006, after which they follow an emissions scenario designed so that the multi-year global mean temperatures never exceed 2°C above pre-industrial levels (Figure 4.2d). Emissions follow the RCP8.5 scenario from 2006 to 2017, after which they start declining rapidly (Figure 4.2a), such that emissions in 2042 are half of the 2017 levels (Sanderson et al., 2017). This low warming

scenario requires a negative emissions phase in order to stay below the 2°C warming target, with combined fossil fuel and land use carbon emissions crossing net zero in 2078 (Figure 4.2a). Note that we take the mean of each ensemble to represent the model response to radiative forcing, and the spread about the mean to represent the internal variability within each scenario ensemble.

From all ensemble simulations, we use the  $u$  and  $v$  components of the sea ice velocity field as well as sea ice concentration (*aiice*), at a monthly time resolution. Each variable is interpolated onto the 25 km Equal-Area Scalable Earth Grid (EASE-Grid; Brodzik et al., 2012) in order to conserve sea ice area during the tracking process (see section 4.2.2 for more details on the ice tracking system). While the CESM-LE also provides sea ice concentration at a daily time resolution for the entire length of the simulation, the  $u$  and  $v$  components of the sea ice velocity field are only available at a 6-hourly time resolution for three periods varying from 10 to 15 yr between 1920 and 2100. In addition, the CESM-LW only provides these variables available at a monthly resolution, which does not allow for an analysis at a higher temporal resolution for this scenario. The effect of the time resolution on our analysis has been tested by comparing weekly and monthly averages for the CESM-LE, and the results show no major change to the conclusions presented here (see Figures S4.1 and S4.2 in the supporting information for more details).

In this study, the CESM analysis is separated into three time periods of 20 yr, separated equally from the end of the 20<sup>th</sup> century to the end of the 21<sup>st</sup> century: (1) 1981 to 2000, (2) 2031 to 2050 and (3) 2081 to 2100. Each period captures a different regime of the transition toward a seasonally ice-free Arctic (see Figures 4.2c and 4.3 for context), allowing us to assess the projected evolution of sea ice exchange:

**1981–2000.** Representative of the state of the Arctic at the end of the twentieth century, before the start of the observed series of record low minima in September sea ice extent of under six million km<sup>2</sup> (can be compared to the pre-2000 period used in Newton et al., 2017);

**2031–2050.** Representative of a thin and dynamic ice pack, mostly consisting of first-year ice except for the region north of Greenland and the Canadian Arctic Archipelago (Figure

4.3b,c);

**2081–2100.** Representative of a fully seasonal ice cover for the CESM-LE, with a nearly ice-free Arctic over three to five months for all 40 ensemble members (Figure 4.2c), and nearly ice-free summers for a maximum of one month every few years for the CESM-LW due to less sea ice loss (Jahn, 2018).

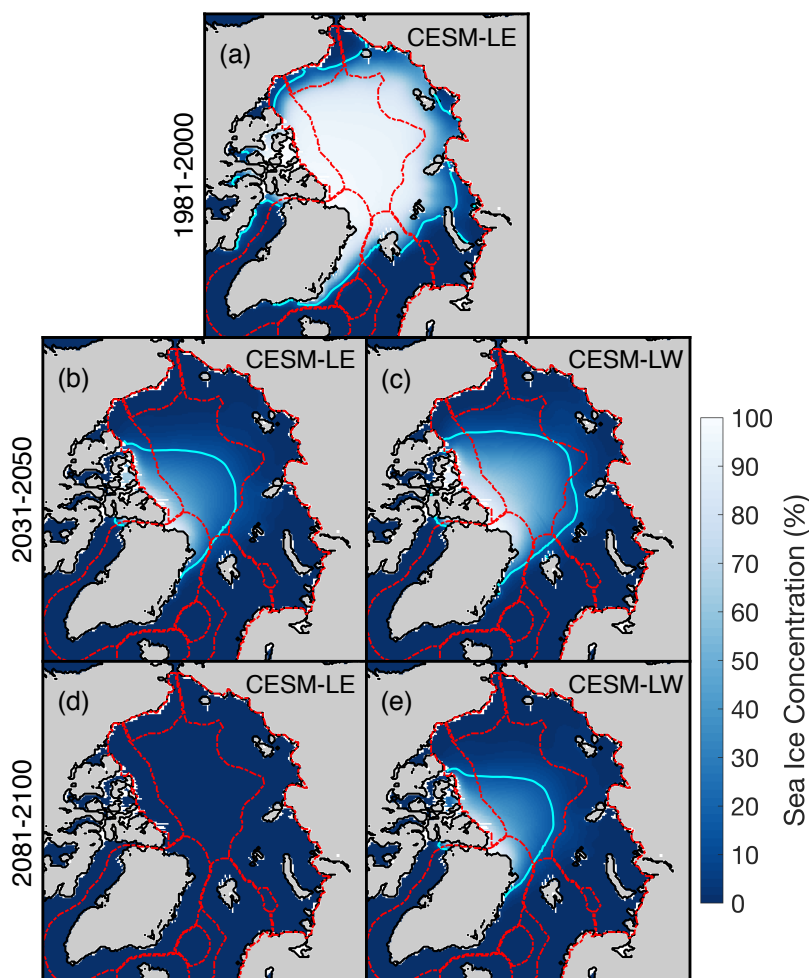


Figure 4.3: Average September sea ice concentration for the CESM-LE over the period of (a) 1981–2000 as well as for (b, d) the CESM-LE and (c, e) the CESM-LW over the periods of (b, c) 2031–2050 and (d, e) 2081–2100. The borders of the EEZs are indicated by red lines. The cyan line shows the 15% sea ice concentration contour.

In order to provide an assessment of the performance of the CESM in simulating sea ice transport between EEZs, we also analyze the CESM-LE over the 20-yr period between 1989 and

2008 and compare it with observational data (section 4.7.2 in the supporting information). This period is slightly shifted compared to the first period of the CESM analysis due to a low bias in satellite-derived drift vectors prior to 1989 (section 4.7.1 in the supporting information). We use data from the National Snow and Ice Data Center’s (NSIDC) Polar Pathfinder project (Tschudi et al., 2016) and the National Oceanic and Atmospheric Administration (NOAA)/NSIDC Climate Data Record (Meier et al., 2017; Peng et al., 2013). We find that the exchange of transnational ice between the different EEZs of the Arctic simulated by the CESM-LE over the period of 1989–2008 is in good general agreement with observations. The small differences between the CESM-LE and observations can be attributed to a bias in the simulated atmospheric circulation over the Arctic during the ice-covered season and the resulting sea ice circulation anomalies (see section 4.7.2 for more details).

#### **4.2.2 Sea Ice Tracking Utility (SITU)**

We use a Lagrangian approach to better understand the potential connections between the Arctic states through the sea ice they exchange. To that end, we use a Lagrangian tracking software called the Sea Ice Tracking Utility (SITU, <http://icemotion.labs.nsidc.org/SITU/>), formerly known as the Lagrangian Ice Tracking System (LITS; DeRepentigny et al., 2016; Williams et al., 2016; Brunette et al., 2019), that tracks ice floes from their formation location to where they ultimately melt. This offline approach to Lagrangian modeling uses saved output from preexisting runs of the model and requires significantly less computational resources compared to the transport of online tracers. SITU allows us to obtain a quantitative assessment of the evolution of ice motion by looking at the exchange of sea ice between the EEZs of different Arctic states and how these patterns are predicted to change in the future. This software has been successfully used to track ice floes forward or backward in time (DeRepentigny et al., 2016; Newton et al., 2017; Williams et al., 2016) and is based on a similar approach that has been widely used to track ice age over several years (Fowler et al., 2004; Maslanik et al., 2007; Pfirman et al., 2004; Rigor and Wallace, 2004).

In the present analysis, SITU is used to track ice area. This requires all of the output

variables to be interpolated to an equal-area grid for the area to be conserved during the tracking process. Note that this method does not aim to fully capture sea ice physics, as it does not track ice volume and uses data at a 25 km resolution. Nonetheless, tracking independent parcels of ice area provides some information on the effect of sea ice convergence, as SITU allows for multiple tracked ice parcels to stack up in the case of convergent flow. This approximates a rise in ice thickness through ridging by increasing the number of tracked areal parcels of ice over a specific location. For this study, we analyze transnational ice exchange in terms of areal flux rather than the areal flux divided by the area covered by each EEZ, as this is more representative of the potential risk for ice-rafted contaminant transport.

First, for every month considered within the analysis, the location of newly formed ice floes is identified. A newly ice-covered grid cell can either be the product of ice formation (freezing) or advection of ice from a nearby location. In order to dissociate the thermodynamic signal from the dynamic signal, we select all grid points along the ice edge (defined as the 15% ice concentration contour), track them forward in time for one month using the sea ice velocity at each grid point along the ice edge, and compare the result with the sea ice edge of the following month. Every grid cell outside of the tracked ice edge that was not covered by ice initially but is ice covered the following month is then considered a new ice parcel (referred to hereafter as an ice formation event). Next, all ice formation events are fed to SITU, which advects each newly formed ice parcel forward in time with a monthly resolution until it ultimately melts, creating a record of ice tracks. An ice parcel is considered to have melted when it is advected to a location that is ice free when compared with the ice concentration field of that month. Melt (and formation explained above) is defined using a sea ice concentration threshold of 15%. The transition between ice and open water is usually abrupt and our results show no sensitivity to the exact choice of cut-off value (not shown).

Using time-averaged velocities (monthly averages in the case of the analysis presented here) can result in floes being advected over land (either an island or the continent) by SITU instead of piling up along the coast. To avoid unrealistic loss of ice floes over land within SITU, we move

the affected parcels back to the last ocean grid cell they crossed prior to reaching land, following a linear trajectory between their initial position and their position after one time step. These parcels continue to be tracked normally, subject to the dynamics of their new location as if they had simply piled up along the coast.

In what follows, we analyze what we refer to as “transnational” sea ice, ice that leaves the EEZ in which it formed, as distinguished from “domestic” ice that melts in the same EEZ where it formed. We also refer to the fraction of transnational ice exchange, defined as the ratio of the areal flux of transnational sea ice to the total areal flux of sea ice, transnational and domestic combined.

## 4.3 Results

### 4.3.1 Increase in Transnational Ice Exchange

Over the last 20 yr of the twentieth century, Russia dominates in terms of formation of transnational ice (74.8% of the total areal flux of transnational ice originates from Russia) and the majority of transnational Russian ice gets exported to Norway (Figure 4.4a), in general agreement with observations (see section 4.7.2 in the supporting information or Newton et al., 2017). Using SITU, we find an increase in the area of ice formed each year from  $1.4 \times 10^6$  km<sup>2</sup>/yr in 1981–2000 for the CESM-LE to between  $4.6$  and  $5.3 \times 10^6$  km<sup>2</sup>/yr in 2031–2050 for the CESM-LW and the CESM-LE, respectively. This large increase in ice formation is accompanied by an increase in the amount of transnational ice exchanged between the different EEZs by midcentury. In fact, the total average areal flux of transnational ice in the Arctic increases by 252% for the CESM-LE and 204% for the CESM-LW between the periods of 1981–2000 and 2031–2050 (Figure 4.4b, c).

The main reason for this large increase in transnational ice flux from 1981–2000 to 2031–2050 is the poleward expansion of the seasonal ice zone (SIZ), defined as the area between the minimum and maximum sea ice extents, due to a continued rise in simulated Arctic temperatures (Figure 4.2e). By midcentury, under both scenarios, the area of annual sea ice formation expands from the peripheral seas to almost the entire Arctic Ocean (Figure 4.5a–f). Over the period of 2031–2050,

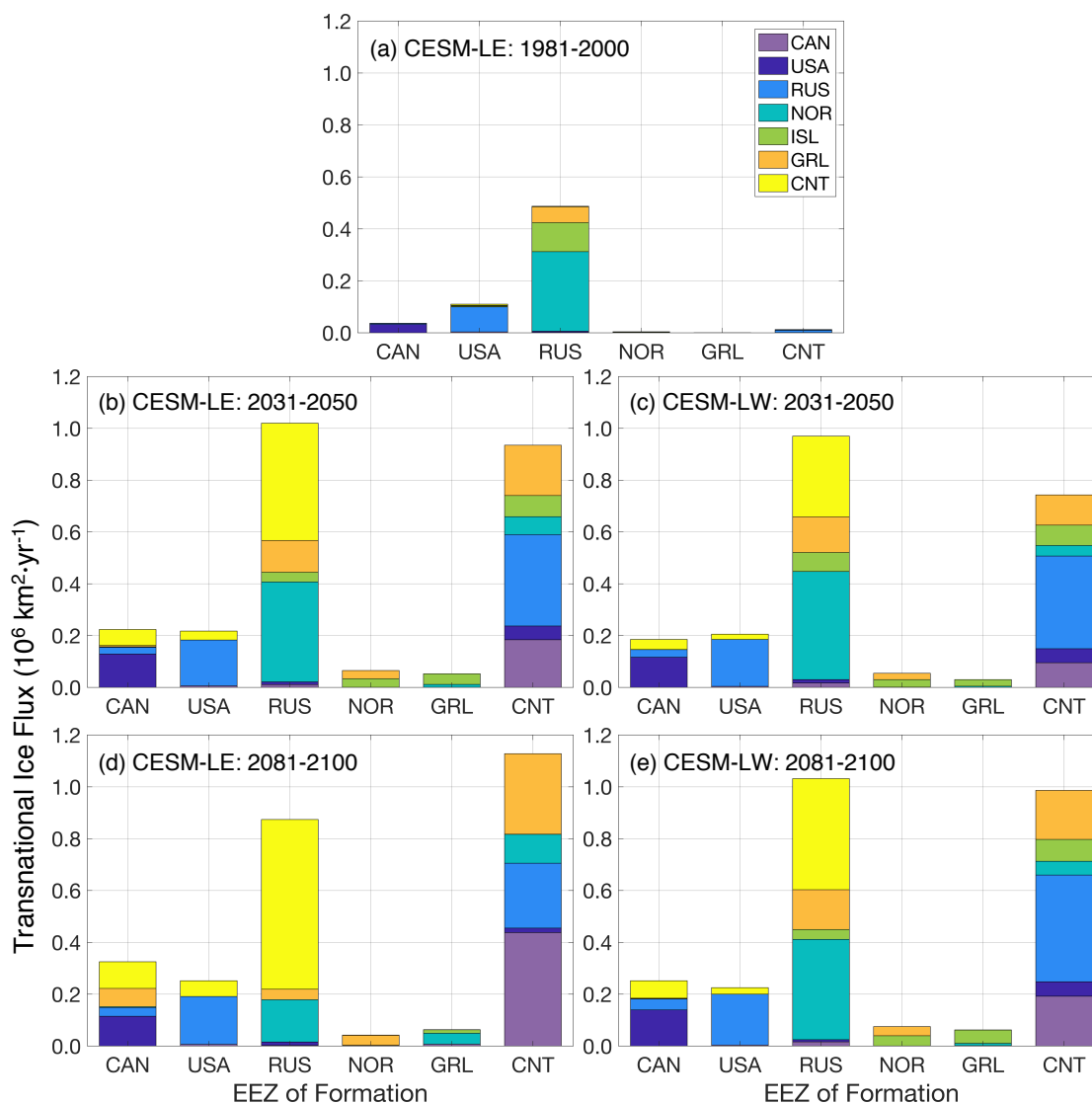


Figure 4.4: Annual mean average areal flux of transnational ice for the CESM-LE over the period of 1981–2000 (a) and for the CESM-LE (b, d) and the CESM-LW (c, e) over the periods of 2031–2050 (b, c) and 2081–2100 (d, e). The height of each colored portion within one bar represents the annual mean areal flux of ice between the EEZ of formation ( $x$  axis) and the EEZ of melt (color). Note that domestic ice is not included in this figure in order to focus on the features of transnational ice exchange. The average amount of ice area exchanged between all EEZs, including domestic ice, for both experiments as well as a statistical assessment of the pathways that are significantly different between the CESM-LE and the CESM-LW can be found in Tables S4.1 and S4.2 in the supporting information.

the spatial differences in ice formation between the CESM-LE and the CESM-LW are small (Figure 4.5c–f), with slightly more extensive ice formation over the Central Arctic for the CESM-LE in the fall due to lower average September sea ice extent (Figures 4.2c and 4.3b, c). By midcentury, only

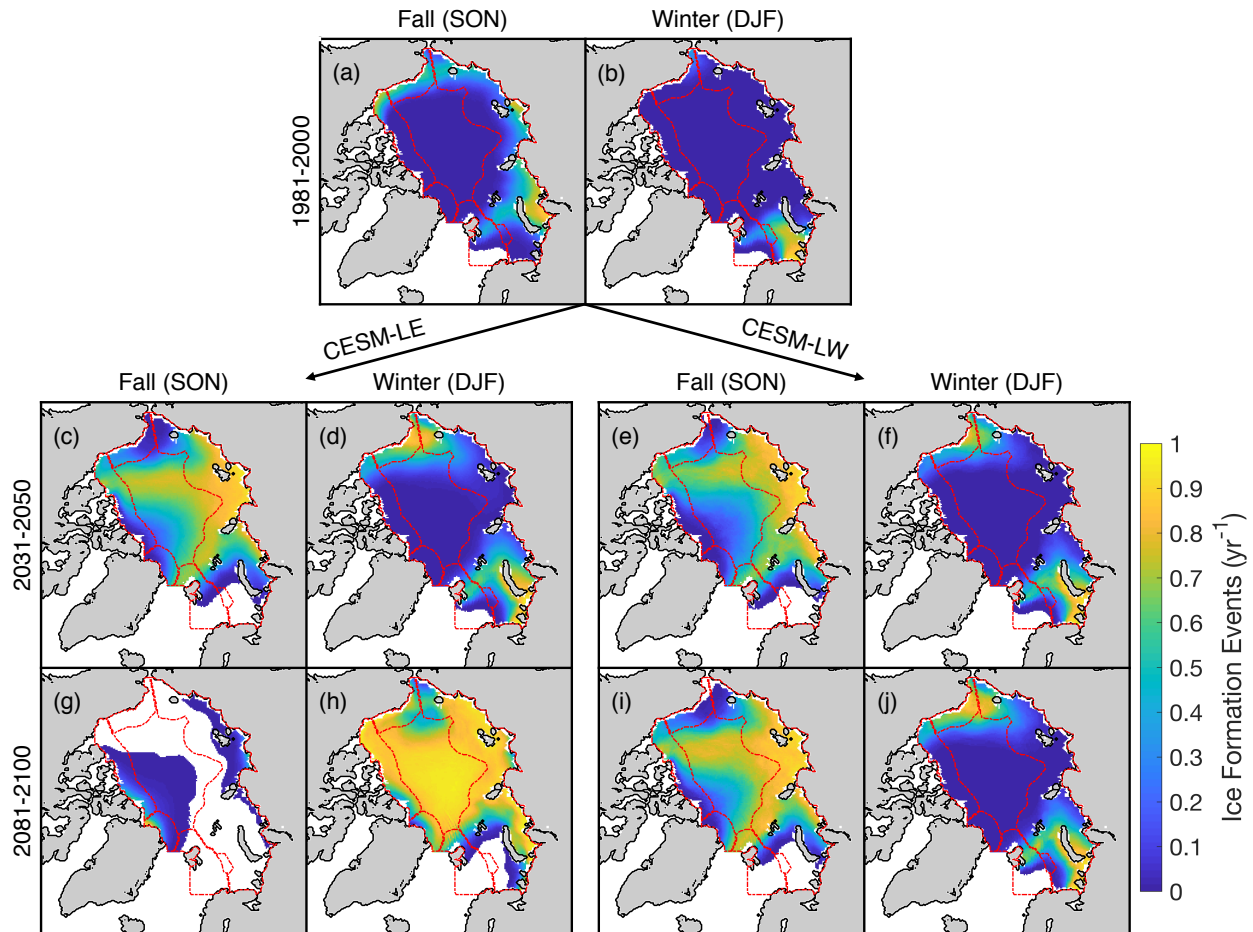


Figure 4.5: Average number of ice formation events per year in fall (SON) and winter (DJF) for the CESM-LE over the period of 1981–2000 (a, b) and for the CESM-LE (c, d, g, and h) and the CESM-LW (e, f, i, and j) over the periods of 2031–2050 (c–f) and 2081–2100 (g–j)]. Only grid cells that are ice covered for at least one month during the specified season and time period and for a least one ensemble member are colored. The borders of the EEZs are indicated by red lines. Only ice floes that formed and melted between the specified time periods are considered.

the region north of Greenland and the Canadian Arctic Archipelago survives the summer melt (Figure 4.6c–f) and is reliably ice covered in September (Figure 4.3b, c). The increase in the area of the SIZ by 2031–2050 allows for more ice to be formed each year and to melt in a different EEZ than the one where it initially formed.

Another key feature of the future projections of sea ice transport is that by midcentury, Russia and the Central Arctic strongly dominate the exchange of transnational ice in the Arctic. The areal flux of transnational ice originating from Russia doubles by midcentury, and for the Central Arctic

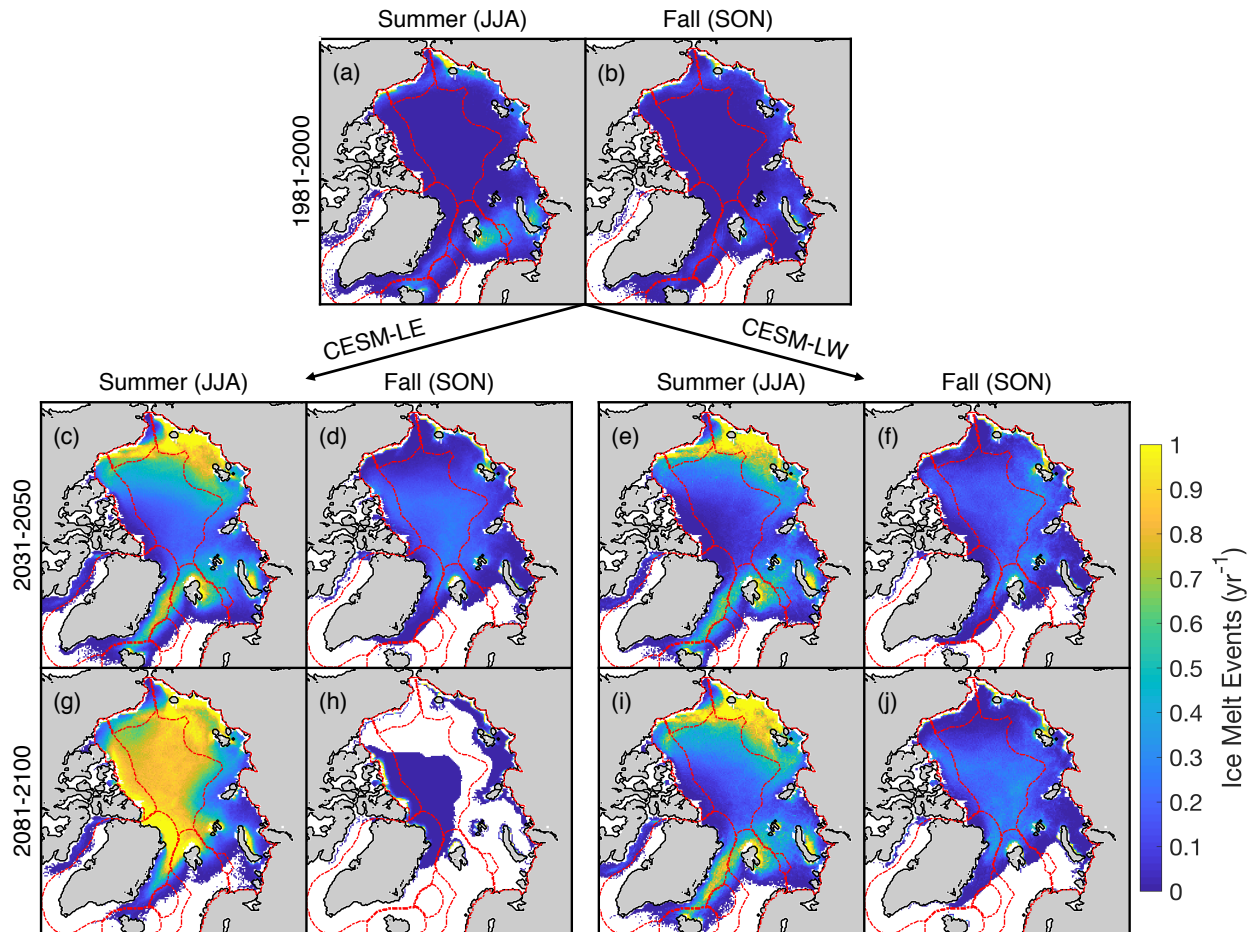


Figure 4.6: As in Figure 4.5, but for the average number of ice melt events per year in summer (JJA) and fall (SON).

it increases from less than 13 thousand  $\text{km}^2/\text{yr}$  to just below one million  $\text{km}^2/\text{yr}$  for the CESM-LE (Figure 4.4a, b). The increase in Russian transnational ice is predicted to occur as the whole area of the Russian EEZ becomes a source and a sink of sea ice in 2031–2050 (Figures 4.5c,e and 4.6c, e), whereas formation and melt is limited to its coastal regions in 1981–2000 (Figures 4.5a and 4.6a). This larger area of sea ice loss in the summer months could potentially promote economic activities in the Russian EEZ and increase the risk of ice-rafted contaminant transport (Newton et al., 2016; Pfirman et al., 1995). As for the Central Arctic, it accounts for 37.2% of the total formation of transnational ice area in 2031–2050 for the CESM-LE (Figure 4.4b), up from less than 2% in 1981–2000 (Figure 4.4a). In addition to becoming an important source region for transnational ice, the

Central Arctic also becomes an important sink, with the percentage of transnational ice melting in this region increasing from 1.1% in 1981–2000 to 21.8% in 2031–2050 for the CESM-LE (Figure 4.4a,b). This can be partly explained by the fact that ice formation/melt is present over most of the Central Arctic by midcentury (Figures 4.5c,e and 4.6c,e), whereas there is little to no ice formation/melt over that region in 1981–2000 (Figures 4.5a and 4.6a). The large contribution of Russia and the Central Arctic to the exchange of transnational ice is not surprising considering the surface area covered by these two EEZs. Note however that it is the total areal flux of transnational ice, not the flux per unit area, that best represent the extent of potential ice-rafted contaminant transport (Newton et al., 2017).

### 4.3.2 Impact of the Future Emissions Scenario

The difference in the response of sea ice transport to the two future emissions scenarios becomes more apparent toward the end of the 21<sup>st</sup> century. Over the last 20 yr of the twentieth century, ice formation and melt peak in October and August, respectively (Figure 4.7a,b). There is a large increase in the total annual amount of areal ice formation and melt by 2031–2050, with the peak in ice formation shifting from October to November for both future emissions scenarios (Figure 4.7c,d). Large differences in the ensemble mean ice formation and melt between the CESM-LE and the CESM-LW are projected by 2081–2100. The ensemble mean represents the best estimate of the forced response to the future emissions scenario, while the spread about the mean is used to assess the confidence of that forced response based on the internal variability of the climate system. The ensemble mean of the CESM-LE has ice formation and melt peak in January and July respectively by the end of the century, compared to November and August for the CESM-LW (Figure 4.7e,f), much more similar to present-day conditions. In addition, the annual cycles of ice formation and melt for the CESM-LE and the CESM-LW are statistically different at the 95% confidence level in 2081–2100 during all months of the growing and melting seasons, respectively. Compared to the period of 1981–2000, the length of the ice-covered season (defined here as the number of months from the peak in ice formation to the peak in ice melt) is predicted to decrease by one month

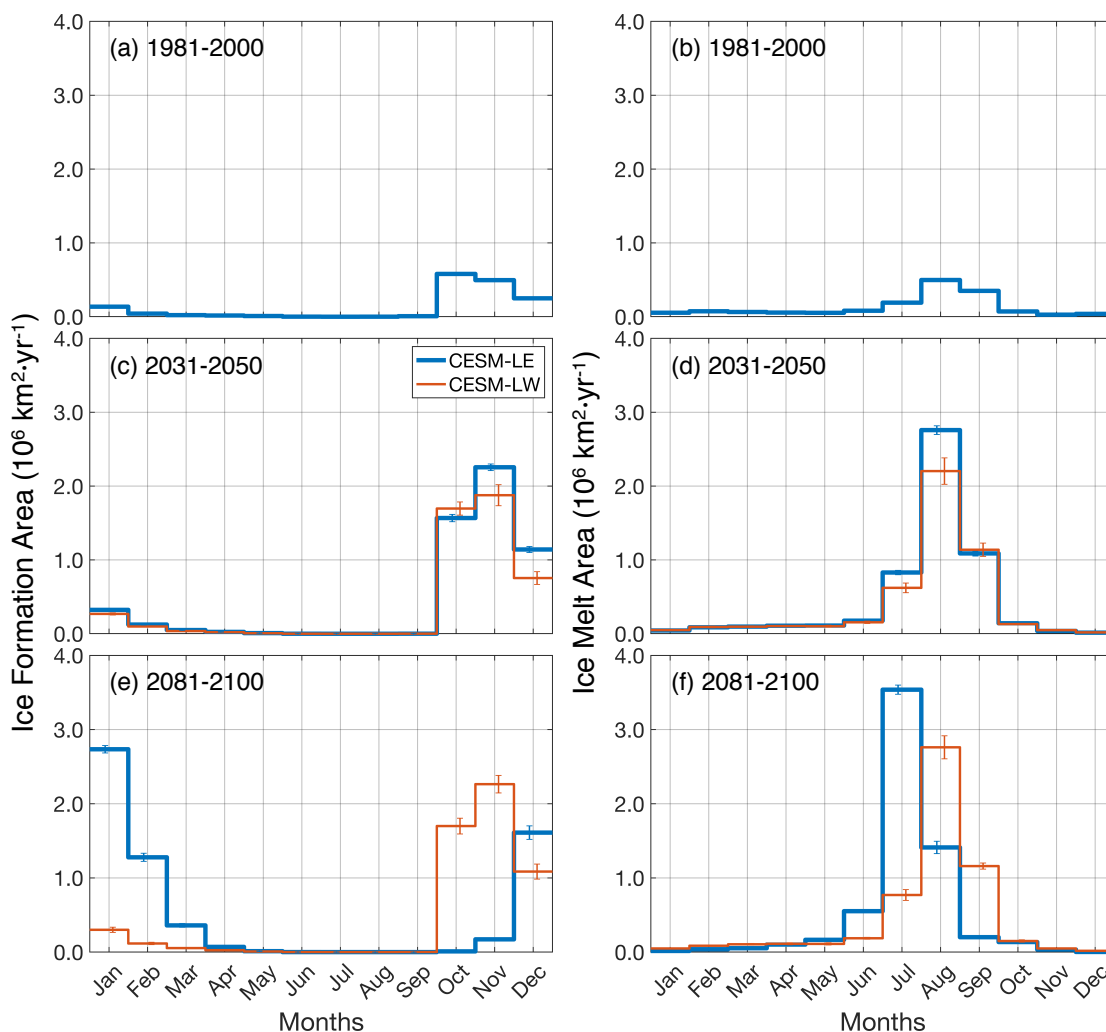


Figure 4.7: Annual cycle of areal ice formation [*left*] and melt [*right*] for the periods of 1981–2000 (a,b), 2031–2050 (c,d) and 2081–2100 (e,f) in the CESM-LE [*blue*] and the CESM-LW [*orange*]. The error bars show the 95% confidence intervals of the 20-year averaged ice formation/melt area for each month across the 40 ensemble members of the CESM-LE and the 11 ensemble members of the CESM-LW. Only ice floes that formed and melted between the specified time periods are considered.

for the CESM-LW and four months for the CESM-LE by 2081–2100 when looking at the forced signal. By the end of the 21<sup>st</sup> century, earlier ice formation as well as later melt in the CESM-LW gives more time for ice floes to transit the Arctic before the start of the melt season compared to the CESM-LE, which has a shorter ice-covered season. In turn, longer travel times allow for larger traveled distances, promoting transnational ice exchange in the CESM-LW compared to the CESM-LE. Note that the annual formation and melt cycles of the CESM-LW over the period of

2081–2100 are very similar to the ones of the CESM-LE in 2031–2050, pointing to a stabilization of the sea ice response under the low emissions scenario around midcentury climate when atmospheric CO<sub>2</sub> starts to slowly decline (Figure 4.2b).

Spatial differences in ice formation and melt between the two future emissions scenarios also manifest at the end of the 21<sup>st</sup> century. By 2081–2100, the ice formation season shifts from fall (SON) to winter (DJF) everywhere in the Arctic for the CESM-LE, as freezing starts and ends later in the year (Figures 4.5g,h and 4.7e; see also Smith and Jahn, 2019). For the CESM-LW on the other hand, most of ice formation still occurs in the fall (Figures 4.5i and 4.7e), with the exception of parts of the Barents, Kara, Beaufort and Chukchi Seas (Figure 4.5j). Moreover, melt occurs over the whole Arctic basin in summer only for the CESM-LE (Figure 4.6g,h), which simulates a nearly ice-free Arctic for several months each year by the late 21<sup>st</sup> century (see also Jahn, 2018). For the CESM-LW, melt still occurs in the fall north of Greenland and the Canadian Arctic Archipelago and into the Central Arctic in the late 21<sup>st</sup> century (Figure 4.6j), similar to midcentury conditions in the CESM-LE (Figure 4.6d). As a result, there is a longer portion of the year when the Arctic is fully ice covered in the CESM-LW, allowing more time for ice floes to move around and increasing the amount of ice exchanged between the different EEZs.

The CESM also projects a large reduction in the average amount of time necessary for sea ice to transit from one EEZ to another by 2031–2050, especially for long pathways that are characterized by an average transit time of more than two years in 1981–2000 (Figure 4.8). This decrease in transit times is related to the poleward expansion of the SIZ, which acts to melt a larger area of ice each summer and greatly reduce the number of multi-year transit pathways, in combination with an increase in ice drift speed, especially in the winter months (not shown; see also Tandon et al., 2018). The increase in ice drift speed is mainly associated with a decrease in ice thickness as we find no significant change in the average wind speed over the Arctic throughout the 21<sup>st</sup> century (not shown). By 2081–2100, all exchange pathways have average transit times of less than one year for the CESM-LE (Figure 4.8). This is the result of a seasonal ice cover over the whole Arctic basin, which prevents the formation of multi-year ice in all of the 40 ensemble members and does

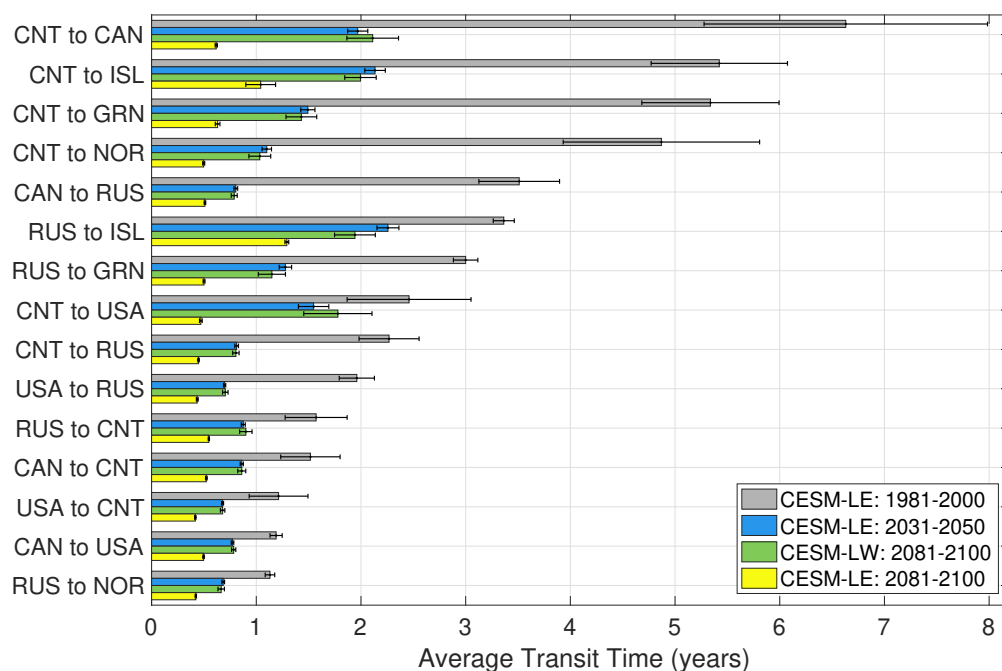


Figure 4.8: Average transit time in years for the 15 pathways exchanging the largest areal flux of transnational ice throughout all three time periods and both experiments. The error bars show the 95% confidence bounds of the 20-year averaged transit time for the 40 ensemble members of the CESM-LE and the 11 ensemble members of the CESM-LW.

not allow for transit times longer than one year. On the other hand, the CESM-LW shows transit times in 2081–2100 that are similar to those of the CESM-LE in 2031–2050 (Figure 4.8), again pointing to a stabilization of the sea ice response to the reduced atmospheric  $\text{CO}_2$  concentration in the CESM-LW scenario toward the end of the century (Figure 4.2b). Note that transit times for all exchange pathways for the CESM-LW by 2081–2100 are statistically different from 1981–2000 transit times at the 95% confidence level, except for ice forming in the Central Arctic and melting in the United States (Figure 4.8). Moreover, for the period of 2081–2100, all transit time differences between the CESM-LE and the CESM-LW are statistically significant.

As the melt season is projected to get longer and average transit times shorten to less than one year for the CESM-LE by the end of the 21<sup>st</sup> century, long-distance ice transport pathways are predicted to diminish in favor of ice exchanged between neighboring EEZs, specifically the ones downstream of each EEZ of formation following the general Arctic sea ice circulation. As a result,

the diversity of EEZs of melt for each EEZ of formation is reduced for the CESM-LE compared to the CESM-LW in 2081–2100, especially for Russia and the Central Arctic where the largest amount of transnational ice originates (Figure 4.4d,e). This implies a continuation in the future of the negative trend in Siberian shelf ice reaching Fram Strait since the beginning of the 21<sup>st</sup> century recently found by Krumpfen et al. (2019). Note that for all exchange pathways over the period of 2081–2100, only the flux of ice from Canada to Russia, from the United States to Russia and from Norway to Greenland (i.e., relatively short-distance downstream fluxes) are not statistically different between the CESM-LE and the CESM-LW at the 95% confidence level. By 2081–2100, consistent nearly ice-free summers in the CESM-LE act to reduce the fraction of transnational ice exchange (as defined in section 4.2.2), whereas the CESM-LW continues to see an increase. Indeed, the fraction of transnational ice exchange grows from 46% to 48% to 49% for the CESM-LW throughout the three time periods of interest, whereas it initially increases from 46% to 47% between the first two time periods for the CESM-LE, but then reduces to 44% by the end of the 21<sup>st</sup> century. Note that the fractions of transnational ice exchange are statistically different from each other at the 95% confidence level between the three time periods only for the CESM-LE. It is important to note that even though the fraction of transnational ice exchange decreases for the CESM-LE between 2031–2050 and 2081–2100, the total areal flux of transnational ice increases slightly over the same period. Nonetheless, this result points to the fact that when the Arctic reaches nearly ice-free conditions and the SIZ covers the full Arctic Ocean, increases in the melt season length associated with continuously warmer Arctic temperatures (Figure 4.2e) will eventually act to reduce the absolute amount of transnational ice exchange, reversing the trend predicted by the CESM-LE over the 21<sup>st</sup> century.

#### 4.4 Discussion

In this contribution, we show that as the SIZ expands the amount of sea ice formed each year increases greatly by midcentury, leading to an increase of more than 200% in the area of sea ice exchanged between the different regions of the Arctic. This increase in transnational ice

exchange amplifies the potential for ice-rafted contaminant transport, raising environmental risks and accentuating emergent political tensions as the Arctic states are effectively brought into closer contact with each other (Arctic Council, 2009; Emmerson and Lahn, 2012; Newton et al., 2016; Pfirman et al., 1995). A prominent example is the export of ice from Russia to Norway. A heated debate persists in Norway about whether their regulations of offshore drilling, which are some of the most extensive in the world, are sufficient. However, our study indicates that the main risk for Norway in the next few years might be from Russian oil spills, since about 400,000 km<sup>2</sup> of ice transit from the Russian to the Norwegian EEZ annually by midcentury. In addition, our results show that the trajectory of future greenhouse gases emissions will have a high impact on export of ice from Russia to Norway, as the low emissions scenario predicts a similar amount of ice transit by 2100 as midcentury conditions, compared to a reduction by more than half under the high emissions scenario.

Pollutants of primary concern in the Arctic are organochlorines, heavy metals, radionuclides and oil (Pfirman et al., 1995), which can take years to biodegrade in the Arctic due to the cold Arctic waters (Fingas and Hollebone, 2003). While freezing ejects many dissolved contaminants found in sea water, ice formed in shallow regions (< 50 m) of the Siberian seas has been shown to entrain sediments and organic material (Smedsrud, 2001, 2002) and hence also incorporates associated contaminants. After several years of transport, due to annual surface melting and ablation, a concentrated lag deposit of sediment, organic material and/or contaminants can form on the surface of the ice (Pfirman et al., 1995; Tremblay et al., 2015). Although some contaminants are lost in meltwater runoff, other pollutants are also added from atmospheric deposition of Arctic haze (Octaviani et al., 2015). Furthermore, potential oil spills or shipping accidents can also add contaminants on the ice surface (Fingas and Hollebone, 2003; Glickson et al., 2014; Izumiyama et al., 2004; Venkatesh et al., 1990; Wilkinson et al., 2017). As a result, the majority of ice-rafted pollutants are released when the entire floe melts despite differences in their sources (Pfirman et al., 1995).

Based on our analysis of sea ice transport between the different EEZs of the Arctic, a little

more than half of the ice melts in the same EEZ where it formed, meaning that a large part of the contaminants introduced into sea ice will be released within the same EEZ (Newton et al., 2017). However, we find that due to a large increase in the area of sea ice formed every year, the absolute amount of transnational ice exchanged between the different Arctic nations increases by a factor of 3 between the end of the 20<sup>th</sup> century and the middle of the 21<sup>st</sup> century. As such, the potential for sea ice to carry contaminants is greatly amplified. The doubling of transnational ice originating from the Russian EEZ by midcentury is of especially high relevance given that most of the Russian EEZ consists of shallow seas where contaminants can be easily incorporated during sea ice formation. In addition, the prospect of undiscovered oil and gas on the Siberian shelves (Bird et al., 2008) and the increase in shipping activities along the Northern Sea Route (Aksenov et al., 2017; Ostreng et al., 2013; Schøyen and Bråthen, 2011; Stephenson et al., 2013) will amplify the risk of pollutants being introduced in these shallow Arctic waters.

The opening of the Central Arctic is also of high significance given the prospect for commercial ships to use the Transpolar Sea Route in order to avoid crossing the EEZ of several Arctic states (Stephenson et al., 2013), increasing the risk of accidental release of contaminants onto sea ice. The lack of risk management policies regulating the release of pollutants in these international waters combined with a short operational season, large distances to ports and other infrastructure, and the generally challenging Arctic environment will likely make this region very vulnerable to long-term contamination. Compared to the Russian shelf seas, the Central Arctic covers mostly deep waters, so contamination of surface waters by oil spills and atmospheric deposition of black carbon and other emissions are likely the main concerns for this region.

## 4.5 Conclusions

In this study, we have addressed the question: “How will the exchange of transnational sea ice evolve in the future?”, using two ensemble experiments of the CESM that range from 2°C to over 4°C of global warming by 2100. We find a large increase in the area of transnational ice exchanged in the Arctic throughout the 21<sup>st</sup> century, continuing the trend reported by Newton et al. (2017)

over the observational period. The CESM captures the exchange of transnational ice in the Arctic well when compared to satellite observations over the 1990s and 2000s, with a few disagreements that can be attributed to a bias in the simulated atmospheric circulation over the Arctic during the ice-covered season. When looking at future projections, we found that the CESM projects the largest increase in the amount of transnational ice exchange between the end of the 20<sup>th</sup> century and the middle of the 21<sup>st</sup> century, under both forcing scenarios. This increase is associated with the expansion of the SIZ from the peripheral seas toward the middle of the Arctic Ocean, as global and Arctic temperatures continue to rise. The expansion of the SIZ in 2031–2050 allows for more ice to be formed each year which, combined with a decrease in the average time it takes for an ice floe to go from one EEZ to another, acts to promote transnational ice exchange in the Arctic.

The increase in transnational ice exchange by midcentury and until 2100 is not uniform everywhere in the Arctic, but is dominated by Russia and the Central Arctic as they include a large fraction of the SIZ. We find that by 2031–2050, 78% of transnational ice originated from these two regions, while also accounting for 44% of the melt of transnational ice in the CESM-LE. Long exchange pathways that are characterized by an average transit time of more than two years in 1981–2000 see a large reduction in travel time as less ice transits along these routes, with all pathways exchanging ice in two years or less by midcentury. We also find that differences in the forced sea ice response to a high versus low emissions scenario become most apparent toward the end of the 21<sup>st</sup> century. By 2081–2100, the CESM-LW has a longer ice-covered period than the CESM-LE, due to earlier ice formation and later ice melt. This gives ice floes more time to travel from one EEZ to another before the start of the melt season, promoting transnational ice exchange in the CESM-LW. Indeed, we find that all exchange pathways have average transit times of one to two years for the CESM-LW that persist through 2081–2100, similar to midcentury transit times for both scenarios. By comparison, average transit times are all less than one year for the CESM-LE by 2081–2100 due to consistent nearly ice-free summers of three to five months for all 40 ensemble members (Jahn, 2018).

Ice transport along long-distance pathways are predicted to diminish in favor of ice exchange

between neighboring EEZs by the end of the 21<sup>st</sup> century under the high emissions scenario, specifically shifting to the EEZs downstream of each EEZ of formation. This is the result of a projected lengthening of the melt season, which decreases average transit times to less than one year for the CESM-LE, continuing the trend recently reported by Krumpfen et al. (2019) and Newton et al. (2017). In fact, the CESM-LE shows a decrease in the fraction of transnational ice exchange between the periods of 2031–2050 and 2081–2100, whereas the CESM-LW continues to see an increase. Even though the total areal flux of transnational ice continues to increase slightly for the CESM-LE over the same time window, the decline of the fraction of transnational ice exchange has important implications for transnational ice exchange after 2100. A previous version of the CESM, the Community Climate System Model Version 4 (CCSM4), RCP8.5 simulations and their extension to 2300 show that September ice extent will not recover under this business-as-usual scenario, and March ice extent will continue to decrease and reach nearly ice-free conditions toward the middle of the 23<sup>rd</sup> century (Jahn and Holland, 2013). Our results suggest that the predicted increase in melt season length associated with continuously warmer Arctic temperatures would eventually act to reduce the total amount of transnational ice exchanged between the EEZs of the Arctic, reversing the trend predicted by the CESM over the 21<sup>st</sup> century for all scenarios.

To conclude, our study shows that the characteristics of transnational ice exchange will change dramatically over the 21<sup>st</sup> century, even under a low warming scenario. As a result, the potential for ice-rafted contaminant transport across EEZs will increase greatly in the next few decades. Given the associated societal risks, our results suggest that in order to support risk management strategies for ice-rafted contaminants, more detailed modeling should be undertaken in the future, to simulate specific pollutants. Such a model would have to include exchange and transport of multiple tracers with a surface deposition source for atmospheric aerosols and particulates, sedimentary inclusion for sea ice formed in shallow waters, and a potential for ice-trapped oil from open-water spills.

## 4.6 Acknowledgements

P. DeRepentigny acknowledges the support of the Natural Sciences and Engineering Council of Canada (NSERC), the Fonds de recherche du Québec – Nature et Technologies (FRQNT) and the Canadian Meteorological and Oceanographic Society (CMOS) through PhD scholarships. P. DeRepentigny is also supported by NSERC Discovery Program funds awarded to L. B. Tremblay, NSF-OPP grant 1504348 (PI: A. Jahn, co-PIs: L. B. Tremblay and M. M. Holland), and A. Jahn’s start-up funds from the University of Colorado Boulder. A. Jahn acknowledges support from NSF-OPP grant 1504348 and start-up funds from the University of Colorado Boulder. L. B. Tremblay is grateful for the financial support of the NSERC Discovery Program and the MEOPAR grant “Forecasting Regional Arctic Sea Ice from a Month to Seasons”. This work is a contribution to the Canadian Sea Ice and Snow Evolution (CanSISE) Network funded by the NSERC Climate Change and Atmospheric Research program. R. Newton’s effort on this project has been supported by the National Science Foundation grants NSF-OCE 14-36666 (Arctic GEOTRACES) and NSF-PLR 15-04404 (Dynamics of Freshwater Components). S. Pfirman’s contribution has been supported by the Arizona State University. This project is part of the grant “A Lagrangian approach to emerging dynamics of the marginal ice zone”, lead PI: L. B. Tremblay, co-PIs: S. Pfirman and R. Newton, ONR N00014-11-1-0977, 2011-2016.

We acknowledge the CESM Large Ensemble Community Project and the CESM Low Warming Ensemble Project. The CESM project is supported primarily by the National Science Foundation (NSF). Computing and data storage resources, including the Cheyenne supercomputer (doi:10.5065/D6RX99HX), were provided by the Computational and Information Systems Laboratory (CISL) at NCAR. Model output for the CESM-LE and the CESM-LW is publicly available on the Earth System Grid website at [www.earthsystemgrid.org](http://www.earthsystemgrid.org). The Polar Pathfinder data set is publicly available on the NSIDC website at <http://nsidc.org/data/NSIDC-0116>. The Climate Data Record product is publicly available on the NSIDC website at <http://nsidc.org/data/G02202>. Shapefiles of maritime boundaries and EEZs are publicly available at <http://http://>

[//www.marineregions.org/](http://www.marineregions.org/).

L. B. Tremblay, S. Pfirman and R. Newton conceived the overall research question, starting from the work of S. Pfirman and W. Haxby (deceased) on Lagrangian sea ice tracking. A. Jahn suggested including the low warming scenario in the analysis. L. B. Tremblay, R. Newton and P. DeRepentigny implemented the Sea Ice Tracking Utility (SITU) and computational framework. P. DeRepentigny carried out the experiments and performed the analysis under the supervision of L. B. Tremblay and A. Jahn. P. DeRepentigny took the lead in writing the manuscript. All authors provided critical feedback and collaborated in shaping the research, analysis and final version of the manuscript. We acknowledge comments on an earlier draft by Dr. Clara Deser, Dr. Marika M. Holland, Dr. Jennifer E. Kay and Dr. Walt N. Meier.

## **4.7 Supplementary Material**

### **4.7.1 Observational Datasets**

The National Snow and Ice Data Center’s (NSIDC) Polar Pathfinder project provides sea ice motion vectors on the 25 km EASE-Grid from the beginning of polar-orbiting satellite observations in November 1978 to 2017 (Tschudi et al., 2016). This gridded product is derived through optimal interpolation of observations from the International Arctic Buoy Program (IABP), as well as the Scanning Multichannel Microwave Radiometer (SMMR), the Special Sensor Microwave Imager (SSM/I), the Special Sensor Microwave Imager Sounder (SSMIS), the Advanced Microwave Scanning Radiometer - Earth Observing System (AMSR-E) and the Advanced Very High Resolution Radiometer (AVHRR) sensors. It is complemented with free drift estimates derived from 10 m winds provided by the National Centers for Environmental Prediction and the National Center for Atmospheric Research (NCEP/NCAR) reanalysis dataset where no observations were available. We also use sea ice concentration data derived from passive microwave brightness temperature from the National Oceanic and Atmospheric Administration (NOAA)/NSIDC Climate Data Record (Meier et al., 2017; Peng et al., 2013). It is a product of different algorithms used to combine observations

made by the SMMR, SSM/I and SSMIS sensors, available from late 1978 to 2017.

The Polar Pathfinder and Climate Data Record datasets were previously used in Newton et al. (2017), where a similar analysis of transnational ice exchange over the observational period was performed. Newton et al. (2017) used a weekly time resolution while we here use a monthly resolution to allow for a direct comparison with model data, which is only available at a monthly resolution for one of the two forcing scenarios analyzed here (see section 2.1). The reduction of temporal resolution from weekly to monthly has been shown to lead to an increase of the error in drift distance when compared to buoy data by approximately 45 km (less than two grid cells) after a year of tracking when using the ice tracking system (DeRepentigny et al., 2016). In the context of this study, we find that the flux of transnational ice is reduced slightly towards the end of the 21<sup>st</sup> century for most pathways when going from a monthly to a weekly resolution (Figure S4.2). However, none of the conclusions from this study are affected by the change in time resolution from monthly to weekly.

All observational analyses presented here use satellite-derived sea ice velocity and concentration between January 1989 and December 2008. We begin the analysis in 1989 to avoid earlier satellite-based drift vectors, based on retrievals from the relatively low-resolution SMMR sensor, that exhibit a low bias in sea ice velocity compared to co-located buoy data (Bruno Tremblay, Robert Newton and Charles Brunette, personal communication, May 16, 2019). Comparison between observations and model data presented in section 4.7.2 is therefore done over the 20-year period of 1989–2008.

#### **4.7.2 Comparison of the CESM with Observations**

To provide an assessment of the performance of the CESM in simulating sea ice transport between the different EEZs of the Arctic, we compare CESM results to results from SITU using satellite observations from the period of 1989 to 2008. We find that the annual cycle of areal ice formation and melt in the CESM-LE compares well with the observations (Figure S4.3). Ice formation peaks in October and ice melt peaks in August (peak of ice formation/melt here refers

to the month with the largest area of simulated ice formation/melt using SITU). Note, however, that the average amount of formation and melt area obtained from the observations does not fall within the spread of internal variability of the CESM-LE during the months of peak ice formation and melt (i.e., October and August, respectively), with the CESM-LE simulating too little ice formation and melt (Figure S4.3). The spatial distributions of areal ice formation and melt are also well represented in the CESM-LE (Figures S4.4 and S4.5) despite slightly larger frequencies of detected fall formation and summer melt over the peripheral seas for the observations (in agreement with results presented in Figure S4.3).

The exchange of transnational ice between the different EEZs of the Arctic simulated by the CESM-LE over the period of 1989–2008 is in good general agreement with observations (Figure S4.6). Both the observations and the CESM-LE show that most of the transnational ice formed in Canada melts in the US EEZ, most of the transnational ice formed in the United States melts in Russia, and most of the Russian transnational ice melts in Norway (Figure S4.6; see also Newton et al., 2017). However, the observed transnational ice transport is slightly outside the range of internal variability of the CESM-LE for two pathways: (1) ice forming in the United States and melting in Russia is underestimated in the CESM, and (2) ice forming in Russia and melting in Norway and Iceland is overestimated in the CESM (Figure S4.6).

The small inconsistencies in areal flux of US ice towards Russia and Russian ice towards Norway and Iceland between observations and the CESM-LE do not extend throughout the full area of the EEZ of formation, but are present only in the region directly upstream of the EEZ of melt, following the general Arctic sea ice circulation (Figure S4.7). For the slightly lower simulated flux of US ice towards Russia by the CESM compared to observations (Figure S4.6), there is a smaller area of high transnational ice promotion probability within the US EEZ close to the Russian border for the CESM-LE compared to the observations (Figures S4.7a, S4.7b, and S4.7d). The slightly higher flux of Russian ice towards Norway and Iceland in the CESM-LE (Figure S4.6) is mainly driven by higher simulated probabilities of transnational ice promotion in the Kara and Barents Seas than what is observed (Figures S4.7a–S4.7c).

Differences in transnational ice exchange between the CESM-LE and observations for US ice melting in Russia and Russian ice melting in Norway and Iceland can be attributed to a bias in the simulated atmospheric circulation over the Arctic during the ice-covered season and the resulting sea ice circulation anomalies. DeRepentigny et al. (2016) showed that the variability in winter sea-level pressure in the CESM-LE results in higher sea ice velocities off the coast of Russia in the Kara and Barents Seas compared to observations, transporting more ice away from the coast and into the Transpolar Drift Stream (see their Figures 6c and 6d). Moreover, the observations are characterized by a strong current along the coast of Alaska, which is not simulated in the years of low winter sea-level pressure in the CESM-LE (see their Figures 6a and 6b). As one would expect, sea ice motion, and consequently transnational ice exchange, is intimately linked to the atmospheric circulation over the Arctic that drives the sea ice.

## 4.7.3 Supplementary Figures

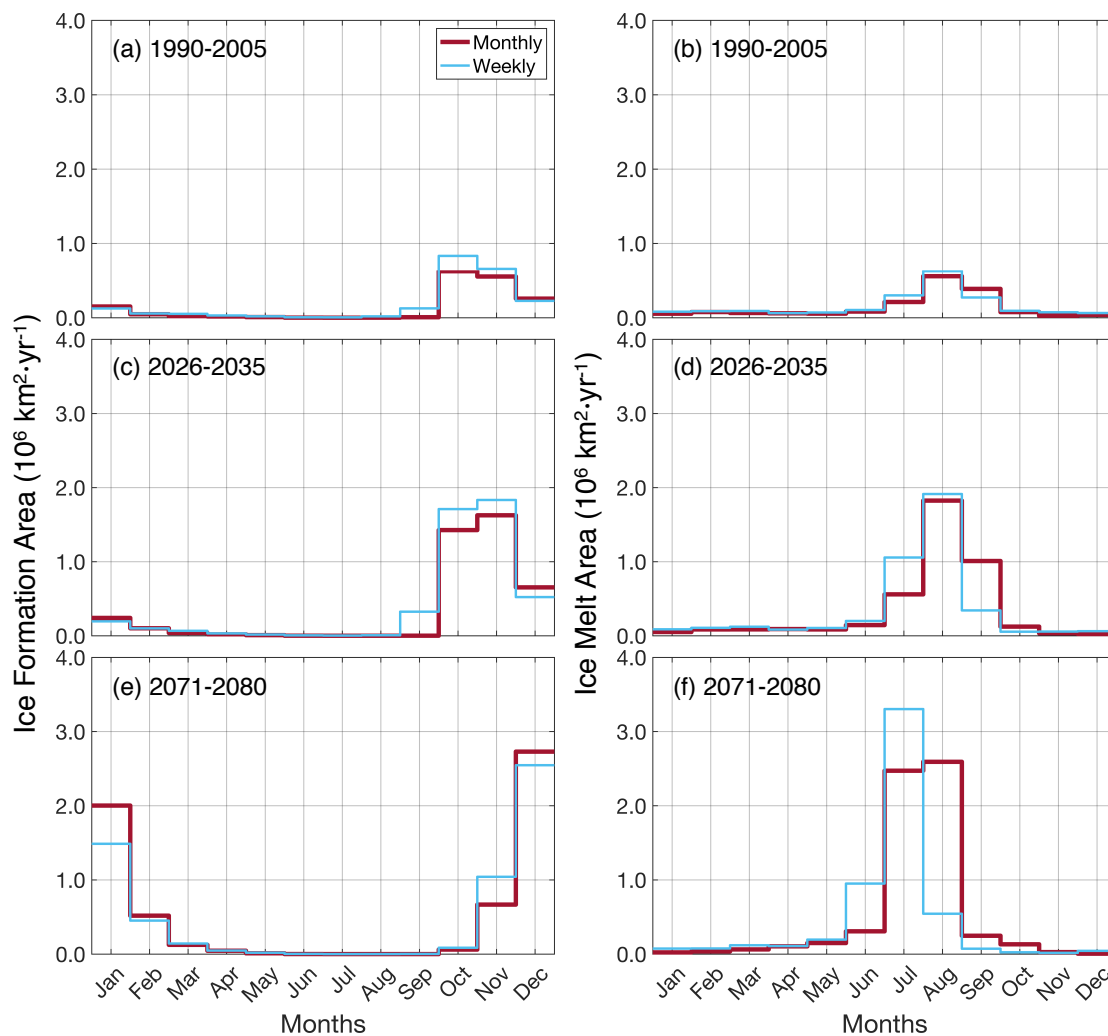


Figure S4.1: Annual cycle of ice formation (a, c, e) and melt (b, d, f) over the periods of 1990–2005 (a, b), 2026–2035 (c, d) and 2071–2080 (e, f) for the first 35 members of the CESM-LE using a monthly (burgundy) and weekly (light blue) time resolutions. Only ice floes that formed and melted between the specified time periods are considered. Note that some of the differences between the weekly and monthly time resolution can be attributed to the way weeks are distributed into months as every month contains either 29, 30 or 31 days and thus always includes part of a week.

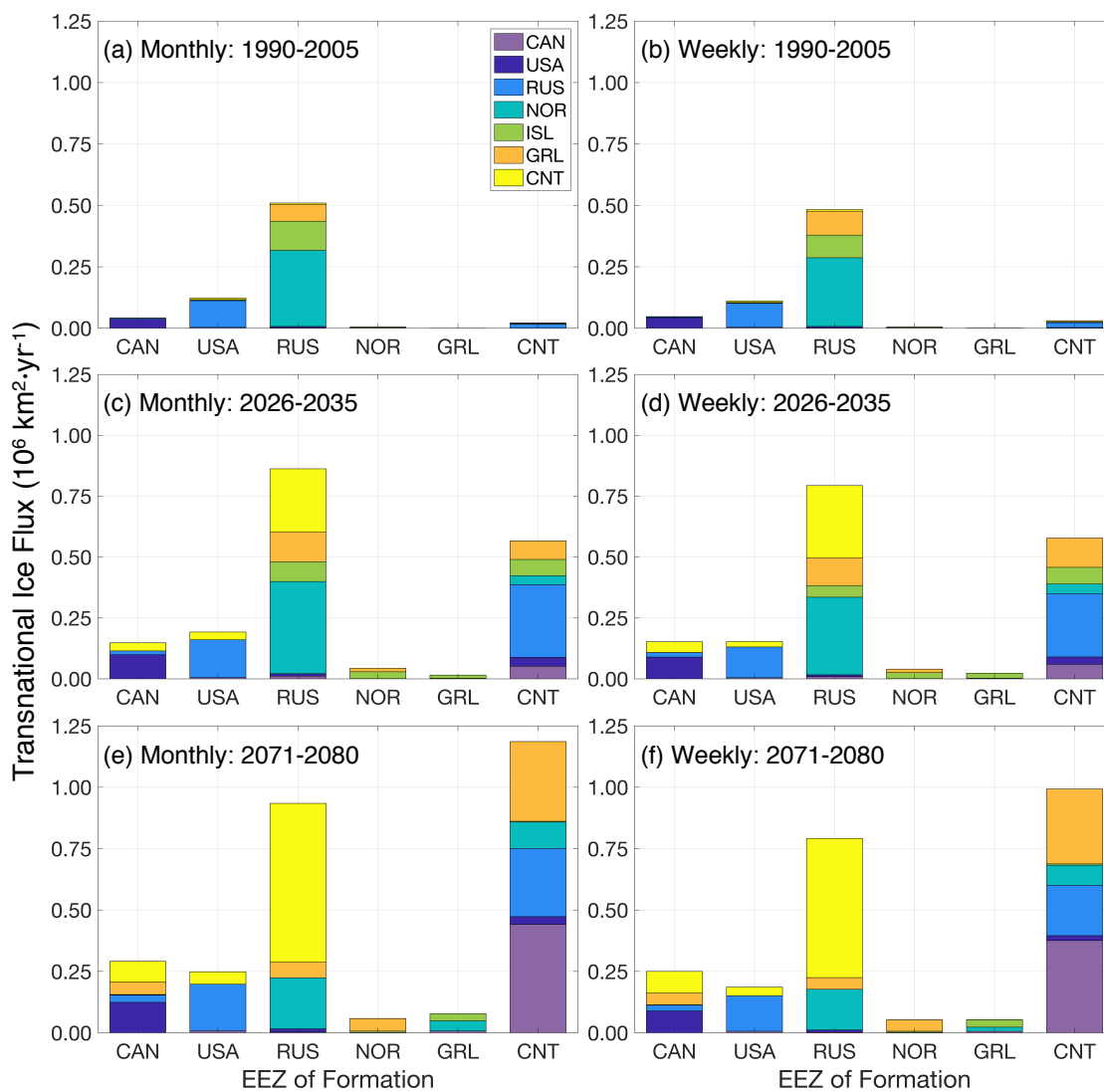


Figure S4.2: Annual mean average areal flux of transnational ice for the CESM-LE over the periods of 1990–2005 (a, b), 2026–2035 (c, d) and 2071–2080 (e, f) using a monthly (a, c, e) and weekly (b, d, f) time resolutions. The height of each colored portion within one bar represents the annual mean areal flux of ice between the EEZ of formation ( $x$  axis) and the EEZ of melt (color). Note that domestic ice is not included in this figure in order to focus on the features of transnational ice exchange.

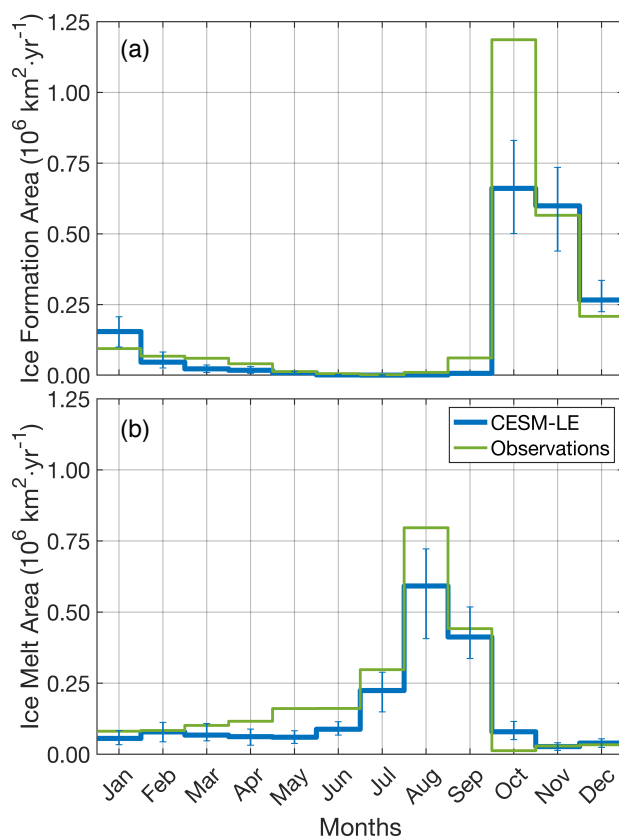


Figure S4.3: Annual cycle of mean areal ice formation (a) and melt (b) in the observations (green) and the CESM-LE (blue) for the period of 1989–2008. The error bars show the maximum and minimum 20-year averaged formation/melt area for each month across the 40 ensemble members of the CESM-LE, showing the range of internal variability for this ensemble. Only ice floes that formed and melted between 1989–2008 are considered. Note that the values shown here are not meant to represent the actual amount of ice that forms and melts in the Arctic every year, but rather the area of ice formation and melt we obtain from SITU (see section 2.2).

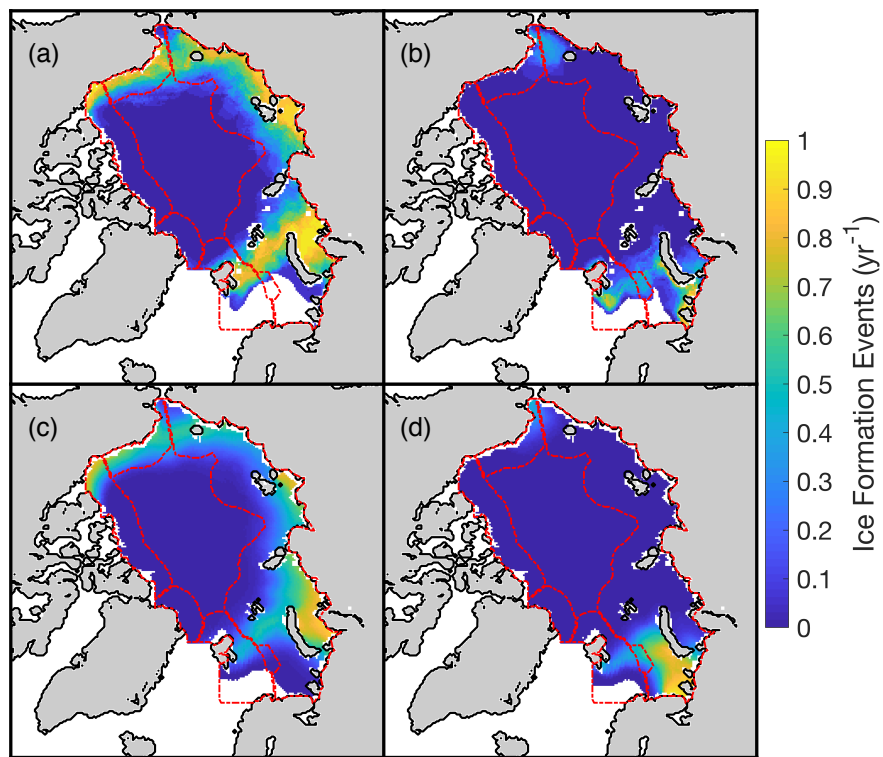


Figure S4.4: Average number of ice formation events per year in fall (SON) (a, c) and winter (DJF) (b, d) over the period of 1989–2008 for both observations (a, b) and the CESM-LE (c, d). The borders of the EEZs are indicated by red lines. Only ice floes that formed and melted between 1989–2008 are considered.

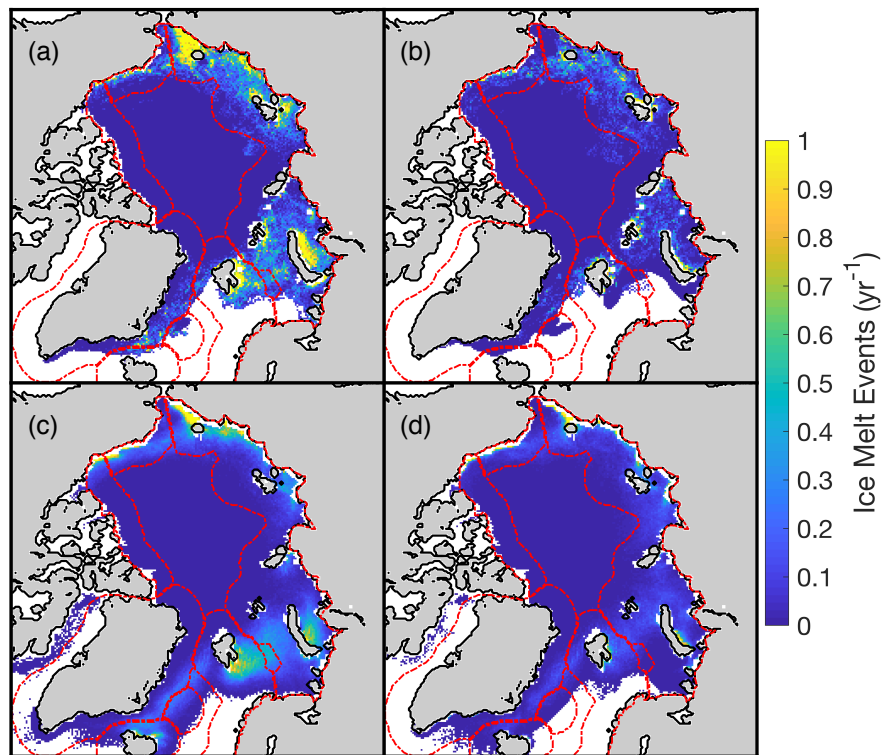


Figure S4.5: As in Figure S4.4, but for the average number of ice melt events per year in summer (JJA) (a, c) and fall (SON) (b, d).

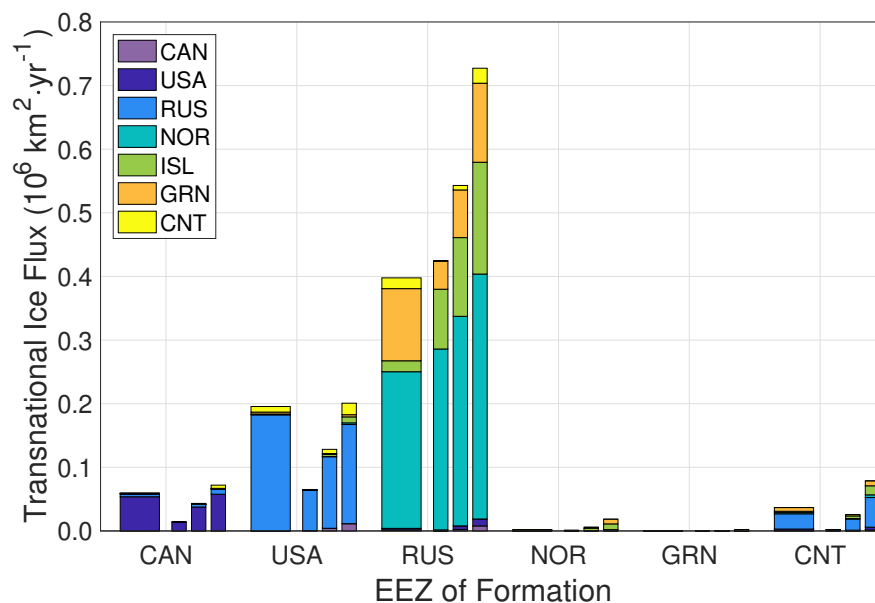


Figure S4.6: Annual mean areal transnational ice flux for the observations (wide bar) and annual mean minimum (left narrow bar), average (middle narrow bar) and maximum (right narrow bar) areal transnational ice flux for the 40 members of the CESM-LE for the period of 1989–2008. The height of each colored portion within one bar represents the annual mean areal flux of ice between the EEZ of formation ( $x$  axis) and the EEZ of melt (color). The CESM-LE is consistent with the observations when the observed value for each pathway lies between the range of the CESM-LE (minimum to maximum). Note that domestic ice is not included in this figure in order to focus on the features of transnational ice exchange.

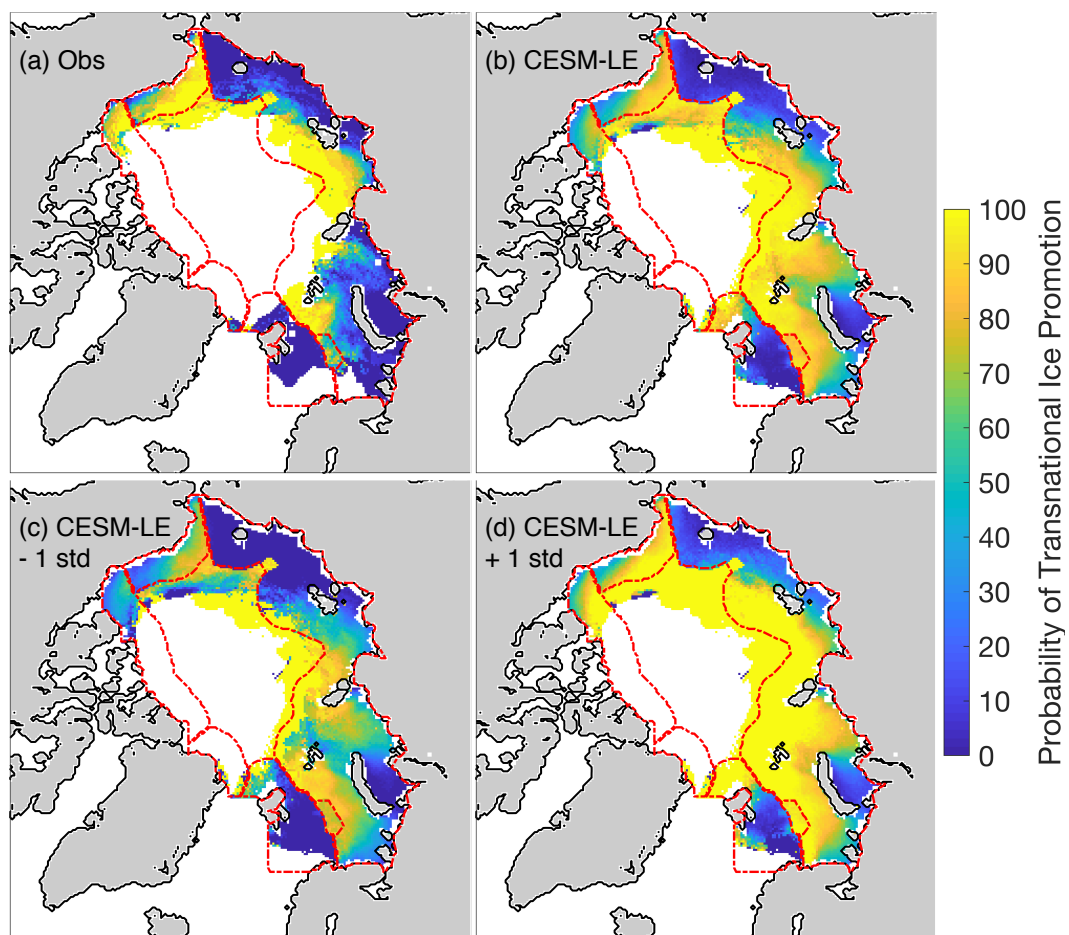


Figure S4.7: Probability of transnational ice promotion for observations (a), the ensemble mean of the CESM-LE (b) as well as the ensemble mean  $\pm$  one standard deviation for the CESM-LE (c, d) over the period of 1989–2008. The color represents the probability that an ice parcel forming at each grid cell gets promoted from domestic ice to transnational ice. The borders of the EEZs are indicated by red lines. Note that the probability is calculated for each grid cell in which at least one ice parcel forms and thus gives no indication of how many ice parcels are considered in the calculation.

Table S4.1: Annual mean average areal flux of ice exchanged between all EEZs for the CESM-LE over the three time periods. The EEZ of formation is indicated in the first column and the EEZ of melt in the first row. All numbers are in km<sup>2</sup>/year. The last column contains the total annual mean average areal flux of ice formed in each EEZ, only considering ice floes that melted before the end of the time period. The numbers in bold highlight the pathways that are statistically different between the CESM-LE and the CESM-LW over a same time period at the 95% confidence level using a t-test.

<b>From/To</b>	<i>Canada</i>	<i>USA</i>	<i>Russia</i>	<i>Norway</i>	<i>Iceland</i>	<i>Greenland</i>	<i>Central</i>	<i>Total</i>
<b>1981–2000</b>								
<i>Canada</i>	39,426	32,741	3,177	32	218	96	631	76,321
<i>USA</i>	3,616	49,083	96,402	546	4,232	1,444	4,184	159,507
<i>Russia</i>	1,635	4,900	563,494	305,730	112,159	60,825	2,217	1,050,960
<i>Norway</i>	0	0	677	108,733	2,331	1,223	0	112,964
<i>Greenland</i>	0	0	0	4	113	31	0	148
<i>Central</i>	163	802	9,026	292	1,585	581	934	13,383
<b>2031–2050</b>								
<i>Canada</i>	107,566	128,998	25,926	441	<b>1,563</b>	<b>4,855</b>	<b>62,049</b>	331,398
<i>USA</i>	6,297	105,809	176,848	0	<b>0</b>	<b>0</b>	<b>34,613</b>	323,567
<i>Russia</i>	<b>11,480</b>	10,188	1,597,911	<b>385,601</b>	<b>37,521</b>	<b>122,715</b>	<b>452,339</b>	2,617,755
<i>Norway</i>	10	0	737	135,196	33,191	<b>31,475</b>	18	200,627
<i>Greenland</i>	<b>789</b>	11	8	<b>10,823</b>	<b>41,205</b>	27,128	51	80,015
<i>Central</i>	<b>184,175</b>	52,953	352,701	<b>69,168</b>	81,513	<b>194,498</b>	833,752	1,768,760
<b>2081–2100</b>								
<i>Canada</i>	327,395	<b>114,877</b>	33,716	<b>3,209</b>	<b>175</b>	<b>70,427</b>	<b>102,810</b>	652,609
<i>USA</i>	6,742	66,614	184,671	0	0	0	<b>60,638</b>	318,665
<i>Russia</i>	<b>2,495</b>	<b>13,346</b>	1,429,691	<b>162,929</b>	<b>4</b>	<b>40,631</b>	<b>654,681</b>	2,303,777
<i>Norway</i>	9	0	<b>1,692</b>	91,323	<b>1,331</b>	38,416	<b>821</b>	133,592
<i>Greenland</i>	<b>7,436</b>	<b>0</b>	64	<b>41,848</b>	<b>13,268</b>	177,128	603	240,347
<i>Central</i>	<b>437,773</b>	<b>17,441</b>	<b>250,289</b>	<b>111,080</b>	<b>410</b>	<b>310,993</b>	1,360,152	2,488,138

Table S4.2: As in Table S4.1, but for the CESM-LW and for the time periods of 2031–2050 and 2081–2100 only.

<b>From/To</b>	<i>Canada</i>	<i>USA</i>	<i>Russia</i>	<i>Norway</i>	<i>Iceland</i>	<i>Greenland</i>	<i>Central</i>	<i>Total</i>
<b>2031–2050</b>								
<i>Canada</i>	67,835	116,784	28,938	9	<b>401</b>	<b>423</b>	<b>38,568</b>	252,958
<i>USA</i>	4,134	102,824	181,077	3	<b>28</b>	20	<b>20,594</b>	308,680
<i>Russia</i>	<b>17,224</b>	13,310	1,529,744	<b>416,960</b>	<b>73,301</b>	<b>137,656</b>	<b>311,557</b>	2,499,752
<i>Norway</i>	0	0	918	137,622	29,449	<b>24,446</b>	0	192,435
<i>Greenland</i>	<b>97</b>	0	0	<b>4,560</b>	<b>25,810</b>	9,903	0	40,370
<i>Central</i>	<b>95,631</b>	53,653	357,849	<b>40,909</b>	78,207	<b>117,193</b>	540,412	1,283,854
<b>2081–2100</b>								
<i>Canada</i>	84,594	<b>139,616</b>	41,702	<b>85</b>	<b>1,153</b>	<b>2,207</b>	<b>67,080</b>	336,437
<i>USA</i>	3,884	95,500	196,153	0	0	0	<b>25,227</b>	320,764
<i>Russia</i>	<b>16,006</b>	<b>8,551</b>	1,600,756	<b>386,994</b>	<b>38,009</b>	<b>153,526</b>	<b>428,526</b>	2,632,368
<i>Norway</i>	51	0	<b>739</b>	130,358	<b>38,855</b>	35,565	<b>0</b>	205,568
<i>Greenland</i>	<b>1,307</b>	<b>125</b>	6	<b>8,969</b>	<b>51,634</b>	24,952	57	87,050
<i>Central</i>	<b>192,349</b>	<b>55,827</b>	<b>411,670</b>	<b>53,332</b>	<b>84,082</b>	<b>189,324</b>	813,423	1,800,007

## CHAPTER 5

### CONCLUSION

#### 5.1 Summary of Major Findings

Climate model projections of Arctic sea ice are crucial tools for understanding how the Arctic will change as global temperatures continue to rise. However, evaluation of sea ice changes in climate models is complicated by the internal variability of the climate system, model differences and scenario uncertainty. In this dissertation we explored processes that lead to Arctic sea ice retreat and their implications in the context of these different sources of uncertainty in climate change projections.

**In Chapter 2, we assessed the current and future states of Arctic sea ice in two different configurations of the CESM2.** We found several differences in the simulated Arctic sea ice cover between the two CESM2 configurations, as well as compared to the previous generation of the CESM model, the CESM-LE. Over the historical period, the CESM2(CAM6) model simulates a winter ice cover that is too thin, which leads to lower summer ice coverage compared to the CESM2(WACCM6) model and observations. In both CESM2 configurations, the timing of first summer ice-free conditions is found to be insensitive to the choice of CMIP6 future emissions scenario, which implies that the year of a first-ice free Arctic will be determined by internal variability and model uncertainty only. This finding is also confirmed in the CMIP6 models overall (SIMIP Community, 2020). In addition, the probability of an ice-free Arctic summer remains low only if global warming stays below 1.5°C, which none of the CMIP6 scenarios achieve in the CESM2. Towards the end of the 21<sup>st</sup> century, the CESM2 simulates a strong acceleration

in winter and spring sea ice decline associated with reduced net surface ocean heat flux during the preceding fall that was not sampled in the CESM-LE simulations. It is important to note, however, that the two versions of the CESM model are consistent in their winter sea ice response to atmospheric CO<sub>2</sub> and Arctic temperature, which suggest that reaching CO<sub>2</sub> concentration higher than 900 ppm and annual mean Arctic temperatures higher than -4°C could lead to an accelerated loss of winter and spring sea ice in the Arctic. This rapid decline in winter ice cover results in open-water conditions for 200 to 365 days of the year depending on the region, which would have tremendous consequences on the polar ecosystems, human activities, as well as the global climate.

**In Chapter 3, we showed that increased inter-annual variability in boreal biomass burning emissions in CMIP6 causes a strong acceleration in sea ice decline in the early 21<sup>st</sup> century in the CESM2-LE and potentially some other CMIP6 models.** Another type of uncertainty that does not affect climate projections but historical simulations is the uncertainty related to the prescribed forcing used in climate models. In CMIP6, a large increase in the inter-annual variability of biomass burning emissions was introduced in 1997 until the end of the historical period in 2014 based on new satellite-based estimates that provide a more realistic depiction of biomass burning emissions in climate models. Using sensitivity experiments in which we removed the biomass burning variability from 1997–2014 but the integrated amount of emissions over that same period is retained, we were able to demonstrate that the excessive early 21<sup>st</sup> century Arctic surface warming and strong decline in September Arctic sea ice area in the CESM2-LE compared to the CESM1-LE can be attributed to the increased biomass burning variability. There is indication that model uncertainty affects how other CMIP6 models respond to this forcing, as a similarly forced sea ice decline is found in some other CMIP6 models but not all. We also show that the increased inter-annual variability in biomass burning emissions explains in large part the increase in sea ice sensitivity to cumulative anthropogenic CO<sub>2</sub> emissions and global warming from the CMIP5-forced to the CMIP6-forced versions of the CESM. Our finding of how biomass burning variability impacts Arctic sea ice, together with the good qualitative match of the sea ice evolution between the CESM2-LE and observations, raises the question as to whether biomass burning emissions could

have also affected the observed Arctic sea ice loss since the late 1990s.

**Finally, in Chapter 4, we evaluated the impact of scenario uncertainty on the amount of sea ice exchanged between the different regions of the Arctic as it transitions towards a thinner, less extensive, more mobile sea ice cover.** The undergoing rapid transition of the Arctic Ocean toward a seasonal ice regime has widespread implications for the polar ecosystem, human activities, as well as the global climate. Using the Sea Ice Tracking Utility, we were able to track ice floes from formation to melt and quantify the exchange of sea ice across the different exclusive economic zones of the Arctic. By the middle of the 21<sup>st</sup> century, transnational ice exchange is projected to triple compared to historical conditions, with most of the transnational ice originating from Russia and the Central Arctic. Scenario uncertainty becomes really important for sea ice transport toward the end of the 21<sup>st</sup> century. Consistent ice-free summers in the high emissions scenario limit the amount of time ice floes have to travel from formation to melt to less than one year, whereas transit times in the low emissions scenario are approximately twice as large. As a result, the total fraction of transnational ice exchange is reduced by 2100 compared to mid-century in the high emissions scenario but the low emissions scenario continues to see an increase in the proportion of transnational ice.

**Overall, this dissertation provides numerous insights into how to best interpret climate projections of Arctic sea ice in the context of the three main sources of projection uncertainty.** We showed that scenario uncertainty does not affect the timing of first summer Arctic ice-free conditions in the CESM2 nor the probability of ice-free conditions for a specific degree of global warming, consistent with other recent studies (Jahn, 2018; SIMIP Community, 2020). When assessing the impact of increased inter-annual variability in biomass burning emissions on Arctic sea ice loss, we focused on the ensemble mean to partly remove the influence of internal variability and isolate the forced response. Even so, CMIP6 models showed a large variety of responses to the biomass burning forcing, which implies a strong influence of model uncertainty on these short-term projections. At long lead times, scenario uncertainty accounts for most of the uncertainty in projections of Arctic sea ice changes (Bonan et al., 2021), and results in large differ-

ences in the amount of ice exchanged between the different regions of the Arctic and the potential for ice-rafted contaminants to be released far away from where they initially originated.

## 5.2 Future Work

The results from this dissertation open up many opportunities for future work. First, the accelerated decline in winter and spring sea ice area towards the end of the 21<sup>st</sup> century in the CESM2 was shown to be driven in large part by changes in ocean heat loss during the preceding fall (Chapter 2). However, the processes that lead to this reduced rate of oceanic heat loss are still unclear. The fact that some other CMIP6 models show a similar acceleration of the March sea ice area decline over the last 20–30 years of the 21<sup>st</sup> century (see Figure 2c of SIMIP Community, 2020) also raises the question as to whether the same processes are driving the late 21<sup>st</sup> century reduction in winter and spring ice area in CMIP6 models in general, while keeping in mind that model uncertainty accounts for most of the uncertainty in long-term projections of Arctic sea ice area change in the winter months (Bonan et al., 2021).

Understanding the effect of changing wildfires on a changing Arctic is very much an understudied problem, particularly when considering coupled climate feedbacks such as cloud feedbacks and aerosol deposition onto sea ice. In Chapter 3, we were able to attribute the excessive Arctic warming and sea ice loss in the CESM2-LE to the increase in inter-annual variability of biomass burning emissions over the GFED era, but the details of the physical mechanisms that drive this warming and reduction in sea ice have not yet been identified. In addition, this high biomass burning variability in the GFED dataset raise the question as to whether the prescribed biomass burning variability in the pre-GFED historical simulations is unrealistically low, and how that affects the simulated 20<sup>th</sup> century Arctic sea ice. Furthermore, the impact of the complete lack of inter-annual variability in the pre-industrial spin-up simulations and in future climate simulations on Arctic sea ice and the global climate in general should to be investigated, as it could have important implications for our estimation of internal climate variability both in the absence and presence of climate change.

The cause of the sea ice trend reversal around the historical-scenario transition in the CESM2 first presented at the end of Chapter 2 and discussed further in Chapter 3 still remains an open question. We were able to rule out a number of forcings as potential explanations for this sea ice recovery, and although its magnitude was much reduced in our sensitivity experiments with homogenized biomass burning emissions, it could not be explain solely by the increased inter-annual variability in biomass burning emissions. As the trend reversal is also present in some but not all CMIP6 models, as well as in observations, this behavior is even more intriguing and deserves to be further investigated, both in models and the real world.

Finally, the Sea Ice Tracking Utility (SITU) is a great tool that allows for a quantitative assessment of sea ice transport in the Arctic (Chapter 4). However, in its current form, SITU only tracks ice area, providing a 2-D picture of the dynamics of sea ice and assuming that any particles trapped in the sea ice will be released into the ocean once the ice floe melts out completely. To more realistically represent the full sea ice physics, further developments of SITU should include tracking sea ice volume and allowing for convergence/divergence of ice floes, such that ridging and lead opening are taken into account. In addition, particle tracers could be incorporated to more robustly quantify the potential risk associated with ice-rafted contaminants.

## BIBLIOGRAPHY

- Aksenov, Y., E. E. Popova, A. Yool, A. G. Nurser, T. D. Williams, L. Bertino, and J. Bergh, 2017: On the future navigability of Arctic sea routes: High-resolution projections of the Arctic Ocean and sea ice. *Marine Policy*, **75**, 300–317, doi:10.1016/j.marpol.2015.12.027.
- AMAP, 2011: AMAP Assessment 2011: Mercury in the Arctic. Technical report, Arctic Monitoring and Assessment Programme (AMAP), Oslo, Norway, available at: <https://www.amap.no/documents/doc/amap-assessment-2011-mercury-in-the-arctic/90>.
- 2015: AMAP Assessment 2015: Black carbon and ozone as Arctic climate forcers. Technical report, Arctic Monitoring and Assessment Programme (AMAP), Oslo, Norway, available at: <https://www.amap.no/documents/doc/amap-assessment-2015-black-carbon-and-ozone-as-arctic-climate-forcers/1299>.
- Arctic Council, 2009: Arctic Marine Shipping Assessment 2009 Report. Technical report, Arctic Council Norwegian Chairmanship, Oslo, Norway, available at: <https://oaarchive.arctic-council.org/handle/11374/54>.
- Assur, A., 1960: *Composition of sea ice and its tensile strength*, volume 44. US Army Snow, Ice and Permafrost Research Establishment.
- Barnes, E. A. and J. A. Screen, 2015: The impact of Arctic warming on the midlatitude jet-stream: Can it? Has it? Will it? *Wiley Interdisciplinary Reviews: Climate Change*, **6**, 277–286, doi:10.1002/wcc.337.
- Barnhart, K. R., C. R. Miller, I. Overeem, and J. E. Kay, 2016: Mapping the future expansion of Arctic open water. *Nature Climate Change*, **6**, 280, doi:10.1038/NCLIMATE2848.
- Baxter, I., Q. Ding, A. Schweiger, M. L’Heureux, S. Baxter, T. Wang, Q. Zhang, K. Harnos, B. Markle, D. Topal, et al., 2019: How tropical Pacific surface cooling contributed to accelerated sea ice melt from 2007 to 2012 as ice is thinned by anthropogenic forcing. *Journal of Climate*, **32**, 8583–8602, doi:10.1175/JCLI-D-18-0783.1.
- Bird, K. J., R. R. Charpentier, D. L. Gautier, D. W. Houseknecht, T. R. Klett, J. K. Pitman, T. E. Moore, C. J. Schenk, M. E. Tennyson, and C. R. Wandrey, 2008: Circum-Arctic resource appraisal: Estimates of undiscovered oil and gas north of the Arctic Circle. Technical report, U.S. Geological Survey, doi:10.3133/fs20083049.
- Bitz, C. and W. Lipscomb, 1999: An energy-conserving thermodynamic model of sea ice. *Journal of Geophysical Research: Oceans*, **104**, 15669–15677, doi:10.1029/1999JC900100.

- Bitz, C. and G. Roe, 2004: A mechanism for the high rate of sea ice thinning in the Arctic Ocean. *Journal of Climate*, **17**, 3623–3632, doi:10.1175/1520-0442(2004)017;3623:AMFTHR;2.0.CO;2.
- Blackport, R. and J. A. Screen, 2020: Insignificant effect of Arctic amplification on the amplitude of midlatitude atmospheric waves. *Science advances*, **6**, eaay2880, doi:10.1126/sciadv.aay2880.
- Blanchard-Wrigglesworth, E., K. C. Armour, C. M. Bitz, and E. DeWeaver, 2011a: Persistence and inherent predictability of Arctic sea ice in a GCM ensemble and observations. *Journal of Climate*, **24**, 231–250, doi:10.1175/2010JCLI3775.1.
- Blanchard-Wrigglesworth, E., C. Bitz, and M. Holland, 2011b: Influence of initial conditions and climate forcing on predicting Arctic sea ice. *Geophysical Research Letters*, **38**, doi:10.1029/2011GL048807.
- Blanken, H., L. B. Tremblay, S. Gaskin, and A. Slavin, 2017: Modelling the long-term evolution of worst-case Arctic oil spills. *Marine Pollution Bulletin*, **116**, 315–331, doi:10.1016/j.marpolbul.2016.12.070.
- Bliss, A. C., M. Steele, G. Peng, W. N. Meier, and S. Dickinson, 2019: Regional variability of Arctic sea ice seasonal change climate indicators from a passive microwave climate data record. *Environmental Research Letters*, doi:10.1088/1748-9326/aafb84.
- Boetius, A., S. Albrecht, K. Bakker, C. Bienhold, J. Felden, M. Fernández-Méndez, S. Hendricks, C. Katlein, C. Lalande, T. Krumpen, et al., 2013: Export of algal biomass from the melting Arctic sea ice. *Science*, **339**, 1430–1432, doi:10.1126/science.1231346.
- Bogenschutz, P. A., A. Gettelman, H. Morrison, V. E. Larson, C. Craig, and D. P. Schanen, 2013: Higher-order turbulence closure and its impact on climate simulations in the Community Atmosphere Model. *Journal of Climate*, **26**, 9655–9676, doi:10.1175/JCLI-D-13-00075.1.
- Bonan, D. B., F. Lehner, and M. M. Holland, 2021: Partitioning uncertainty in projections of Arctic sea ice. *Environmental Research Letters*, doi:10.1088/1748-9326/abe0ec.
- Boucher, O., S. Denvil, G. Levvasseur, A. Cozic, A. Caubel, M.-A. Foujols, Y. Meurdesoif, P. Cadule, M. Devilliers, E. Dupont, and T. Lurton, 2019: IPSL IPSL-CM6A-LR model output prepared for CMIP6 ScenarioMIP ssp370. Version 20190119, doi:10.22033/ESGF/CMIP6.5265.
- Boucher, O., S. Denvil, G. Levvasseur, A. Cozic, A. Caubel, M.-A. Foujols, Y. Meurdesoif, P. Cadule, M. Devilliers, J. Ghattas, N. Lebas, T. Lurton, L. Mellul, I. Musat, J. Mignot, and F. Cheruy, 2018: IPSL IPSL-CM6A-LR model output prepared for CMIP6 CMIP historical. Version 20180803, doi:10.22033/ESGF/CMIP6.5195.
- Brodzik, M. J., B. Billingsley, T. Haran, B. Raup, and M. H. Savoie, 2012: EASE-Grid 2.0: Incremental but significant improvements for Earth-gridded data sets. *ISPRS International Journal of Geo-Information*, **1**, 32–45, doi:10.3390/ijgi1010032.
- Brunette, C., B. Tremblay, and R. Newton, 2019: Winter coastal divergence as a predictor for the minimum sea ice extent in the Laptev Sea. *Journal of Climate*, **32**, 1063–1080, doi:10.1175/JCLI-D-18-0169.1.
- Budikova, D., 2009: Role of Arctic sea ice in global atmospheric circulation: A review. *Global and Planetary Change*, **68**, 149–163, doi:10.1016/j.gloplacha.2009.04.001.

- Bunzel, F., D. Notz, and L. T. Pedersen, 2018: Retrievals of Arctic Sea-Ice Volume and Its Trend Significantly Affected by Interannual Snow Variability. *Geophysical Research Letters*, **45**, 11–751, doi:10.1029/2018GL078867.
- Bushuk, M., R. Msadek, M. Winton, G. Vecchi, X. Yang, A. Rosati, and R. Gudgel, 2019: Regional Arctic sea-ice prediction: Potential versus operational seasonal forecast skill. *Climate Dynamics*, **52**, 2721–2743, doi:10.1007/s00382-018-4288-y.
- Chevallier, M., G. C. Smith, F. Dupont, J.-F. Lemieux, G. Forget, Y. Fujii, F. Hernandez, R. Msadek, K. A. Peterson, A. Storto, et al., 2017: Intercomparison of the Arctic sea ice cover in global ocean–sea ice reanalyses from the ORA-IP project. *Climate Dynamics*, **49**, 1107–1136, doi:10.1007/s00382-016-2985-y.
- Cohen, J., J. A. Screen, J. C. Furtado, M. Barlow, D. Whittleston, D. Coumou, J. Francis, K. Dethloff, D. Entekhabi, J. Overland, et al., 2014: Recent Arctic amplification and extreme mid-latitude weather. *Nature geoscience*, **7**, 627–637, doi:10.1038/ngeo2234.
- Collins, W. J., J.-F. Lamarque, M. Schulz, O. Boucher, V. Eyring, M. I. Hegglin, A. Maycock, G. Myhre, M. Prather, D. Shindell, and S. J. Smith, 2017: AerChemMIP: quantifying the effects of chemistry and aerosols in CMIP6. *Geoscientific Model Development*, **10**, 585–607, doi:10.5194/gmd-10-585-2017.
- Comiso, J. C., 2012: Large decadal decline of the Arctic multiyear ice cover. *Journal of Climate*, **25**, 1176–1193, doi:10.1175/JCLI-D-11-00113.1.
- Comiso, J. C., W. N. Meier, and R. Gersten, 2017: Variability and trends in the Arctic sea ice cover: Results from different techniques. *Journal of Geophysical Research: Oceans*, **122**, 6883–6900, doi:10.1002/2017JC012768.
- Comiso, J. C., C. L. Parkinson, R. Gersten, and L. Stock, 2008: Accelerated decline in the Arctic sea ice cover. *Geophysical Research Letters*, **35**, doi:10.1029/2007GL031972.
- Coumou, D., G. Di Capua, S. Vavrus, L. Wang, and S. Wang, 2018: The influence of Arctic amplification on mid-latitude summer circulation. *Nature Communications*, **9**, 1–12, doi:10.1038/s41467-018-05256-8.
- Cox, P. and D. Stephenson, 2007: A changing climate for prediction. *Science*, **317**, 207–208, doi:10.1126/science.1145956.
- Dai, A., D. Luo, M. Song, and J. Liu, 2019: Arctic amplification is caused by sea-ice loss under increasing CO<sub>2</sub>. *Nature communications*, **10**, 1–13, doi:10.1038/s41467-018-07954-9.
- Danabasoglu, G., 2019a: NCAR CESM2 model output prepared for CMIP6 CMIP historical. Version 20190514, doi:10.22033/ESGF/CMIP6.7627.
- 2019b: NCAR CESM2 model output prepared for CMIP6 ScenarioMIP ssp126. Version 20200528, doi:10.22033/ESGF/CMIP6.7746.
- 2019c: NCAR CESM2 model output prepared for CMIP6 ScenarioMIP ssp245. Version 20200528, doi:10.22033/ESGF/CMIP6.7748.

- 2019d: NCAR CESM2 model output prepared for CMIP6 ScenarioMIP ssp370. Version 20200528, doi:10.22033/ESGF/CMIP6.7753.
  - 2019e: NCAR CESM2 model output prepared for CMIP6 ScenarioMIP ssp585. Version 20200528, doi:10.22033/ESGF/CMIP6.7768.
  - 2019f: NCAR CESM2-WACCM model output prepared for CMIP6 AerChemMIP hist-1950HC. Version 20190606, doi:10.22033/ESGF/CMIP6.10060.
  - 2019g: NCAR CESM2-WACCM model output prepared for CMIP6 AerChemMIP hist-piNTCF. Version 20190531, doi:10.22033/ESGF/CMIP6.10062.
  - 2019h: NCAR CESM2-WACCM model output prepared for CMIP6 AerChemMIP ssp370-lowNTCF. Version 20200107, doi:10.22033/ESGF/CMIP6.10104.
  - 2019i: NCAR CESM2-WACCM model output prepared for CMIP6 CMIP historical. Version 20190227, doi:10.22033/ESGF/CMIP6.10071.
  - 2019j: NCAR CESM2-WACCM model output prepared for CMIP6 ScenarioMIP ssp126. Version 20190815, doi:10.22033/ESGF/CMIP6.10100.
  - 2019k: NCAR CESM2-WACCM model output prepared for CMIP6 ScenarioMIP ssp245. Version 20190815, doi:10.22033/ESGF/CMIP6.10101.
  - 2019l: NCAR CESM2-WACCM model output prepared for CMIP6 ScenarioMIP ssp370. Version 20190815, doi:10.22033/ESGF/CMIP6.10102.
  - 2019m: NCAR CESM2-WACCM model output prepared for CMIP6 ScenarioMIP ssp585. Version 20190815, doi:10.22033/ESGF/CMIP6.10115.
- Danabasoglu, G., S. C. Bates, B. P. Briegleb, S. R. Jayne, M. Jochum, W. G. Large, S. Peacock, and S. G. Yeager, 2012: The CCSM4 ocean component. *Journal of Climate*, **25**, 1361–1389, doi:10.1175/JCLI-D-11-00091.1.
- Danabasoglu, G., J.-F. Lamarque, J. Bacmeister, D. Bailey, A. DuVivier, J. Edwards, L. Emmons, J. Fasullo, R. Garcia, A. Gettelman, et al., 2020: The Community Earth System Model Version 2 (CESM2). *Journal of Advances in Modeling Earth Systems*, **12**, e2019MS001916, doi:10.1029/2019MS001916.
- Davy, R. and S. Outten, 2020: The Arctic surface climate in CMIP6: status and developments since CMIP5. *Journal of Climate*, **33**, 8047–8068, doi:10.1175/JCLI-D-19-0990.1.
- Day, J. J., J. Hargreaves, J. Annan, and A. Abe-Ouchi, 2012: Sources of multi-decadal variability in Arctic sea ice extent. *Environmental Research Letters*, **7**, 034011, doi:10.1088/1748-9326/7/3/034011.
- de Groot, W. J., M. D. Flannigan, and A. S. Cantin, 2013: Climate change impacts on future boreal fire regimes. *Forest Ecology and Management*, **294**, 35–44, doi:10.1016/j.foreco.2012.09.027.
- DeRepentigny, P., A. Jahn, M. M. Holland, and A. Smith, 2020: Arctic sea ice in two configurations of the CESM2 during the 20th and 21st centuries. *Journal of Geophysical Research: Oceans*, **125**, e2020JC016133, doi:10.1029/2020JC016133.

- DeRepentigny, P., L. B. Tremblay, R. Newton, and S. Pfirman, 2016: Patterns of sea ice retreat in the transition to a seasonally ice-free Arctic. *Journal of Climate*, **29**, 6993–7008, doi:10.1175/JCLI-D-15-0733.1.
- Deser, C., A. Phillips, V. Bourdette, and H. Teng, 2012: Uncertainty in climate change projections: the role of internal variability. *Climate dynamics*, **38**, 527–546, doi:10.1007/s00382-010-0977-x.
- Ding, Q., A. Schweiger, M. L’Heureux, D. S. Battisti, S. Po-Chedley, N. C. Johnson, E. Blanchard-Wrigglesworth, K. Harnos, Q. Zhang, R. Eastman, et al., 2017: Influence of high-latitude atmospheric circulation changes on summertime Arctic sea ice. *Nature Climate Change*, **7**, 289–295, doi:10.1038/nclimate3241.
- Ding, Q., A. Schweiger, M. L’Heureux, E. J. Steig, D. S. Battisti, N. C. Johnson, E. Blanchard-Wrigglesworth, S. Po-Chedley, Q. Zhang, K. Harnos, et al., 2019: Fingerprints of internal drivers of Arctic sea ice loss in observations and model simulations. *Nature Geoscience*, **12**, 28–33, doi:10.1038/s41561-018-0256-8.
- Dix, M., D. Bi, P. Dobrohotoff, R. Fiedler, I. Harman, R. Law, C. Mackallah, S. Marsland, S. O’Farrell, H. Rashid, J. Srbinovsky, A. Sullivan, C. Trenham, P. Vohralik, I. Watterson, G. Williams, M. Woodhouse, R. Bodman, F. B. Dias, C. Domingues, N. Hannah, A. Heerdegen, A. Savita, S. Wales, C. Allen, K. Druken, B. Evans, C. Richards, S. M. Ridzwan, D. Roberts, J. Smillie, K. Snow, M. Ward, and R. Yang, 2019a: CSIRO-ARCCSS ACCESS-CM2 model output prepared for CMIP6 CMIP historical. Version 20200817, doi:10.22033/ESGF/CMIP6.4271.
- 2019b: CSIRO-ARCCSS ACCESS-CM2 model output prepared for CMIP6 ScenarioMIP ssp370. Version 20200817, doi:10.22033/ESGF/CMIP6.4323.
- DuVivier, A. K., M. M. Holland, J. E. Kay, S. Tilmes, A. Gettelman, and D. Bailey, 2020: Arctic and Antarctic sea ice mean state in the Community Earth System Model Version 2 and the influence of atmospheric chemistry. *Journal of Geophysical Research: Oceans*, **125**, e2019JC015934, doi:10.1029/2019JC015934.
- EC-Earth Consortium (EC-Earth), 2019a: EC-Earth-Consortium EC-Earth3-Veg model output prepared for CMIP6 CMIP historical. Version 20200919, doi:10.22033/ESGF/CMIP6.4706.
- 2019b: EC-Earth-Consortium EC-Earth3-Veg model output prepared for CMIP6 ScenarioMIP ssp370. Version 20200919, doi:10.22033/ESGF/CMIP6.4886.
- Eicken, H., 2004: The role of Arctic sea ice in transporting and cycling terrigenous organic matter. *The Organic Carbon Cycle in the Arctic Ocean*, Springer Berlin, 45–53.
- Eicken, H., J. Kolatschek, J. Freitag, F. Lindemann, H. Kassens, and I. Dmitrenko, 2000: A key source area and constraints on entrainment for basin-scale sediment transport by Arctic sea ice. *Geophysical Research Letters*, **27**, 1919–1922, doi:10.1029/1999GL011132.
- Emmerson, C. and G. Lahn, 2012: Arctic Opening: Opportunity and Risk in the High North. Technical report, Chatham House, London, United Kingdom, available at: <https://www.chathamhouse.org/publications/papers/view/182839>.
- England, M., A. Jahn, and L. Polvani, 2019: Nonuniform Contribution of Internal Variability to Recent Arctic Sea Ice Loss. *Journal of Climate*, **32**, 4039–4053, doi:10.1175/JCLI-D-18-0864.1.

- Eyring, V., S. Bony, G. A. Meehl, C. A. Senior, B. Stevens, R. J. Stouffer, and K. E. Taylor, 2016: Overview of the Coupled Model Intercomparison Project Phase 6 (CMIP6) experimental design and organization. *Geoscientific Model Development (Online)*, **9**, doi:10.5194/gmd-9-1937-2016.
- Fasullo, J. T., J.-F. Lamarque, C. Hannay, N. Rosenbloom, S. Tilmes, P. DeRepentigny, A. Jahn, and C. Deser, 2021: Spurious Late Historical-Era Warming in CESM2 and Other CMIP6 Climate Simulations Driven by Prescribed Biomass Burning Emissions. *Nature Climate Change*, under review.
- Fernández-Méndez, M., C. Katlein, B. Rabe, M. Nicolaus, I. Peeken, K. Bakker, H. Flores, and A. Boetius, 2015: Photosynthetic production in the central Arctic Ocean during the record sea-ice minimum in 2012. *Biogeosciences*, **12**, 3525–3549, doi:10.5194/bg-12-3525-2015.
- Fetterer, F., K. Knowles, W. Meier, M. Savoie, and A. Windnagel, 2017: Sea Ice Index, Version 3 [monthly values from 1979 to 2020]. National Snow and Ice Data Center, Boulder, Colorado, USA, accessed May 2020, doi:10.7265/N5K072F8.
- Fingas, M. and B. Hollebone, 2003: Review of behaviour of oil in freezing environments. *Marine Pollution Bulletin*, **47**, 333–340, doi:10.1016/S0025-326X(03)00210-8.
- Flanders Marine Institute, 2018: Maritime Boundaries Geodatabase: Maritime Boundaries and Exclusive Economic Zones (200NM), version 10. Doi:10.14284/312.
- Fowler, C., W. Emery, and J. Maslanik, 2004: Satellite-derived evolution of Arctic sea ice age: October 1978 to March 2003. *Geoscience and Remote Sensing Letters, IEEE*, **1**, 71–74, doi:10.1109/LGRS.2004.824741.
- Francis, J. A., 2017: Why are Arctic linkages to extreme weather still up in the air? *Bulletin of the American Meteorological Society*, **98**, 2551–2557, doi:10.1175/BAMS-D-17-0006.1.
- Francis, J. A. and S. J. Vavrus, 2012: Evidence linking Arctic amplification to extreme weather in mid-latitudes. *Geophysical research letters*, **39**, doi:10.1029/2012GL051000.
- 2015: Evidence for a wavier jet stream in response to rapid Arctic warming. *Environmental Research Letters*, **10**, 014005, doi:10.1088/1748-9326/10/1/014005.
- Francis, J. A., S. J. Vavrus, and J. Cohen, 2017: Amplified Arctic warming and mid-latitude weather: new perspectives on emerging connections. *Wiley Interdisciplinary Reviews: Climate Change*, **8**, e474, doi:10.1002/wcc.474.
- Gagné, M.-E., M. Kirchmeier-Young, N. Gillett, and J. Fyfe, 2017: Arctic sea ice response to the eruptions of Agung, El Chichón, and Pinatubo. *Journal of Geophysical Research: Atmospheres*, **122**, 8071–8078, doi:10.1002/2017JD027038.
- Gettelman, A., C. Hannay, J. Bacmeister, R. Neale, A. Pendergrass, G. Danabasoglu, J.-F. Lamarque, J. Fasullo, D. Bailey, D. Lawrence, et al., 2019a: High Climate Sensitivity in the Community Earth System Model Version 2 (CESM2). *Geophysical Research Letters*, **46**, 8329–8337, doi:10.1029/2019GL083978.
- Gettelman, A., M. Mills, D. Kinnison, R. Garcia, A. Smith, D. Marsh, S. Tilmes, F. Vitt, C. Bardeen, J. McInerney, et al., 2019b: The Whole Atmosphere Community Climate Model Version 6 (WACCM6). *Journal of Geophysical Research: Atmospheres*, doi:10.1029/2019JD030943.

- Gettelman, A. and H. Morrison, 2015: Advanced two-moment bulk microphysics for global models. Part I: Off-line tests and comparison with other schemes. *Journal of Climate*, **28**, 1268–1287, doi:10.1175/JCLI-D-14-00102.1.
- Gillett, N. P., V. K. Arora, K. Zickfeld, S. J. Marshall, and W. J. Merryfield, 2011: Ongoing climate change following a complete cessation of carbon dioxide emissions. *Nature Geoscience*, **4**, 83–87, doi:10.1038/ngeo1047.
- GISTEMP Team, 2021: GISS Surface Temperature Analysis (GISTEMP), version 4. NASA Goddard Institute for Space Studies, dataset accessed at <https://data.giss.nasa.gov/gistemp/>.
- Glickson, D., M. Grabowski, T. Coolbaugh, D. Dickins, R. Glenn, K. Lee, L. Majors, M. Myers, B. Norcross, M. Reed, et al., 2014: Responding to oil spills in the U.S. Arctic marine environment. *International Oil Spill Conference Proceedings*, American Petroleum Institute, volume 2014, 283740, doi:10.7901/2169-3358-2014-1-283740.1.
- Global Carbon Project, 2019: Supplemental data of Global Carbon Budget 2019 (Version 1.0). Global Carbon Project, doi:10.18160/gcp-2019.
- Gradinger, R. R., M. R. Kaufman, and B. A. Bluhm, 2009: Pivotal role of sea ice sediments in the seasonal development of near-shore Arctic fast ice biota. *Marine Ecology Progress Series*, **394**, 49–63, doi:10.3354/meps08320.
- Guemas, V., E. Blanchard-Wrigglesworth, M. Chevallier, J. J. Day, M. Déqué, F. J. Doblas-Reyes, N. S. Fučkar, A. Germe, E. Hawkins, S. Keeley, et al., 2016: A review on Arctic sea-ice predictability and prediction on seasonal to decadal time-scales. *Quarterly Journal of the Royal Meteorological Society*, **142**, 546–561, doi:10.1002/qj.2401.
- Hanes, C. C., X. Wang, P. Jain, M.-A. Parisien, J. M. Little, and M. D. Flannigan, 2019: Fire-regime changes in Canada over the last half century. *Canadian Journal of Forest Research*, **49**, 256–269, doi:10.1139/cjfr-2018-0293.
- Hawkins, E. and R. Sutton, 2009: The potential to narrow uncertainty in regional climate predictions. *Bulletin of the American Meteorological Society*, **90**, 1095–1108, doi:10.1175/2009BAMS2607.1.
- Holland, M. M., C. M. Bitz, and B. Tremblay, 2006: Future abrupt reductions in the summer Arctic sea ice. *Geophysical research letters*, **33**, doi:10.1029/2006GL028024.
- Huang, Y., Y. Jin, M. W. Schwartz, and J. H. Thorne, 2020: Intensified burn severity in California’s northern coastal mountains by drier climatic condition. *Environmental Research Letters*, **15**, 104033, doi:10.1088/1748-9326/aba6af.
- Hunke, E. C., D. A. Hebert, and O. Lecomte, 2013: Level-ice melt ponds in the Los Alamos sea ice model, CICE. *Ocean Modelling*, **71**, 26–42, doi:10.1016/j.ocemod.2012.11.008.
- Hunke, E. C., W. H. Lipscomb, A. K. Turner, N. Jeffery, and S. Elliot, 2015: CICE: The Los Alamos Sea Ice Model Documentation and Software User’s Manual Version 5.1. Technical Report LA-CC-06-012, Los Alamos National Laboratory.

- Huntington, H. P., S. L. Danielson, F. K. Wiese, M. Baker, P. Boveng, J. J. Citta, A. De Robertis, D. M. Dickson, E. Farley, J. C. George, et al., 2020: Evidence suggests potential transformation of the Pacific Arctic ecosystem is underway. *Nature Climate Change*, **10**, 342–348, doi:10.1038/s41558-020-0695-2.
- Hurrell, J. W., M. M. Holland, P. R. Gent, S. Ghan, J. E. Kay, P. J. Kushner, J.-F. Lamarque, W. G. Large, D. Lawrence, K. Lindsay, et al., 2013: The Community Earth System Model: A Framework for Collaborative Research. *Bulletin of the American Meteorological Society*, **94**, 1339–1360, doi:10.1175/BAMS-D-12-00121.1.
- Huserbråten, M. B. O., E. Eriksen, H. Gjøsæter, and F. Vikebø, 2019: Polar cod in jeopardy under the retreating Arctic sea ice. *Communications biology*, **2**, 1–8, doi:10.1038/s42003-019-0649-2.
- IPCC, 2014: *Climate Change 2013 – The Physical Science Basis: Working Group I Contribution to the Fifth Assessment Report of the Intergovernmental Panel on Climate Change*. Cambridge University Press.
- Izumiyama, K., S. Uto, S. Sakai, et al., 2004: Prediction of oil-ice sandwich formation. *International Journal of Offshore and Polar Engineering*, **14**.
- Jahn, A., 2018: Reduced probability of ice-free summers for 1.5 C compared to 2 C warming. *Nature Climate Change*, **8**, 409, doi:10.1038/s41558-018-0127-8.
- Jahn, A. and M. M. Holland, 2013: Implications of Arctic sea ice changes for North Atlantic deep convection and the meridional overturning circulation in CCSM4-CMIP5 simulations. *Geophysical Research Letters*, **40**, 1206–1211, doi:10.1002/grl.50183.
- Jahn, A., J. E. Kay, M. M. Holland, and D. M. Hall, 2016: How predictable is the timing of a summer ice-free Arctic? *Geophysical Research Letters*, **43**, 9113–9120, doi:10.1002/2016GL070067.
- Jin, M., C. Deal, J. Wang, V. Alexander, R. Gradinger, S.-I. Saitoh, T. Iida, Z. Wan, and P. Stabeno, 2007: Ice-associated phytoplankton blooms in the southeastern Bering Sea. *Geophysical Research Letters*, **34**, doi:10.1029/2006GL028849.
- Jones, C., E. Robertson, V. Arora, P. Friedlingstein, E. Shevliakova, L. Bopp, V. Brovkin, T. Hajima, E. Kato, M. Kawamiya, et al., 2013: Twenty-first-century compatible CO<sub>2</sub> emissions and airborne fraction simulated by CMIP5 earth system models under four representative concentration pathways. *Journal of Climate*, **26**, 4398–4413, doi:10.1175/JCLI-D-12-00554.1.
- Jungclaus, J., M. Bittner, K.-H. Wieners, F. Wachsman, M. Schupfner, S. Legutke, M. Giorgetta, C. Reick, V. Gayler, H. Haak, P. de Vrese, T. Raddatz, M. Esch, T. Mauritsen, J.-S. von Storch, J. Behrens, V. Brovkin, M. Claussen, T. Crueger, I. Fast, S. Fiedler, S. Hagemann, C. Hohenegger, T. Jahns, S. Kloster, S. Kinne, G. Lasslop, L. Kornblueh, J. Marotzke, D. Matei, K. Meraner, U. Mikolajewicz, K. Modali, W. Müller, J. Nabel, D. Notz, K. Peters, R. Pincus, H. Pohlmann, J. Pongratz, S. Rast, H. Schmidt, R. Schnur, U. Schulzweida, K. Six, B. Stevens, A. Voigt, and E. Roeckner, 2019: MPI-M MPI-ESM1.2-HR model output prepared for CMIP6 CMIP historical. Version 20190710, doi:10.22033/ESGF/CMIP6.6594.
- Kay, J. E., C. Deser, A. Phillips, A. Mai, C. Hannay, G. Strand, J. M. Arblaster, S. Bates, G. Danabasoglu, J. Edwards, et al., 2015: The Community Earth System Model (CESM) large ensemble project: A community resource for studying climate change in the presence of internal climate

- variability. *Bulletin of the American Meteorological Society*, **96**, 1333–1349, doi:10.1175/BAMS-D-13-00255.1.
- Kay, J. E., M. M. Holland, and A. Jahn, 2011: Inter-annual to multi-decadal Arctic sea ice extent trends in a warming world. *Geophysical Research Letters*, **38**, doi:10.1029/2011GL048008.
- Kirchmeier-Young, M. C., F. W. Zwiers, and N. P. Gillett, 2017: Attribution of extreme events in Arctic sea ice extent. *Journal of Climate*, **30**, 553–571, doi:10.1175/JCLI-D-16-0412.1.
- Koenigk, T., J. Key, and T. Vihma, 2020: Climate Change in the Arctic. *Physics and Chemistry of the Arctic Atmosphere*, A. Kokhanovsky and C. Tomasi, eds., Springer, Cham, 673–705, doi:10.1007/978-3-030-33566-3\_11.
- Krumpen, T., H. J. Belter, A. Boetius, E. Damm, C. Haas, S. Hendricks, M. Nicolaus, E.-M. Nöthig, S. Paul, I. Peeken, R. Ricker, and R. Stein, 2019: Arctic warming interrupts the Transpolar Drift and affects long-range transport of sea ice and ice-rafted matter. *Scientific Reports*, **9**, 1–9, doi:10.1038/s41598-019-41456-y.
- Kwok, R., 2018: Arctic sea ice thickness, volume, and multiyear ice coverage: losses and coupled variability (1958–2018). *Environmental Research Letters*, **13**, 105005, doi:10.1088/1748-9326/aae3ec.
- Labe, Z., G. Magnusdottir, and H. Stern, 2018: Variability of Arctic sea ice thickness using PIOMAS and the CESM Large Ensemble. *Journal of Climate*, **31**, 3233–3247, doi:10.1175/JCLI-D-17-0436.1.
- Lamarque, J.-F., T. C. Bond, V. Eyring, C. Granier, A. Heil, Z. Klimont, D. Lee, C. Liou, A. Mieville, B. Owen, et al., 2010: Historical (1850–2000) gridded anthropogenic and biomass burning emissions of reactive gases and aerosols: methodology and application. *Atmospheric Chemistry and Physics*, **10**, 7017–7039, doi:10.5194/acp-10-7017-2010.
- Landrum, L. and M. M. Holland, 2020: Extremes become routine in an emerging new Arctic. *Nature Climate Change*, **10**, 1108–1115, doi:10.1038/s41558-020-0892-z.
- Lawrence, D. M., R. A. Fisher, C. D. Koven, K. W. Oleson, S. C. Swenson, G. Bonan, N. Collier, B. Ghimire, L. van Kampen, D. Kennedy, et al., 2019: The Community Land Model version 5: Description of new features, benchmarking, and impact of forcing uncertainty. *Journal of Advances in Modeling Earth Systems*, doi:10.1029/2018MS001583.
- Lehner, F., C. Deser, N. Maher, J. Marotzke, E. M. Fischer, L. Brunner, R. Knutti, and E. Hawkins, 2020: Partitioning climate projection uncertainty with multiple large ensembles and CMIP5/6. *Earth System Dynamics*, **11**, 491–508, doi:10.5194/esd-11-491-2020.
- Lenssen, N. J., G. A. Schmidt, J. E. Hansen, M. J. Menne, A. Persin, R. Ruedy, and D. Zyss, 2019: Improvements in the GISTEMP uncertainty model. *Journal of Geophysical Research: Atmospheres*, **124**, 6307–6326, doi:10.1029/2018JD029522.
- Li, L., 2019a: CAS FGOALS-g3 model output prepared for CMIP6 CMIP historical. Version 20191029, doi:10.22033/ESGF/CMIP6.3356.
- 2019b: CAS FGOALS-g3 model output prepared for CMIP6 ScenarioMIP ssp370. Version 20191029, doi:10.22033/ESGF/CMIP6.3480.

- Liu, X., R. C. Easter, S. J. Ghan, R. Zaveri, P. Rasch, X. Shi, J.-F. Lamarque, A. Gettelman, H. Morrison, F. Vitt, et al., 2012: Toward a minimal representation of aerosols in climate models: Description and evaluation in the Community Atmosphere Model CAM5. *Geoscientific Model Development*, **5**, 709–739, doi:10.5194/gmd-5-709-2012.
- Liu, X., P.-L. Ma, H. Wang, S. Tilmes, B. Singh, R. Easter, S. Ghan, and P. Rasch, 2016: Description and evaluation of a new four-mode version of the Modal Aerosol Module (MAM4) within version 5.3 of the Community Atmosphere Model. *Geoscientific Model Development*, **9**, 505–522, doi:10.5194/gmd-9-505-2016.
- Long, M., L. Zhang, S. Hu, and S. Qian, 2021: Multi-Aspect Assessment of CMIP6 Models for Arctic Sea Ice Simulation. *Journal of Climate*, **34**, 1515–1529, doi:10.1175/JCLI-D-20-0522.1.
- Macias-Fauria, M. and E. Post, 2018: Effects of sea ice on Arctic biota: An emerging crisis discipline. *Biology letters*, **14**, 20170702, doi:10.1098/rsbl.2017.0702.
- Mahlstein, I. and R. Knutti, 2012: September Arctic sea ice predicted to disappear near 2°C global warming above present. *Journal of Geophysical Research: Atmospheres*, **117**, doi:10.1029/2011JD016709.
- Markus, T., J. C. Stroeve, and J. Miller, 2009: Recent changes in Arctic sea ice melt onset, freezeup, and melt season length. *Journal of Geophysical Research: Oceans*, **114**, doi:10.1029/2009JC005436.
- Maslanik, J., C. Fowler, J. Stroeve, S. Drobot, J. Zwally, D. Yi, and W. Emery, 2007: A younger, thinner Arctic ice cover: Increased potential for rapid, extensive sea-ice loss. *Geophysical Research Letters*, **34**, doi:10.1029/2007GL032043.
- Massonnet, F., T. Fichefet, H. Goosse, C. M. Bitz, G. Philippon-Berthier, M. M. Holland, and P.-Y. Barriat, 2012: Constraining projections of summer Arctic sea ice. *The Cryosphere*, **6**, 1383–1394, doi:10.5194/tc-6-1383-2012.
- Massonnet, F., M. Vancoppenolle, H. Goosse, D. Docquier, T. Fichefet, and E. Blanchard-Wrigglesworth, 2018: Arctic sea-ice change tied to its mean state through thermodynamic processes. *Nature Climate Change*, **8**, 599, doi:10.1038/s41558-018-0204-z.
- McIlhattan, E. A., J. E. Kay, and T. S. L'Ecuyer, 2020: Arctic clouds and precipitation in the community earth system model version 2. *Journal of Geophysical Research: Atmospheres*, **125**, e2020JD032521, doi:10.1029/2020JD032521.
- Meehl, G. A., J. M. Arblaster, S. Bates, J. H. Richter, C. Tebaldi, A. Gettelman, B. Medeiros, J. Bacmeister, P. DeRepentigny, N. Rosenbloom, et al., 2020: Characteristics of future warmer base states in cesm2. *Earth and Space Science*, **7**, e2020EA001296, doi:10.1029/2020EA001296.
- Meier, W., F. Fetterer, M. Savoie, S. Mallory, R. Duerr, and J. Stroeve, 2017: NOAA/NSIDC Climate Data Record of Passive Microwave Sea Ice Concentration, Version 3 [September averages 1980 to 2009]. National Snow and Ice Data Center, Boulder, Colorado, USA, accessed July 2018, doi:10.7265/N59P2ZTG.
- Meier, W. N., G. K. Hovelsrud, B. E. Van Oort, J. R. Key, K. M. Kovacs, C. Michel, C. Haas, M. A. Granskog, S. Gerland, D. K. Perovich, et al., 2014: Arctic sea ice in transformation: A review

- of recent observed changes and impacts on biology and human activity. *Reviews of Geophysics*, **52**, 185–217, doi:10.1002/2013RG000431.
- Melnikov, I. A., E. G. Kolosova, H. E. Welch, and L. S. Zhitina, 2002: Sea ice biological communities and nutrient dynamics in the Canada Basin of the Arctic Ocean. *Deep Sea Research Part I: Oceanographic Research Papers*, **49**, 1623–1649, doi:10.1016/S0967-0637(02)00042-0.
- Moore, S. E. and H. P. Huntington, 2008: Arctic marine mammals and climate change: impacts and resilience. *Ecological Applications*, **18**, S157–S165, doi:10.1890/06-0571.1.
- Morrison, H. and A. Gettelman, 2008: A new two-moment bulk stratiform cloud microphysics scheme in the Community Atmosphere Model, version 3 (CAM3). Part I: Description and numerical tests. *Journal of Climate*, **21**, 3642–3659, doi:10.1175/2008JCLI2105.1.
- Newton, R., S. Pfirman, P. Schlosser, B. Tremblay, M. Murray, and R. Pomerance, 2016: White Arctic vs. Blue Arctic: A case study of diverging stakeholder responses to environmental change. *Earth's Future*, **4**, 396–405, doi:10.1002/2016EF000356.
- Newton, R., S. Pfirman, B. Tremblay, and P. DeRepentigny, 2017: Increasing transnational sea-ice exchange in a changing Arctic Ocean. *Earth's Future*, **5**, 633–647, doi:10.1002/2016EF000500.
- Newton, R., P. Schlosser, R. Mortlock, J. Swift, and R. MacDonald, 2013: Canadian Basin freshwater sources and changes: Results from the 2005 Arctic Ocean Section. *Journal of Geophysical Research: Oceans*, **118**, 2133–2154, doi:10.1002/jgrc.20101.
- Ng, A. K., J. Andrews, D. Babb, Y. Lin, and A. Becker, 2018: Implications of climate change for shipping: Opening the Arctic seas. *Wiley Interdisciplinary Reviews: Climate Change*, **9**, e507, doi:10.1002/wcc.507.
- Niederdrenk, A. L. and D. Notz, 2018: Arctic sea ice in a 1.5 C warmer world. *Geophysical Research Letters*, **45**, 1963–1971, doi:10.1002/2017GL076159.
- Nordquist, M., 2011: *United Nations Convention on the Law of the Sea 1982, Volume VII: A Commentary*. Brill.
- Notz, D., 2014: Sea-ice extent and its trend provide limited metrics of model performance. *The Cryosphere*, **8**, 229–243, doi:10.5194/tc-8-229-2014.
- 2015: How well must climate models agree with observations? *Philosophical Transactions of the Royal Society A: Mathematical, Physical and Engineering Sciences*, **373**, 20140164, doi:10.1098/rsta.2014.0164.
- Notz, D., A. Jahn, M. Holland, E. Hunke, F. Massonnet, J. Stroeve, B. Tremblay, and M. Van-coppenolle, 2016: The CMIP6 Sea-Ice Model Intercomparison Project (SIMIP): understanding sea ice through climate-model simulations. *Geoscientific Model Development (Online)*, **9**, doi:10.5194/gmd-9-3427-2016.
- Notz, D. and J. Marotzke, 2012: Observations reveal external driver for Arctic sea-ice retreat. *Geophysical Research Letters*, **39**, doi:10.1029/2012GL051094.
- Notz, D. and J. Stroeve, 2016: Observed Arctic sea-ice loss directly follows anthropogenic CO<sub>2</sub> emission. *Science*, **354**, 747–750, doi:10.1126/science.aag2345.

- Nürnberg, D., I. Wollenburg, D. Dethleff, H. Eicken, H. Kassens, T. Letzig, E. Reimnitz, and J. Thiede, 1994: Sediments in Arctic sea ice: Implications for entrainment, transport and release. *Marine Geology*, **119**, 185–214, doi:10.1016/0025-3227(94)90181-3.
- Obbard, R. W., S. Sadri, Y. Q. Wong, A. A. Khitun, I. Baker, and R. C. Thompson, 2014: Global warming releases microplastic legacy frozen in Arctic Sea ice. *Earth's Future*, **2**, 315–320, doi:10.1002/2014EF000240.
- Octaviani, M., I. Stemmler, G. Lammel, and H. F. Graf, 2015: Atmospheric transport of persistent organic pollutants to and from the Arctic under present-day and future climate. *Environmental science & technology*, **49**, 3593–3602, doi:10.1021/es505636g.
- Ogi, M. and I. G. Rigor, 2013: Trends in Arctic sea ice and the role of atmospheric circulation. *Atmospheric Science Letters*, **14**, 97–101, doi:10.1002/asl2.423.
- Olsen, L. M., S. R. Laney, P. Duarte, H. M. Kauko, M. Fernández-Méndez, C. J. Mundy, A. Rösel, A. Meyer, P. Itkin, L. Cohen, et al., 2017: The seeding of ice algal blooms in Arctic pack ice: the multiyear ice seed repository hypothesis. *Journal of Geophysical Research: Biogeosciences*, **122**, 1529–1548, doi:10.1002/2016JG003668.
- O'Neill, B. C., C. Tebaldi, D. P. v. Vuuren, V. Eyring, P. Friedlingstein, G. Hurtt, R. Knutti, E. Kriegler, J.-F. Lamarque, J. Lowe, et al., 2016: The scenario model intercomparison project (ScenarioMIP) for CMIP6. *Geoscientific Model Development*, **9**, 3461–3482, doi:10.5194/gmd-9-3461-2016.
- Ostreg, W., K. M. Eger, B. Fløistad, A. Jørgensen-Dahl, L. Lothe, M. Mejlænder-Larsen, and T. Wergeland, 2013: *Shipping in Arctic waters: a comparison of the Northeast, Northwest and trans polar passages*. Springer Science & Business Media.
- O'Neill, B. C., E. Kriegler, K. Riahi, K. L. Ebi, S. Hallegatte, T. R. Carter, R. Mathur, and D. P. van Vuuren, 2014: A new scenario framework for climate change research: the concept of shared socioeconomic pathways. *Climatic change*, **122**, 387–400, doi:10.1007/s10584-013-0905-2.
- Parkinson, C. L., 2014: Spatially mapped reductions in the length of the Arctic sea ice season. *Geophysical Research Letters*, **41**, 4316–4322, doi:10.1002/2014GL060434.
- Peeken, I., S. Primpke, B. Beyer, J. Gütermann, C. Katlein, T. Krumpfen, M. Bergmann, L. Hehemann, and G. Gerdt, 2018: Arctic sea ice is an important temporal sink and means of transport for microplastic. *Nature communications*, **9**, 1505, doi:10.1038/s41467-018-03825-5.
- Peng, G., W. Meier, D. Scott, and M. Savoie, 2013: A long-term and reproducible passive microwave sea ice concentration data record for climate studies and monitoring. *Earth System Science Data*, **5**, 311–318, doi:10.5194/essd-5-311-2013.
- Perovich, D., W. Meier, M. Tschudi, S. Hendricks, A. A. Petty, D. Divine, S. Farrell, S. Gerland, C. Haas, L. Kaleschke, O. Pavlova, R. Ricker, X. Tian-Kunze, M. Webster, and K. Wood, 2020: Sea ice. *Arctic Report Card 2020*, R. L. Thoman, J. Richter-Menge, and M. L. Druckenmiller, eds., NOAA, doi:10.25923/n170-9h57.
- Perovich, D. K., S. V. Nghiem, T. Markus, and A. Schweiger, 2007: Seasonal evolution and inter-annual variability of the local solar energy absorbed by the Arctic sea ice–ocean system. *Journal of Geophysical Research: Oceans*, **112**, doi:10.1029/2006JC003558.

- Perovich, D. K. and C. Polashenski, 2012: Albedo evolution of seasonal Arctic sea ice. *Geophysical Research Letters*, **39**, doi:10.1029/2012GL051432.
- Peterson, C. H., S. D. Rice, J. W. Short, D. Esler, J. L. Bodkin, B. E. Ballachey, and D. B. Irons, 2003: Long-term ecosystem response to the Exxon Valdez oil spill. *Science*, **302**, 2082–2086, doi:10.1126/science.1084282.
- Pfirman, S., H. Eicken, D. Bauch, and W. Weeks, 1995: The potential transport of pollutants by Arctic sea ice. *Science of the Total Environment*, **159**, 129–146, doi:10.1016/0048-9697(95)04174-Y.
- Pfirman, S., W. F. Haxby, R. Colony, and I. Rigor, 2004: Variability in Arctic sea ice drift. *Geophysical Research Letters*, **31**, doi:10.1029/2004GL020063.
- Pfirman, S., J. Kögeler, and I. Rigor, 1997: Potential for rapid transport of contaminants from the Kara Sea. *Science of the Total Environment*, **202**, 111–122, doi:10.1016/S0048-9697(97)00108-3.
- Polvani, L. M., M. Previdi, M. R. England, G. Chiodo, and K. L. Smith, 2020: Substantial twentieth-century Arctic warming caused by ozone-depleting substances. *Nature Climate Change*, **10**, 130–133, doi:10.1038/s41558-019-0677-4.
- Post, E., R. B. Alley, T. R. Christensen, M. Macias-Fauria, B. C. Forbes, M. N. Gooseff, A. Iler, J. T. Kerby, K. L. Laidre, M. E. Mann, et al., 2019: The polar regions in a 2°C warmer world. *Science Advances*, **5**, eaaw9883, doi:10.1126/sciadv.aaw9883.
- Post, E., U. S. Bhatt, C. M. Bitz, J. F. Brodie, T. L. Fulton, M. Hebblewhite, J. Kerby, S. J. Kutz, I. Stirling, and D. A. Walker, 2013: Ecological consequences of sea-ice decline. *Science*, **341**, 519–524, doi:10.1126/science.1235225.
- Post, E., M. C. Forchhammer, M. S. Bret-Harte, T. V. Callaghan, T. R. Christensen, B. Elberling, A. D. Fox, O. Gilg, D. S. Hik, T. T. Høye, et al., 2009: Ecological dynamics across the Arctic associated with recent climate change. *Science*, **325**, 1355–1358, doi:10.1126/science.1173113.
- Previdi, M., T. P. Janoski, G. Chiodo, K. L. Smith, and L. M. Polvani, 2020: Arctic amplification: A rapid response to radiative forcing. *Geophysical Research Letters*, **47**, e2020GL089933, doi:10.1029/2020GL089933.
- Rigor, I. G. and J. M. Wallace, 2004: Variations in the age of Arctic sea-ice and summer sea-ice extent. *Geophysical Research Letters*, **31**, doi:10.1029/2004GL019492.
- Rinke, A., M. Maturilli, R. M. Graham, H. Matthes, D. Handorf, L. Cohen, S. R. Hudson, and J. C. Moore, 2017: Extreme cyclone events in the Arctic: Wintertime variability and trends. *Environmental Research Letters*, **12**, 094006, doi:10.1088/1748-9326/aa7def.
- Rodgers, K. B., S.-S. Lee, N. Rosenbloom, A. Timmermann, G. Danabasoglu, C. Deser, J. Edwards, J.-E. Kim, I. Simpson, K. Stein, M. F. Stuecker, R. Yamaguchi, T. Bodai, E.-S. Chung, L. Huang, W. Kim, J.-F. Lamarque, D. Lombardozzi, W. R. Wieder, and S. G. Yeager, 2021: Ubiquity of human-induced changes in climate variability. *Earth System Dynamics*, doi:10.5194/esd-2021-50, under review.
- Rosenblum, E. and I. Eisenman, 2016: Faster Arctic sea ice retreat in CMIP5 than in CMIP3 due to volcanoes. *Journal of Climate*, **29**, 9179–9188, doi:10.1175/JCLI-D-16-0391.1.

- 2017: Sea ice trends in climate models only accurate in runs with biased global warming. *Journal of Climate*, **30**, 6265–6278, doi:10.1175/JCLI-D-16-0455.1.
- Sanderson, B. M., Y. Xu, C. Tebaldi, M. Wehner, B. C. O’Neill, A. Jahn, A. G. Pendergrass, F. Lehner, W. G. Strand, L. Lin, et al., 2017: Community climate simulations to assess avoided impacts in 1.5 and 2 C futures. *Earth System Dynamics*, **8**, 827–847, doi:10.3929/ethz-b-000191578.
- Schøyen, H. and S. Bråthen, 2011: The Northern Sea Route versus the Suez Canal: cases from bulk shipping. *Journal of Transport Geography*, **19**, 977–983, doi:10.1016/j.jtrangeo.2011.03.003.
- Schupfner, M., K.-H. Wieners, F. Wachsmann, C. Steger, M. Bittner, J. Jungclaus, B. Früh, K. Pankatz, M. Giorgetta, C. Reick, S. Legutke, M. Esch, V. Gayler, H. Haak, P. de Vrese, T. Raddatz, T. Mauritsen, J.-S. von Storch, J. Behrens, V. Brovkin, M. Claussen, T. Crueger, I. Fast, S. Fiedler, S. Hagemann, C. Hohenegger, T. Jahns, S. Kloster, S. Kinne, G. Lasslop, L. Kornblueh, J. Marotzke, D. Matei, K. Meraner, U. Mikolajewicz, K. Modali, W. Müller, J. Nabel, D. Notz, K. Peters, R. Pincus, H. Pohlmann, J. Pongratz, S. Rast, H. Schmidt, R. Schnur, U. Schulzweida, K. Six, B. Stevens, A. Voigt, and E. Roeckner, 2019: DKRZ MPI-ESM1.2-HR model output prepared for CMIP6 ScenarioMIP ssp370. Version 20190815, doi:10.22033/ESGF/CMIP6.4399.
- Screen, J. A., 2018: Arctic sea ice at 1.5 and 2 C. *Nature Climate Change*, **8**, 362–363, doi:10.1038/s41558-018-0137-6.
- Screen, J. A., C. Deser, and I. Simmonds, 2012: Local and remote controls on observed Arctic warming. *Geophysical Research Letters*, **39**, doi:10.1029/2012GL051598.
- Screen, J. A. and I. Simmonds, 2010: The central role of diminishing sea ice in recent Arctic temperature amplification. *Nature*, **464**, 1334–1337, doi:10.1038/nature09051.
- Screen, J. A. and D. Williamson, 2017: Ice-free Arctic at 1.5 C? *Nature Climate Change*, **7**, 230, doi:10.1038/nclimate3248.
- Seland, Ø., M. Bentsen, D. J. L. Olivie, T. Toniazzo, A. Gjermundsen, L. S. Graff, J. B. Debernard, A. K. Gupta, Y. He, A. Kirkevåg, J. Schwinger, J. Tjiputra, K. S. Aas, I. Bethke, Y. Fan, J. Griesfeller, A. Grini, C. Guo, M. Ilicak, I. H. H. Karset, O. A. Landgren, J. Liakka, K. O. Moseid, A. Nummelin, C. Spensberger, H. Tang, Z. Zhang, C. Heinze, T. Iversen, and M. Schulz, 2019a: NCC NorESM2-LM model output prepared for CMIP6 CMIP historical. Version 20191108, doi:10.22033/ESGF/CMIP6.8036.
- 2019b: NCC NorESM2-LM model output prepared for CMIP6 ScenarioMIP ssp370. Version 20191108, doi:10.22033/ESGF/CMIP6.8268.
- Serreze, M. C. and R. G. Barry, 2011: Processes and impacts of Arctic amplification: A research synthesis. *Global and planetary change*, **77**, 85–96, doi:10.1016/j.gloplacha.2011.03.004.
- Serreze, M. C. and J. Stroeve, 2015: Arctic sea ice trends, variability and implications for seasonal ice forecasting. *Philosophical Transactions of the Royal Society A: Mathematical, Physical and Engineering Sciences*, **373**, 20140159, doi:10.1098/rsta.2014.0159.

- Sherstyukov, B. and A. Sherstyukov, 2014: Assessment of increase in forest fire risk in Russia till the late 21st century based on scenario experiments with fifth-generation climate models. *Russian Meteorology and Hydrology*, **39**, 292–301, doi:10.3103/S1068373914050021.
- Shevchenko, V. P., A. A. Vinogradova, A. P. Lisitzin, A. N. Novigatsky, M. V. Panchenko, and V. V. Pol'kin, 2016: *Aeolian and Ice Transport of Matter (Including Pollutants) in the Arctic*, Springer Berlin Heidelberg, Berlin, Heidelberg. 59–73, doi:10.1007/978-3-642-12315-3\_5.
- Shiogama, H., M. Abe, and H. Tatebe, 2019: MIROC MIROC6 model output prepared for CMIP6 ScenarioMIP ssp370. Version 20190627, doi:10.22033/ESGF/CMIP6.5752.
- Sigmond, M., J. C. Fyfe, and N. C. Swart, 2018: Ice-free Arctic projections under the Paris Agreement. *Nature Climate Change*, **8**, 404, doi:10.1038/s41558-018-0124-y.
- SIMIP Community, 2020: Arctic Sea Ice in CMIP6. *Geophysical Research Letters*, **47**, e2019GL086749, doi:10.1029/2019GL086749.
- Smedsrud, L. H., 2001: Frazil-ice entrainment of sediment: large-tank laboratory experiments. *Journal of Glaciology*, **47**, 461–471, doi:10.3189/172756501781832142.
- 2002: A model for entrainment of sediment into sea ice by aggregation between frazil-ice crystals and sediment grains. *Journal of Glaciology*, **48**, 51–61, doi:10.3189/172756502781831520.
- Smith, A. and A. Jahn, 2019: Definition differences and internal variability affect the simulated Arctic sea ice melt season. *The Cryosphere*, **13**, 1–20, doi:10.5194/tc-13-1-2019.
- Smith, R., P. Jones, B. Briegleb, F. Bryan, G. Danabasoglu, J. Dennis, J. Dukowicz, C. Eden, B. Fox-Kemper, P. Gent, et al., 2010: The Parallel Ocean Program (POP) Reference Manual: Ocean Component of the Community Climate System Model (CCSM) and Community Earth System Model (CESM). *Rep. LAUR-01853*, **141**, 1–140.
- Sørstrøm, S. E., P. J. Brandvik, I. Buist, P. Daling, D. Dickins, L.-G. Faksness, S. Potter, J. Fritt-Rasmussen, and I. Singaas, 2010: *Joint industry program on oil spill contingency for Arctic and ice-covered waters: Summary report*. SINTEF, Trondheim, Norway.
- Stephenson, S. R., L. C. Smith, L. W. Brigham, and J. A. Agnew, 2013: Projected 21st-century changes to Arctic marine access. *Climatic Change*, **118**, 885–899, doi:10.1007/s10584-012-0685-0.
- Stroeve, J., A. Barrett, M. Serreze, and A. Schweiger, 2014a: Using records from submarine, aircraft and satellites to evaluate climate model simulations of Arctic sea ice thickness. *Cryosphere*, **8**, doi:10.5194/tc-8-1839-2014.
- Stroeve, J., M. M. Holland, W. Meier, T. Scambos, and M. Serreze, 2007: Arctic sea ice decline: Faster than forecast. *Geophysical research letters*, **34**, doi:10.1029/2007GL029703.
- Stroeve, J., V. Kattsov, A. Barrett, M. Serreze, T. Pavlova, M. Holland, and W. N. Meier, 2012a: Trends in Arctic sea ice extent from CMIP5, CMIP3 and observations. *Geophysical Research Letters*, **39**, doi:10.1029/2012GL052676.
- Stroeve, J., T. Markus, L. Boisvert, J. Miller, and A. Barrett, 2014b: Changes in Arctic melt season and implications for sea ice loss. *Geophysical Research Letters*, **41**, 1216–1225, doi:10.1002/2013GL058951.

- Stroeve, J. and D. Notz, 2015: Insights on past and future sea-ice evolution from combining observations and models. *Global and Planetary Change*, **135**, 119–132, doi:10.1016/j.gloplacha.2015.10.011.
- 2018: Changing state of Arctic sea ice across all seasons. *Environmental Research Letters*, **13**, 103001, doi:10.1088/1748-9326/aade56.
- Stroeve, J., M. Serreze, M. M. Holland, J. E. Kay, J. Malanik, and A. P. Barrett, 2012b: The Arctic’s rapidly shrinking sea ice cover: a research synthesis. *Climatic Change*, **110**, 1005–1027, doi:10.1007/s10584-011-0101-1.
- Stuecker, M. F., C. M. Bitz, K. C. Armour, C. Proistosescu, S. M. Kang, S.-P. Xie, D. Kim, S. McGregor, W. Zhang, S. Zhao, et al., 2018: Polar amplification dominated by local forcing and feedbacks. *Nature Climate Change*, **8**, 1076–1081, doi:10.1038/s41558-018-0339-y.
- Swart, N. C., J. N. Cole, V. V. Kharin, M. Lazare, J. F. Scinocca, N. P. Gillett, J. Anstey, V. Arora, J. R. Christian, Y. Jiao, W. G. Lee, F. Majaess, O. A. Saenko, C. Seiler, C. Seinen, A. Shao, L. Solheim, K. von Salzen, D. Yang, B. Winter, and M. Sigmond, 2019a: CCCma CanESM5 model output prepared for CMIP6 CMIP historical. Version 20190429, doi:10.22033/ESGF/CMIP6.3610.
- 2019b: CCCma CanESM5 model output prepared for CMIP6 ScenarioMIP ssp370. Version 20190429, doi:10.22033/ESGF/CMIP6.3690.
- Swart, N. C., J. C. Fyfe, E. Hawkins, J. E. Kay, and A. Jahn, 2015: Influence of internal variability on Arctic sea-ice trends. *Nature Climate Change*, **5**, 86, doi:10.1038/nclimate2483.
- Tandon, N. F., P. J. Kushner, D. Docquier, J. J. Wettstein, and C. Li, 2018: Reassessing Sea Ice Drift and Its Relationship to Long-Term Arctic Sea Ice Loss in Coupled Climate Models. *Journal of Geophysical Research: Oceans*, **123**, 4338–4359, doi:10.1029/2017JC013697.
- Tang, W., S. Tilmes, D. M. Lawrence, F. Li, C. He, L. K. Emmons, and R. R. Buchholz, 2021: Wildfires in the 21st Century under Different Shared Socioeconomic Pathways (SSPs) and Geo-engineering Scenarios in CESM2/WACCM6. *Earth’s Future*, under review.
- Tatebe, H. and M. Watanabe, 2018: MIROC MIROC6 model output prepared for CMIP6 CMIP historical. Version 20181212, doi:10.22033/ESGF/CMIP6.5603.
- Tilmes, S., A. Hodzic, L. K. Emmons, M. J. Mills, A. Gettelman, D. E. Kinnison, M. Park, J.-F. Lamarque, F. Vitt, M. Shrivastava, P. Campuzano Jost, J. Jimenez, and X. Liu, 2019: Climate forcing and trends of organic aerosols in the Community Earth System Model (CESM2). *Journal of Advances in Modeling Earth Systems*, doi:10.1029/2019MS001827.
- Tremblay, L., G. Schmidt, S. Pfirman, R. Newton, and P. Derepentigny, 2015: Is ice-rafted sediment in a North Pole marine record evidence for perennial sea-ice cover? *Philosophical Transactions of the Royal Society A: Mathematical, Physical and Engineering Sciences*, **373**, 20140168, doi:10.1098/rsta.2014.0168.
- Tschudi, M., C. Fowler, J. Maslanik, J. S. Stewart, and W. Meier, 2016: Polar Pathfinder Daily 25 km EASE-Grid Sea Ice Motion Vectors, Version 3 [monthly averages from January 1989 to December 2008]. *NASA National Snow and Ice Data Center Distributed Active Archive Center, Boulder, Colorado, USA*, Accessed March 2016, doi:10.5067/O57VAIT2AYYY.

- Turner, A. K. and E. C. Hunke, 2015: Impacts of a mushy-layer thermodynamic approach in global sea-ice simulations using the CICE sea-ice model. *Journal of Geophysical Research: Oceans*, **120**, 1253–1275, doi:10.1002/2014JC010358.
- UNFCCC, 2015: Adoption of the Paris Agreement, FCCC/CP/2015/10/Add.1, available at: <https://unfccc.int/resource/docs/2015/cop21/eng/10a01.pdf>.
- Van Marle, M. J., S. Kloster, B. I. Magi, J. R. Marlon, A.-L. Daniau, R. D. Field, A. Arneth, M. Forrest, S. Hantson, N. M. Kehrwald, et al., 2017: Historic global biomass burning emissions for CMIP6 (BB4CMIP) based on merging satellite observations with proxies and fire models (1750–2015). *Geoscientific Model Development*, **10**, 3329–3357, doi:10.5194/gmd-10-3329-2017.
- Van Vuuren, D. P., J. Edmonds, M. Kainuma, K. Riahi, A. Thomson, K. Hibbard, G. C. Hurtt, T. Kram, V. Krey, J.-F. Lamarque, et al., 2011: The representative concentration pathways: an overview. *Climatic change*, **109**, 5, doi:10.1007/s10584-011-0148-z.
- Varotsos, C. A. and V. F. Krapivin, 2018: Pollution of Arctic Waters Has Reached a Critical Point: an Innovative Approach to This Problem. *Water, Air, & Soil Pollution*, **229**, 343, doi:10.1007/s11270-018-4004-x.
- Vavrus, S. J., 2018: The influence of Arctic amplification on mid-latitude weather and climate. *Current Climate Change Reports*, **4**, 238–249, doi:10.1007/s40641-018-0105-2.
- Venkatesh, S., H. El-Tahan, G. Comfort, and R. Abdelnour, 1990: Modelling the behaviour of oil spills in ice-infested waters. *Atmosphere-Ocean*, **28**, 303–329, doi:10.1080/07055900.1990.9649380.
- Vihma, T., 2014: Effects of Arctic sea ice decline on weather and climate: A review. *Surveys in Geophysics*, **35**, 1175–1214, doi:10.1007/s10712-014-9284-0.
- Wang, M. and J. E. Overland, 2009: A sea ice free summer Arctic within 30 years? *Geophysical Research Letters*, **36**, doi:10.1029/2009GL037820.
- 2012: A sea ice free summer Arctic within 30 years: An update from CMIP5 models. *Geophysical Research Letters*, **39**, doi:10.1029/2012GL052868.
- Wang, M., Q. Yang, J. E. Overland, and P. Stabeno, 2018: Sea-ice cover timing in the Pacific Arctic: The present and projections to mid-century by selected CMIP5 models. *Deep Sea Research Part II: Topical Studies in Oceanography*, **152**, 22–34, doi:10.1016/j.dsr2.2017.11.017.
- Werf, G. R., J. T. Randerson, L. Giglio, T. T. v. Leeuwen, Y. Chen, B. M. Rogers, M. Mu, M. J. Van Marle, D. C. Morton, G. J. Collatz, et al., 2017: Global fire emissions estimates during 1997–2016. *Earth System Science Data*, **9**, 697–720, doi:10.5194/essd-9-697-2017.
- Wieners, K.-H., M. Giorgetta, J. Jungclaus, C. Reick, M. Esch, M. Bittner, V. Gayler, H. Haak, P. de Vrese, T. Raddatz, T. Mauritsen, J.-S. von Storch, J. Behrens, V. Brovkin, M. Claussen, T. Crueger, I. Fast, S. Fiedler, S. Hagemann, C. Hohenegger, T. Jahns, S. Kloster, S. Kinne, G. Lasslop, L. Kornbluh, J. Marotzke, D. Matei, K. Meraner, U. Mikolajewicz, K. Modali, W. Müller, J. Nabel, D. Notz, K. Peters, R. Pincus, H. Pohlmann, J. Pongratz, S. Rast, H. Schmidt, R. Schnur, U. Schulzweida, K. Six, B. Stevens, A. Voigt, and E. Roeckner, 2019a: MPI-M MPI-ESM1.2-LR model output prepared for CMIP6 ScenarioMIP ssp370. Version 20190710, doi:10.22033/ESGF/CMIP6.6695.

- Wieners, K.-H., M. Giorgetta, J. Jungclaus, C. Reick, M. Esch, M. Bittner, S. Legutke, M. Schupfner, F. Wachsmann, V. Gayler, H. Haak, P. de Vrese, T. Raddatz, T. Mauritsen, J.-S. von Storch, J. Behrens, V. Brovkin, M. Claussen, T. Crueger, I. Fast, S. Fiedler, S. Hagemann, C. Hohenegger, T. Jahns, S. Kloster, S. Kinne, G. Lasslop, L. Kornblueh, J. Marotzke, D. Matei, K. Meraner, U. Mikolajewicz, K. Modali, W. Müller, J. Nabel, D. Notz, K. Peters, R. Pincus, H. Pohlmann, J. Pongratz, S. Rast, H. Schmidt, R. Schnur, U. Schulzweida, K. Six, B. Stevens, A. Voigt, and E. Roeckner, 2019b: MPI-M MPI-ESM1.2-LR model output prepared for CMIP6 CMIP historical. Version 20190710, doi:10.22033/ESGF/CMIP6.6595.
- Wilhelmsen, J. M. and K. L. Gjerde, 2018: Norway and Russia in the Arctic: New Cold War Contamination? *Arctic Review on Law and Politics*, **9**, 381–407, doi:10.23865/arctic.v9.1334.
- Wilkinson, J., C. J. Beegle-Krause, K.-U. Evers, N. Hughes, A. Lewis, M. Reed, and P. Wadhams, 2017: Oil spill response capabilities and technologies for ice-covered Arctic marine waters: A review of recent developments and established practices. *Ambio*, **46**, 423–441, doi:10.1007/s13280-017-0958-y.
- Williams, J., B. Tremblay, R. Newton, and R. Allard, 2016: Dynamic preconditioning of the minimum September sea-ice extent. *Journal of Climate*, **29**, 5879–5891, doi:10.1175/JCLI-D-15-0515.1.
- Winton, M., 2011: Do climate models underestimate the sensitivity of Northern Hemisphere sea ice cover? *Journal of Climate*, **24**, 3924–3934, doi:10.1175/2011JCLI4146.1.
- Witze, A., 2020: The arctic is burning like never before — and that’s bad news for climate change. *Nature*, **585**, 336–337, doi:10.1038/d41586-020-02568-y.
- Yukimoto, S., T. Koshiro, H. Kawai, N. Oshima, K. Yoshida, S. Urakawa, H. Tsujino, M. Deushi, T. Tanaka, M. Hosaka, H. Yoshimura, E. Shindo, R. Mizuta, M. Ishii, A. Obata, and Y. Adachi, 2019a: MRI MRI-ESM2.0 model output prepared for CMIP6 CMIP historical. Version 20190904, doi:10.22033/ESGF/CMIP6.6842.
- 2019b: MRI MRI-ESM2.0 model output prepared for CMIP6 ScenarioMIP ssp370. Version 20190904, doi:10.22033/ESGF/CMIP6.6915.
- Zappa, G., F. Pithan, and T. G. Shepherd, 2018: Multimodel evidence for an atmospheric circulation response to Arctic sea ice loss in the CMIP5 future projections. *Geophysical research letters*, **45**, 1011–1019, doi:10.1002/2017GL076096.
- Zhang, J., T. Wu, X. Shi, F. Zhang, J. Li, M. Chu, Q. Liu, J. Yan, Q. Ma, and M. Wei, 2018: BCC BCC-ESM1 model output prepared for CMIP6 CMIP historical. Version 20200218, doi:10.22033/ESGF/CMIP6.2949.
- 2019: BCC BCC-ESM1 model output prepared for CMIP6 AerChemMIP ssp370. Version 20200219, doi:10.22033/ESGF/CMIP6.3036.
- Zhang, R., 2015: Mechanisms for low-frequency variability of summer Arctic sea ice extent. *Proceedings of the National Academy of Sciences*, **112**, 4570–4575, doi:10.1073/pnas.1422296112.
- Ziehn, T., M. Chamberlain, A. Lenton, R. Law, R. Bodman, M. Dix, Y. Wang, P. Dobrohotoff, J. Srbinovsky, L. Stevens, P. Vohralik, C. Mackallah, A. Sullivan, S. O’Farrell, and K. Druken,

2019a: CSIRO ACCESS-ESM1.5 model output prepared for CMIP6 CMIP historical. Version 20200817, doi:10.22033/ESGF/CMIP6.4272.

— 2019b: CSIRO ACCESS-ESM1.5 model output prepared for CMIP6 ScenarioMIP ssp370. Version 20200817, doi:10.22033/ESGF/CMIP6.4324.